

# DISSERTATION

## **Characterizing the Fluorescence Intermittency of Individual CdSe/ZnS Quantum Dot Clusters with Spatially Correlated Single Molecule Fluorescence Spectroscopy and Atomic Force Microscopy**

Submitted by

Ming Yu

Department of Chemistry

In partial fulfillment of the requirements

For the Degree of Doctor of Philosophy

Colorado State University

Fort Collins, Colorado

Summer, 2008

UMI Number: 3332719

## INFORMATION TO USERS

The quality of this reproduction is dependent upon the quality of the copy submitted. Broken or indistinct print, colored or poor quality illustrations and photographs, print bleed-through, substandard margins, and improper alignment can adversely affect reproduction.

In the unlikely event that the author did not send a complete manuscript and there are missing pages, these will be noted. Also, if unauthorized copyright material had to be removed, a note will indicate the deletion.

**UMI**<sup>®</sup>

---

UMI Microform 3332719

Copyright 2008 by ProQuest LLC.

All rights reserved. This microform edition is protected against unauthorized copying under Title 17, United States Code.

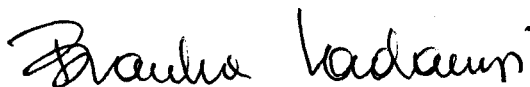
ProQuest LLC  
789 E. Eisenhower Parkway  
PO Box 1346  
Ann Arbor, MI 48106-1346

COLORADO STATE UNIVERSITY

April 22<sup>nd</sup>, 2008

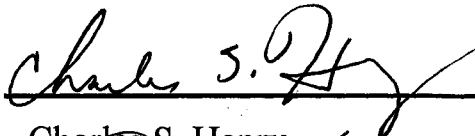
WE HEREBY RECOMMEND THAT THE DISSERTATION PREPARED UNDER OUR SUPERVISION BY **MING YU** ENTITLED "CHARACTERIZING THE FLUORESCENCE INTERMITTENCY OF INDIVIDUAL CdSe/ZnS QUANTUM DOT CLUSTERS WITH SPATIALLY CORRELATED SINGLE MOLECULE FLUORESCENCE SPECTROSCOPY AND ATOMIC FORCE MICROSCOPY" BE ACCEPTED AS FULLFILING IN PART REQUIREMENTS FOR THE DEGREE OF DOCTOR OF PHILOSOPHY.

Committee on Graduate Work



---

Branka M. Ladanyi



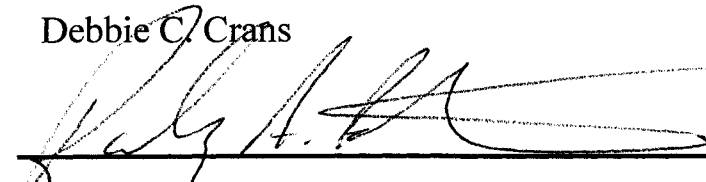
---

Charles S. Henry



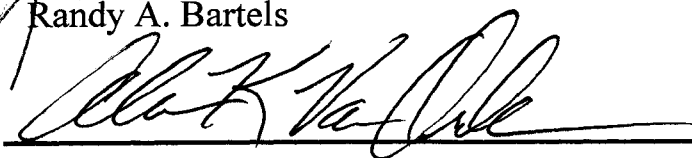
---

Debbie C. Crans



---

Randy A. Bartels



---

Adviser – Alan K. Van Orden



---

Department Head – Anthony K. Rappe

## ABSTRACT OF DISSERTATION

### **Characterizing the Fluorescence Intermittency of Individual CdSe/ZnS Quantum Dot Clusters with Spatially Correlated Single Molecule Fluorescence Spectroscopy and Atomic Force Microscopy**

In this thesis, I describe work done to study the optical behaviors of CdSe/ZnS quantum dots, especially the fluorescence blinking behavior of small quantum dot clusters. QDs have unique optical properties that impart several key advantages over molecular dyes. However, when examined at the single-molecule level, QDs emission exhibit novel fluorescence intermittency, or “blinking,” behavior. This blinking is believed to be caused by trapping and de-trapping of the photoexcited carriers, causing the QDs to fluctuate between emissive and non-emissive states.

A spatially correlated single molecule fluorescence spectroscopy and atomic force microscopy (AFM) apparatus was used to carry out these studies. Single molecule spectroscopy examines the blinking behavior of individual, isolated QDs and QD clusters, while the AFM images the nanometer scale topography of the particles. When multiple isolated QDs were probed simultaneously, the fluorescence behavior was consistent with independent blinking of the individual QDs. However, when close-packed QD clusters were probed, the fluorescence intermittency became much more rapid and intense than could be explained by the summation of multiple particles blinking independently. This suggests when the small QDs aggregate together, they become electronically coupled in some way that enhances the fluorescence blinking. Subsequently, we studied variations of the emission wavelengths of isolated small QD clusters possessing the enhanced blinking behavior. The emission wavelength of the coupled enhanced blinking is red

shifted relative to that of normal blinking. We propose that red-shifting in emission is one of the characteristics of electronic coupling in the QD clusters and resulted from the quantum confinement Stark effect.

In the following chapters, environment and substrate dependence were also studied. Compared with ambient air, dry nitrogen decreases the population, intensity and/or durations of “on” times. Both CTAB- and  $Mg^{2+}$ -mica substrates quench the fluorescence of single QDs and QD clusters, which is due to the dissociation of electron hole pairs of excited QDs by the electron attractive sites in CTAB molecules and  $Mg^{2+}$  ions.

Ming Yu  
Department of Chemistry  
Colorado State University  
Fort Collins, CO 80523  
Summer, 2008

## Acknowledgments

This dissertation would not be completed without the help of others. I first want to thank my advisor, Alan, for his constant support and help during my time here. You are so smart and approachable that I have learned much from you.

Jaemyeong was always willing to answer my questions. Thanks for being there each and every time. Keir is one of most responsible, organized and cheerful fellows I have met. “Ask Keir,” jumps into my mind whenever I am in need of help. Jon inspired me of the independency and initiative in doing research. Dale was the first person I worked with and I learned a lot from you about biochemistry.

Yunfeng, my husband, is my lover and soul mate. Without your support and encouragement, I would not have achieved this goal.

Last but not least, I would like to thank Colorado State University to give me a chance to study in the United States. It has been a precious experience.

# Contents

<b>1</b>	<b>Introduction.....</b>	<b>1</b>
1.1	Quantum Dots	
1.2	Quantum Confinement	
1.3	QD Surface (Core/Shell Structure)	
1.4	General Synthesis Methods	
1.5	QDs Blinking	
1.6	Physical Models of Single QDs Blinking	
1.6.1	Quantum Jump and Auger Ionization	
1.6.2	Fluctuated Tunneling and Charge Diffusion	
1.6.3	Diffusion Controlled Electron Transfer (DCET)	
1.6.4	Fluctuating Electronic States Model	
1.7	QD-QD Interactions	
1.8	Fluorescence Blinking Data Analysis	
1.8.1	Autocorrelation Analysis	
1.8.2	“On”/ “Off” Time Density Distribution	



3.4.2	On-/Off-time Probability Density Distributions	
3.4.3	ACF Analysis	
3.5	Conclusion	
<b>4</b>	<b>Fluorescence Blinking of Small Close-packed Clusters of QD Nanocrystals.....</b>	<b>68</b>
4.1	Introduction	
4.2	Experimental Section	
4.3	Observations	
4.3.1	AFM Images of Single QDs and Small QD Clusters	
4.3.2	Probing Single QD Nanocrystals and Small QD Clusters	
4.3.3	QD Size Dependence of the Enhanced Blinking	
4.4	Data Analysis	
4.4.1	On/Off Times Probability Density Distributions	
4.4.2	Autocorrelation Analysis	
4.4.3	Kinetics Analysis with a Hybrid MEM/NLS	
4.5	Discussion	
4.6	Conclusion	
<b>5</b>	<b>Distinguishable Difference in PL between Enhanced Blinking and Normal Blinking.....</b>	<b>90</b>
5.1	Introduction	
5.2	Experimental Section	
5.2.1	Instrumentation	
5.2.2	Sample Preparation	

5.3	Results and Observations	
5.3.1	Emission Wavelength of the Small QD Clusters	
5.3.2	Initial PL Positions of Isolated QD Clusters	
5.3.3	Bluing of Individual QDs and Small QD Clusters	
5.4	Discussion	
5.5	Conclusion	
<b>6</b>	<b>Environment Dependence of QDs Fluorescence Blinking.....</b>	<b>114</b>
6.1	Introduction	
6.2	Experimental Section	
6.2.1	Instrumentation	
6.2.2	Sample Preparation	
6.3	Results and Discussion	
6.4	Conclusion	
<b>7</b>	<b>Surface Dependence of QDs Fluorescence Blinking.....</b>	<b>127</b>
7.1	Introduction	
7.2	Experimental Section	
7.3	Results and Discussion	
7.4	Conclusion	
<b>8</b>	<b>Conclusions and Future Work.....</b>	<b>134</b>
8.1	Altering Capping Ligands	
8.2	Altering Inter Particle Distances of QD Clusters	
8.3	Altering Shell Thickness	
8.4	Altering QD Clusters Shapes	

- 8.5 Altering the Single Quantum Units by Using Small Quantum Rods (QRs)
- 8.6 Influence of Gold Nanoparticles
- 8.7 Temperature Dependence

**Appendix Programming with MatLab.....145**

- 1 Probability Density Distribution of “on” and “off” Times in a Blinking Trajectory
- 2 Threshold for Distinguishing “on” and “off” States
- 3 Photon Counting Histogram for the Single Detector Setup
- 4 Photon Counting Histogram for the Two-detector Setup
- 5 Auto-correlation Function for the Single Detector Setup
- 6 Auto-correlation Function for the Two-detector Setup
- 7 Auto-correlation and Cross-correlation Functions for the Two-detector Setup
- 8 Auto-correlation and Cross-correlation Functions for the Two-detector Setup

# List of Figures

1-1	Low-dimensional structures.....	3
1-2	Schematic of energy levels of bulk and low-dimensional structure.....	6
1-3	Schematic of deep trap emission and band-edge emission.....	7
1-4	Fluorescence trajectory of a single CdSe/ZnS QD.....	11
1-5	Probability density distributions of off- and on-times of a single QD.....	12
1-6	Schematic of quantum jump model and Auger ionization model.....	14
1-7	Schematic of fluctuated tunneling model.....	16
1-8	Schematic of the charge diffusion model.....	16
1-9	Schematic of the DCET model.....	18
1-10	Schematic of the fluctuating electronic states model.....	20
2-1	Schematic of spatially correlated single molecule fluorescence spectroscopy and AFM method.....	32
2-2	Schematic of the experimental operation method for smaller particles.....	36
2-3	Schematic of the experimental operation method for bigger particles.....	37
2-4	Fluorescence confocal images of nanobeads.....	40

2-5	Concurrent topographical and probe region images of nanobeads.....	41
3-1	TappingMode and phase AFM images of individual QD-bioconjugates.....	49
3-2	Fluorescence trajectory segment, corresponding photon counting histogram, and on-/off- time density distributions of one QD605 streptavidin conjugate.....	50
3-3	Fluorescence trajectory segment, corresponding photon counting histogram, and on-/off- time density distributions of two isolated QD605 streptavidin conjugate..	52
3-4	Fluorescence trajectory segment, corresponding photon counting histogram, and on-/off- time density distributions of an QD605 streptavidin conjugate cluster.....	54
3-5	Autocorrelation functions of the individual QD, multiple QDs, and QD cluster....	56
3-6	Fluorescence trajectory segments, corresponding photon counting histograms, and ACFs of the same single QD605 streptavidin conjugate probing at different excitation power.....	58
3-7	Fluorescence trajectories and corresponding TappingMode AFM images of one isolated QD, three isolated QDs, a QD chain, and a QD blob.....	60
3-8	On-/off-time density distributions of the single QD, the multiple single QDs, the QD chain, and the QD blob.....	62
3-9	ACFs of the single QD, multiple QDs, QD chain, and QD blob.....	64
4-1	TEM images, size histograms and PL spectra of QD samples of green Evidots, yellow Evidots and red Evidots.....	71
4-2	AFM topography images and effective volume histograms of individual isolated Evidot QDs and QD clusters on mica.....	72
4-3	Fluorescence trajectory segments, photon count histograms, and AFM topography images of a single QD, a QD cluster, three isolated QDs probed	

simultaneously, and multiple isolated QDs in the same QD samples of green Evidots.....	74
4-4 Fluorescence trajectory segments and photon count histograms of a single QD and a QD cluster in the same QD sample of red Evidots.....	77
4-5 Off-/on- time density distributions of the single QD and the QD cluster.....	78
4-6 $m_{\text{off}}$ and $m_{\text{on}}$ of the power law vs. effective AFM volume for 18 particles in a QD sample of green Evidots containing a mixture of individual QDs and QD clusters.....	79
4-7 Normalized autocorrelation functions of the fluorescence trajectories shown in Figure 4-3.....	81
4-8 A bar graph histogram summarizing the blinking behavior of 25 particles in a sample of green Evidots containing a mixture of individual QDs and QD clusters, plotted vs. effective particle volume.....	83
4-9 MemExp output of the single QD and the QD cluster.....	86
4-10 MemExp outcomes of the lifetime distributions recovered from the autocorrelation functions of single QDs and small close-packed QD clusters.....	87
5-1 The two-detector setup of the spatially correlated single molecule fluorescence/AFM.....	93
5-2 PL spectrum of the single yellow Evidots and transmission spectra of the 650 nm short pass filter, the 605/40 nm band pass filter, the 565/40 nm band pass filter and the 590/40 nm band pass filter.....	95
5-3 Fluorescence trajectories of a QD clusters in two detecting channels under the constant laser excitation.....	97

5-4	Fluorescence trajectory segments and the corresponding photon counting histograms in different detecting channels of two different QD clusters in the same sample.....	100
5-5	A bar graph histogram summarizing PL position of 18 QD clusters in the same sample, plotted vs. effective particle volume.....	103
5-6	Fluorescence trajectories of multiple isolated single QDs, up to 3, near the probe region.....	104
5-7	Fluorescence trajectory segments and corresponding photon counting histograms of the same QD cluster under different radiation periods.....	106
6-1	Schematic diagram of the gas hood modified single-detector correlation setup...	117
6-2	2-D scanning confocal fluorescence images of isolated QD nanocrystals of yellow Evidots dispersed on AP-mica under ambient air and dry N <sub>2</sub> .....	120
6-3	Fluorescence trajectory segment of a big QD blob under ambient air and constant illumination.....	121
6-4	Fluorescence trajectories of two single nanocrystals in the same sample on AP-mica under alternative atmospheres of ambient air and dry N <sub>2</sub> .....	123
6-5	Fluorescence trajectories of two QD clusters in the same sample on AP-mica under alternative atmospheres of ambient air and dry N <sub>2</sub> .....	124
7-1	3-D scanning confocal fluorescence images of small close-packed QD clusters dispersed on CATB-mica and AP-mica.....	132

# List of Tables

1-1	Exciton Bohr diameters and band gap energies for semiconductors.....	4
1-2	Comparison of reported QD-QD interactions.....	21
3-1	Parameters from $P[t]$ fittings of the single QD, multiple QDs, QD chain, and QD blob.....	63

# Chapter 1

## Introduction

### 1.1 Quantum Dots

Colloidal quantum dots (QDs) are nanometer-scaled semiconductor crystals, containing a total of 100 to 100,000 atoms within a single QD. QDs are also called as artificial atoms because of their atomic like quantized energy states resulting from the small size scale. Under radiation of light with certain energy, QDs can emit fluorescence or visible light of lower energy. Since the successful synthesis of colloidal QDs 10 years ago, research on QDs has exploded because of their promising applications in biology<sup>1-3</sup> and solar cells<sup>4-7</sup>. Every year, there are thousands of papers about QDs are published. As the biological labels, QDs have several advantages over molecular dyes. They have broad absorption with narrow symmetric emission spectra, large Stokes shifts, high resistance to photobleaching and chemical degradation and tunable fluorescence emission

as a function of core size or chemical composition<sup>8</sup>. These features help to simplify instrumentation and processing in simultaneous detection of multiple signals, consequently cost and time. In solar cell applications, specific advantages of using QDs as light harvesting assemblies in solar cells exist. First and foremost, size quantization allows people to tune the visible response and vary the band offsets to modulate the charge transfer across different sized particles. In addition, these QDs open up new ways to increase the photovoltaic conversion efficiency by utilizing hot electrons or generate multiple charge carriers with a single photon. It has been reported that up to seven excitons could be generated in PbSe nanocrystals with a single photon.<sup>9, 10</sup>

However one drawback of the QDs applications is the fluctuation or inconsistency in their fluorescence emission.<sup>11-14</sup> Under continuous radiation, QDs display fluorescence intermittency or blinking. It is considered as an intrinsic limitation difficult to overcome, which is unfortunate because booming applications in biology labeling/sensing and solar cells could greatly benefit from long-lasting and nonblinking single-molecule emitters. Fully understood fluorescence intermittency of QDs will help to avoid and finally suppress its occurrence. We suggest that QD blinking can be exploited to study the interactions between neighboring QDs, or between QDs and other types of particles. Moreover, small QD clusters are potential building blocks of advanced devices, like the optoelectronic devices and light harvesting ensemble. Examining the cooperative optical behavior of small QD clusters is beneficial for fabricating QD devices. As a first step in that direction, individual QDs and small QD aggregates, or “clusters,” containing two or more QDs are studied with spatially correlated atomic force microscopy (AFM) and

single molecule fluorescence spectroscopy, which will be introduced in Chapter 2. We take CdSe/ZnS QDs as examples in the project because they have become the best systems in terms of the overall control of the size, shape, size/shape distribution, and optical quality.

## 1.2 Quantum Confinement

Interest in QDs is motivated by the fact that QDs have novel optical/electrical properties that are distinctly different from bulk behavior. At the mention of these novel intriguing properties, we have to introduce the concept of *quantum confinement*. The term quantum confinement describes the confinement of the exciton (bound electron-hole pair) within the physical boundaries of the semiconductor. Figure 1-1 shows typical low-dimensional structures<sup>15</sup>. QDs have a Zero-dimensional (0-D) structure, in which the motion of excitons is confined in all three dimensions. In contrast, a bulk material has the 3-D structure, in which the electronic carriers are free in all three directions. A completely free bulk material spatially confined in one direction results in a thin film—2-D quantum well. Confinement in two dimensions produces 1-D quantum wires.

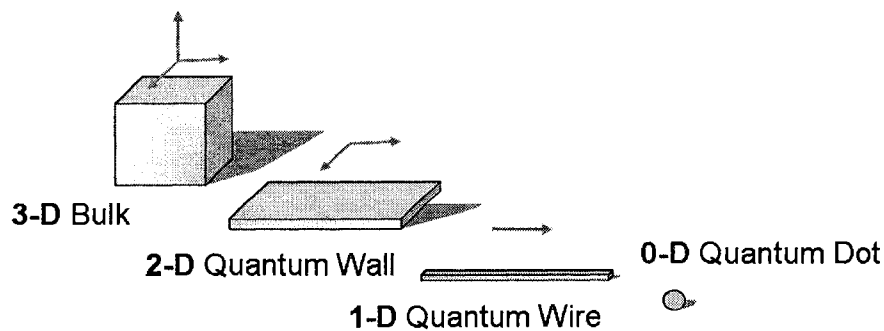


**Figure 1-1.** Low-dimensional structures.<sup>15</sup>

Excitons are bound electron and hole pairs. An exciton is very similar to the hydrogen atom. It has an average physical separation between the electron and hole, referred to as the exciton Bohr radius. A Bohr approximation of the atom can be used to calculate the exciton Bohr radius ( $a_{ex}$ ) by

$$a_{ex} = \frac{\kappa \hbar^2}{\mu^* e^2}$$

where  $\kappa$  is the semiconductor permittivity (the dielectric constant of the semiconductor),  $\mu^*$  is the reduced mass of the electron-hole pair,  $\hbar$  is the Planck's constant, and  $e$  is the charge on the electron.<sup>16</sup> This physical distance is often used as a meter-stick to judge the extent of confinement. Table 1-1 summarizes the exciton Bohr diameters and band gap energies for semiconductors.<sup>15</sup>

**Table 1-1.** Exciton Bohr diameters and band gap energies for semiconductors.<sup>15</sup>

Semiconductor	Exciton Bohr Diameter (Å)	Band Gap Energy (eV)
ZnSe	84	2.58
CdS	56	2.53
CdSe	106	1.74
CdTe	150	1.50
GaAs	280	1.43
Si	37 (longitudinal) 90 (transverse)	1.11
Ge	50 (longitudinal) 200(transverse)	0.67
PbS	400	0.41

The dimension of a bulk material is much bigger than its exciton Bohr diameter. Energy levels in valence or conduction bands are very close together, so close that they are described as continuous, as illustrated in Figure 1-2(a). Moreover, the band gap

energy is fixed. When the diameter of the crystal approaches the size of its exciton Bohr diameter, the electron energy levels can no longer be treated as continuous - they must be treated as discrete, meaning that there is a small and finite separation between energy levels, and the bandgap energy is also increased. When the size of the crystal is smaller than the size of the Bohr diameter, strong confinement is formed. Instead of a band of energies, energy levels are quantized, as shown in Figure 1-2(b). It is in the strongly-confined regime that the bandgap energy is very sensitive to the size of the crystal.

In the case of strong confinement, the energy of a spherical confined system is expressed as:

$$\Delta E_{nl} = \frac{\hbar^2 \alpha_{nl}^2}{2\mu^* a^2}$$

where  $\alpha_{nl}$  is the Bessel function term,  $\mu^*$  is effective carrier reduced mass, and  $a$  is the radius of the crystal.<sup>15</sup> As a QD getting smaller, its band gap energy gets bigger and the emission wavelength is shorter. It is established that the great majority of excited electrons, when falling from the conduction band (CB) back to the valence band (VB), tend to jump from near the bottom of the conduction band to the top of the valence band, schematically illustrated in Figure 1-2(b). In other words, they travel from one edge of the bandgap to the other and emit fluorescence with a wavelength corresponding to the bandgap energy. This is called as band -edge emission<sup>17</sup>. The wavelength of the emission is a function of the composition and size of the dot. Therefore it is possible to control the output wavelength by adjusting the size and composition of a QD. QDs offer the ability to tune the bandgap and hence the emission wavelength.

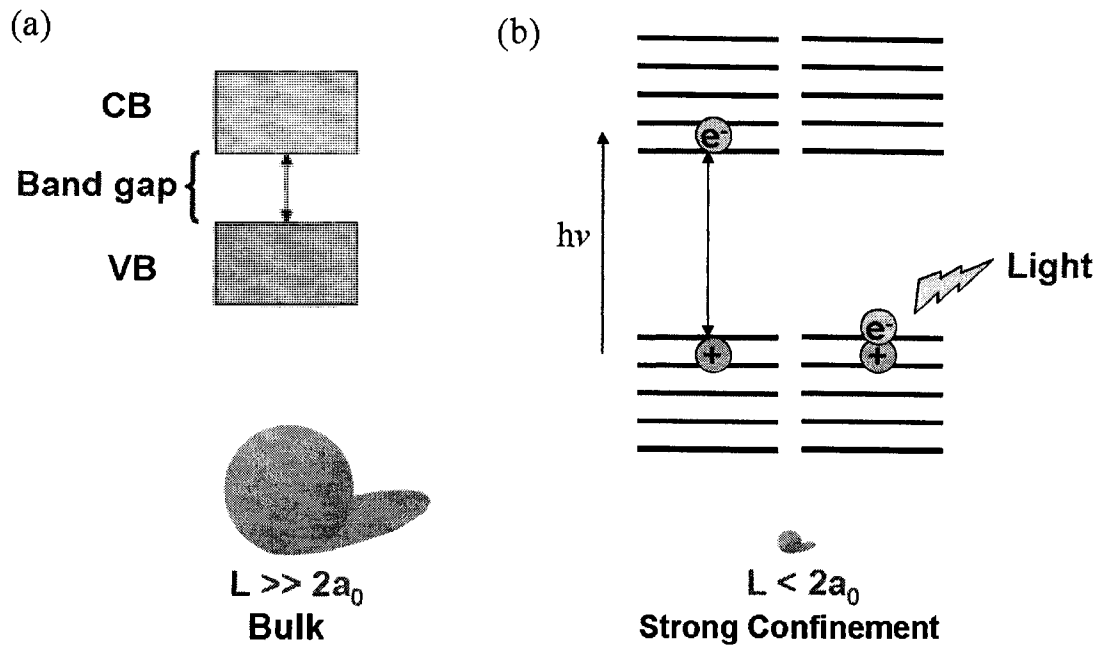


**Figure 1-2.** Schematic of (a) continuous energy levels of bulk and (b) discrete energy levels of low-dimensional structure with strong confinement.  $L$  is the diameter of the structure;  $a_0$  is the Bohr radius of the material. Band-edge emission, corresponding to band gap energy, is a function of the composition and size of the dot.

### 1.3 QDs Surface (Core/Shell Structure)

We have talked about the quantum confinement occurring on the small size scale. Another characteristic of being small is the big surface to volume ratio. Because of this, there are many trap states deep in band gap of QDs for electrons and holes. These trap states are caused by defects, such as vacancies, lattice mismatches, and dangling bonds.<sup>18</sup> The excited electron or hole might be trapped by these trap states, which results in broad deep trap emission of lower energy, schematically illustrated in Figure 1-3(a). Surface passivation is a well-known phenomenon that decreases the possibility of charge carriers residing in traps. Silicon, for example, is passivated with a layer of silicon dioxide. For QDs, surface passivation has been achieved by overcoating the QD with a higher-bandgap shell<sup>19</sup>, such as a ZnS shell on the surface of a CdSe QD in Figure 1-3(b). The shell reduces the number of trap states, confines the electrons and holes away from the surface, suppresses broad deep trap emission<sup>17</sup>, and increases the band-edge emission. The quantum yield (QY) can increase from 15% for bare dots to 50% for core/shell dots.

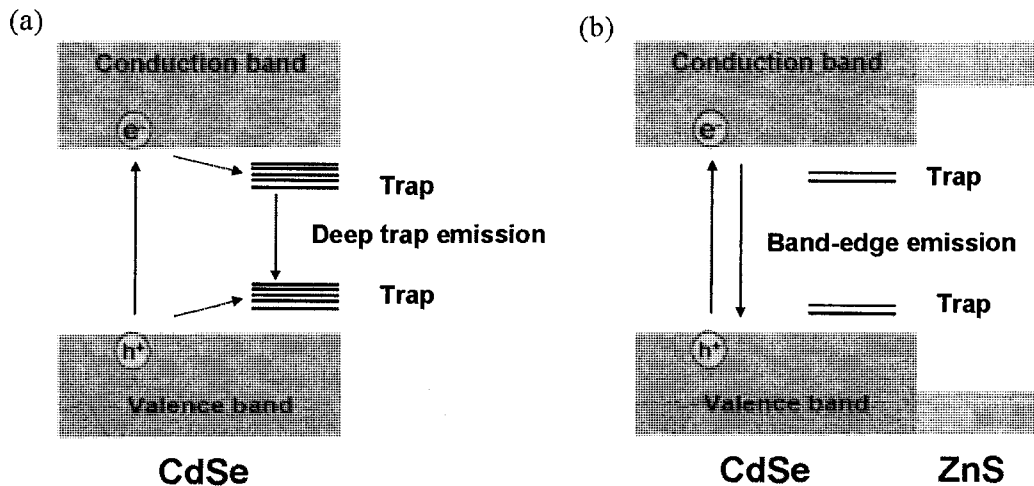


**Figure 1-3.** Energy-level diagram showing (a) deep trap emission of bare core QDs and (b) band-edge emission of core/shell QDs, following<sup>18</sup>.

At last, a layer of organic coating is put on the surface. The functions of this layer are preventing flocculation, further passivating the surface, and/or generating available chemical modification sites. Colloidal QDs attract strongly each other by van der Waals forces.<sup>20</sup> The larger the particles are, the greater the attractive forces are the particles experiencing. Flocculation or aggregation of QDs can be prevented by an existing sufficient repulsive force to counteract the van der Waals attraction. Chemisorption of amphiphilic species on the surface of the QDs brings amphiphilic steric barrier to the aggregation. For example, the dispersions of CdSe/ZnS core/shell QDs are often sterically stabilized by trioctylphosphine and trioctylphosphine oxide (TOP/TOPO) molecules.

## 1.4 General Synthesis Methods

The synthesis method of CdSe/ZnS nanocrystals is most widely adopted methods in the field and the produced QDs are among those of most high quality. Organometallic approaches in coordinating solvents were invented in the early 1990s by Steigerwald et al.<sup>21</sup> and developed to a practical level by Murray et al.<sup>20</sup>. The typical reaction conditions are organometallic precursors, such as Cd(CH<sub>3</sub>)<sub>2</sub>, Zn(CH<sub>3</sub>)<sub>2</sub>, S(TMS)<sub>2</sub>, P(TMS)<sub>3</sub>, etc, coordinating solvents, trioctylphosphine (TOP) and trioctylphosphine oxide (Tech TOPO), and high reaction temperatures, typically between 150 and 400 °C.<sup>22</sup> However because the organometallic precursors are extremely reactive and toxic, the non-aqueous and air-free environments or a glovebox is required for their handling. In fact, some groups have tried to carry out the entire chemical synthesis inside a large glove box.

Very recently, alternative approaches using air-stable precursors, such as inorganic salts, organic salts, oxides, and metals have been found to work<sup>23,24</sup>. Today, most high quality CdSe nanocrystals are produced by alternative approaches. The shape of the CdSe nanocrystals can also be more controllable.<sup>25</sup> The ligands used in the alternative routes are also very versatile. In addition to the traditional Tech TOPO used in the organometallic approaches, fatty acids, phosphonic acids, phosphine oxides, and amines are all possible choices<sup>24</sup>. The alternative approaches, also called “greener” approaches, are gradually becoming the most widely adopted methods in the field.<sup>22</sup>

Although alternative approaches in coordinating solvents have yielded CdSe nanocrystals of high quality, attempts to extend those approaches to other types of semiconductor nanocrystals proved difficult in most cases. Non-coordinating solvents were then introduced and the results have been very encouraging.<sup>26</sup> The key difference between coordinating solvents and non-coordinating solvents is that the reactivity of the monomers can be tuned by varying the ligand concentrations in the non-coordinating solvents.<sup>26</sup> This tunable reactivity of the monomers provides a key to balancing nucleation and growth, and thus makes it possible to controllably synthesize high quality nanocrystals.

The first system using non-coordinating solvents was CdS nanocrystals<sup>26</sup>. The non-coordinating solvent used most is 1-octadecene (ODE); Its relatively low melting point (below 20 °C), relatively high boiling point (about 320 °C), low cost, low toxicity, low

reactivity to precursors, and excellent solvation power for many compounds at elevated temperatures make ODE an ideal solvent for the growth of high-quality nanocrystals in general.<sup>27</sup> Oleic acid, a natural surfactant, or other fatty acids were chosen as the ligands for stabilizing the resulting nanocrystals and the cationic precursors.

## 1.5 QDs Blinking

Single QDs blinking was first described by Nirmal et al.<sup>13</sup>. Figure 1-4 shows a fluorescence trajectory of a single CdSe/ZnS QD. The first question is why does fluorescence of single QDs turn off under illumination? It has been suggested a neutral QD is in its bright state and a charged one in its dark state.<sup>4, 28</sup> The charged QD is created if one of the charge carriers (electrons or holes) is ejected into a trap state, leaving behind a charge in the QD states. The trap states could be from the vacancies, lattice mismatches, or dangling bonds of the QDs themselves, as mentioned before, and/or from the surrounding matrices or substrates, near but outside the QD. Subsequent photogenerated excitons recombine non-radiatively through Auger recombination. The excitons transfer their energy to the charge, which then loses its surplus energy as heat through phonon emission. This means that no light is produced and fluorescence shuts off. The fluorescence emission restores upon recovery of charge neutrality.

From the fluorescence trajectory of a single QD, Kuno et al. did the statistical analysis on “on” and “off” times and found an inverse power-law behavior in the probability density distributions<sup>12</sup>,  $P[t_{\text{on}}]$  and  $P[t_{\text{off}}]$ :

$$P(t) \propto t^{-m}$$

where  $m$  has a range of 1 to 2. The distributions and switching times spread a very broad range for both “off” and “on” times, up to several orders (See Figure 1-5). The inverse power law is common to all immobilized QD systems have been studied.<sup>29-31</sup> It is also reported that the power law behavior for the “off” time distribution is independent of temperature, excitation intensity, surface morphology or size.<sup>30,32,33</sup> However, “on” time probability distributions break down the power law behavior with a bending or truncated tail at elevated temperature or illumination intensity.<sup>33</sup> For uncapped QDs, the “on” times exhibit exponential distribution and “off” times have a power law distribution.<sup>34</sup>

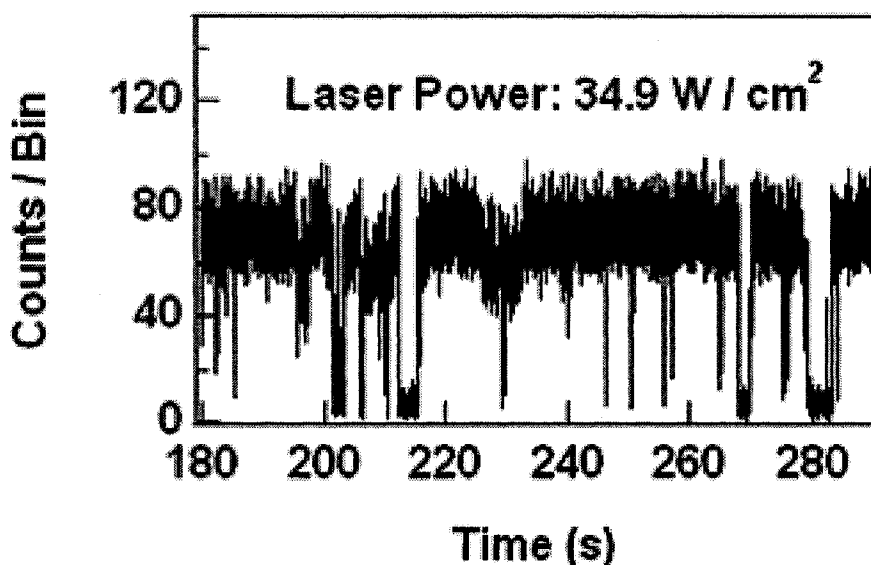


**Figure 1-4.** Fluorescence trajectory of a single CdSe/ZnS QD.

Strong evidence for the correlation between the blinking events with spectral diffusion has been obtained in several studies.<sup>35-37</sup> Spectral diffusion is the fact that the photoluminescence (PL) a single QD shifts randomly in its peak position and line width. Particularly, large spectral shifts usually follow after a return from an “off” event.<sup>36</sup>

Bawendi *et al.* proposed that the spectral diffusion might be caused by the quantum confined Stark effect (QCSE)<sup>35</sup>. The charge density around a QD is changing randomly with time, which produces a varying net electric field. This electric field modifies the emission wavelength of the single QDs through QCSE.

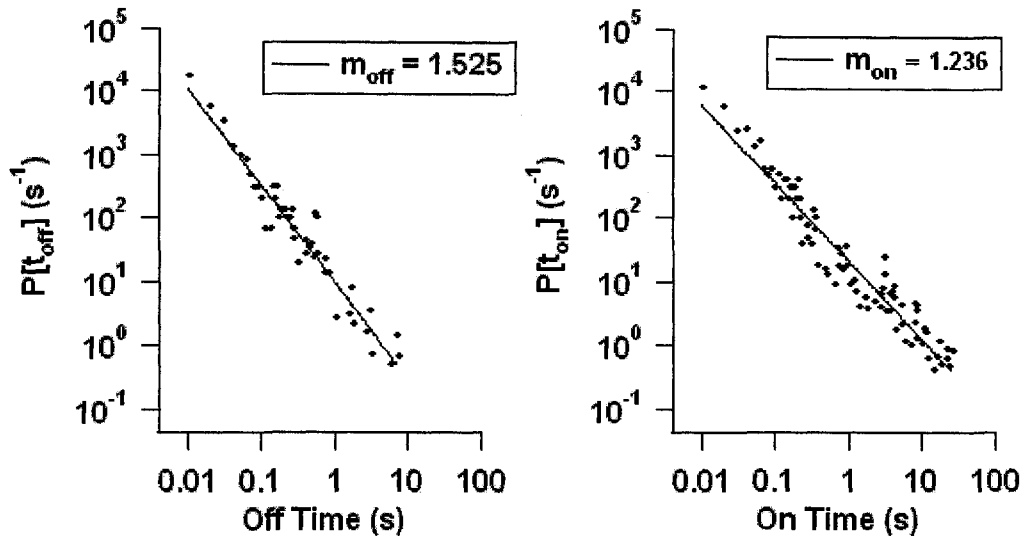


**Figure 1-5.** Probability density distributions of “off” times (left) and “on” times (right) from the fluorescence trajectory in **Figure 1-4**.

How is the QD blinking happening and how could the switching between bright and dark states give such broad distributions? To date, we still do not have clear answers for these questions yet. However, people are making attempts towards explaining this mystery. Several proposed physical models along the developing research path will be introduced briefly in the following section.

## 1.6 Physical Models of Single QDs Blinking

### 1.6.1 Quantum Jump and Auger Ionization

Figure 1-6 shows the schematic of two proposed models: quantum jump<sup>31, 38, 39</sup> and Auger ionization<sup>13, 28, 31</sup>. Quantum jump model is the simplest model for single molecule blinking. It is based on fast fluorescence cycling between ground state  $|1\rangle$  and excited state  $|2\rangle$ , followed by infrequent ‘jumps’ to a nonradiative triplet state  $|3\rangle$ , which subsequently recovers to the ground state. Because of constant on and off rate, such a model is described by a single exponential behavior which is inconsistent with the power-law dynamics.

Auger ionization model was proposed soon after the first reports of blinking. In the “on” times, single electron-hole pairs are photoexcited and subsequently recombine radiatively. However, there is a probability that a particle will absorb two photons, either in a single step or sequentially, generating two electron hole pairs. Recombination of a second electron-hole pair leads to ejection of one charge outside the dot. In such ionized QDs, the emission is quenched because of the excess charge. Bright state is not recovered until the QD is neutralized again. Since this model contains single rate processes for ionization and recombination, it naturally predicts single exponential probability densities in both  $P[t_{on}]$  and  $P[t_{off}]$ . This also is in conflict with the experimental results.

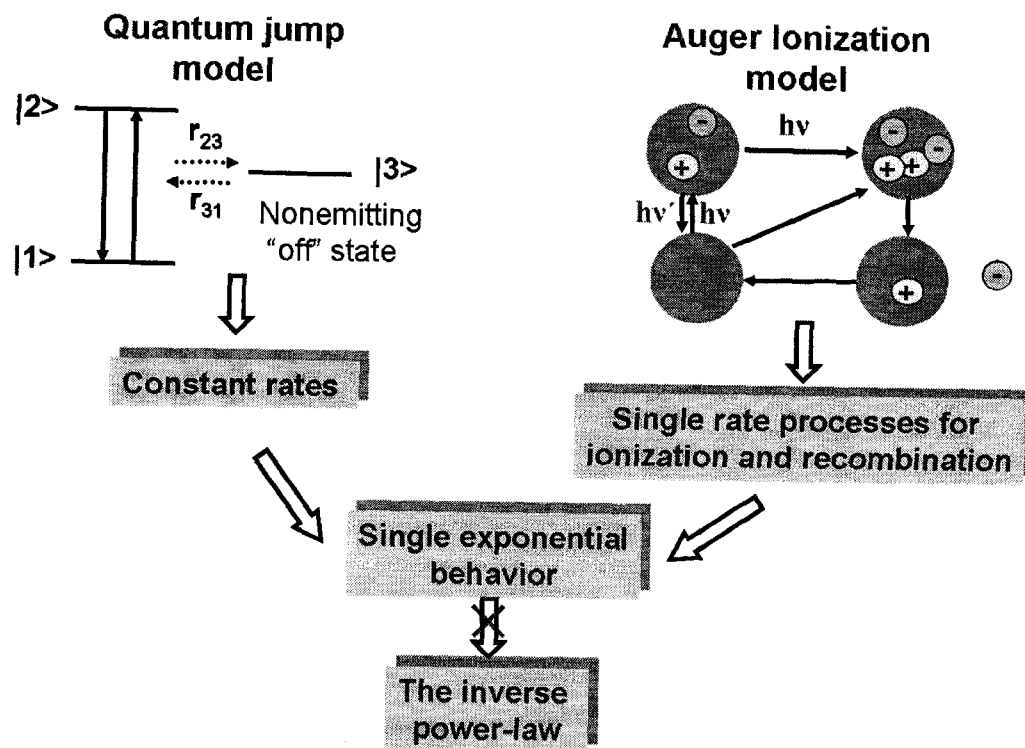
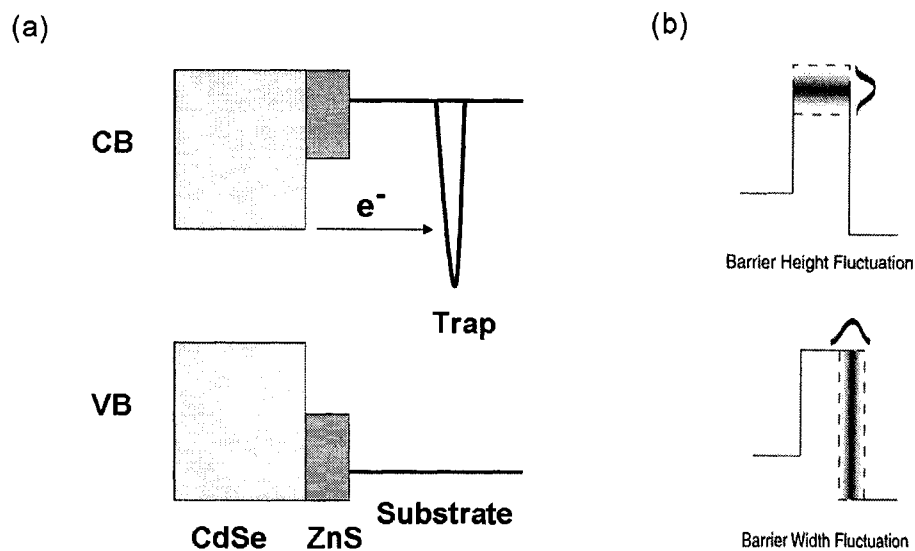


Figure 1-6. Schematic of quantum jump model and Auger ionization model.<sup>39</sup>

## 1.6.2 Fluctuated Tunneling and Charge Diffusion

Kuno *et al.* proposed the fluctuating tunneling model<sup>31, 39</sup> for the blinking in immobilized single QDs. In this model, a charge carrier, especially an electron, tunnels directly through the barrier to trap states external to the QD, essentially in or on the surface of the substrate (See Figure 1-7(a)). Instead of being static, tunneling barriers are assumed to change randomly in height and width after each on/off event, probably due to relatively slow conformational changes in the organic molecules on the QD surface or site-to-site movement of charges on the substrate (See Figure 1-7(b)). However, the absence of effects of shell thickness on the QD blinking statistics observed in a recent study<sup>40</sup> suggests the fluctuating tunneling model is unlikely the dominant mechanism for single QDs blinking, because an exponential decrease in the tunneling rate with shell thickness would be expected.

Charge diffusion model, proposed by Verberk *et al.*<sup>34</sup>, is schematically illustrated in Figure 1-8. It was assumed that neutral capped QDs corresponded to short “on” states; charged capped QDs had two opposite possible states. If the charge remained close to the center or in the core of the QD, the dot was dark. Alternatively, if the charge was trapped in vicinity of capping, bright states could be produced with longer durations compared to those of neutral QDs. The trapped charge did not quench fluorescence, but prevented further ionization of the QD by Coulomb blockade. However, the blinking statistics in the model would be dependent on the QD environment, which contradicts the experimental observations<sup>41</sup>.



**Figure 1-7.** (a) Band energy diagram of a positively charged CdSe/ZnS QD, following<sup>39</sup>. (b) Description of the tunneling barrier fluctuating in the height (top) or in the barrier width (bottom).<sup>31</sup>

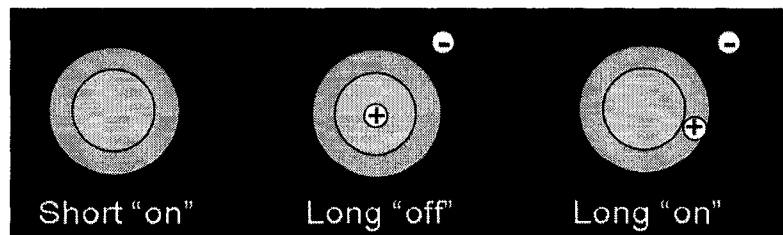


**Figure 1-8.** Schematic of the charge diffusion model, following<sup>34</sup>.

### 1.6.3 Diffusion Controlled Electron Transfer (DCET)

The idea of DCET, illustrated schematically in Figure 1-9, was developed into a detailed model by Tang and Marcus<sup>32</sup>, which is consistent with recent experimental observation<sup>42</sup>. The model consists of 4 states: ground state  $|G\rangle$  and excited state  $|L^*\rangle$  of a neutral bright QD; the ground state  $|D\rangle$  and excited state  $|D^*\rangle$  of the charged dark QD.  $|L^*\rangle$  is the band-edge excited state.  $|D\rangle$  is a charge-separated state of a dark QD with a charge in the core and a countercharge trapped in surface states, just below the edge of conduction band or just above the edge of valence band.  $|D^*\rangle$  is the excited charge-separated state of  $|D\rangle$  with an additional exciton. When a carrier switches from  $|L^*\rangle$  state to the  $|D\rangle$  state, the QD turns off; when the charge jumps back, the fluorescence turns on.

How could the charge jump between  $|L^*\rangle$  and  $|D\rangle$  states? In Figure 1-9(b) parabolic potentials with  $Q$  as the reaction coordinate are assumed. Slow diffusion of the system along a reaction coordinate,  $Q$ , controls the transitions between  $|D\rangle$  and  $|L^*\rangle$  and the time intervals between blinking events. The transitions are phonon assisted and occur at the crossing point  $Q^\ddagger$  of the two parabolic potential energy curves. It was claimed that in such a model one trap state was sufficient for the power law behavior.<sup>42</sup>

### 1.6.4 Fluctuating Electronic States Model

Another alternative physical model of single QD blinking, illustrated in Figure 1-10, was developed by Frantsuzov and Marcus<sup>43</sup> and has been discussed and supported in recent study<sup>40, 42</sup>. The existence of a band of hole trap states<sup>44</sup> of dangling bonds above the  $1S_{3/2}$  valence band level, deep in the band gap, is the basic of the model. The

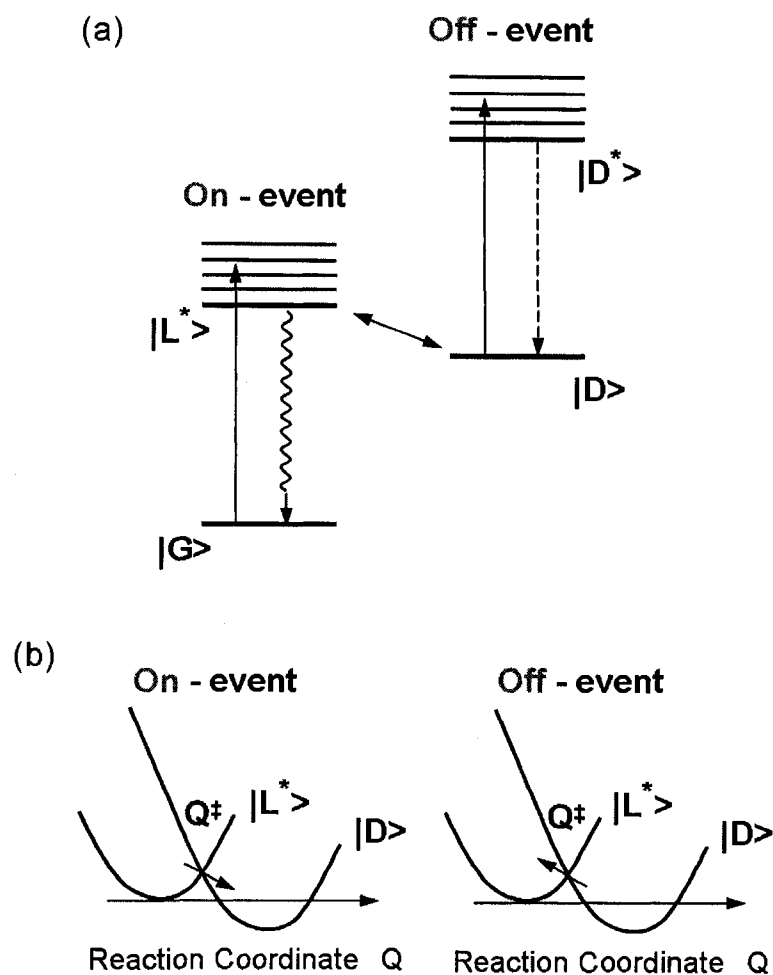


**Figure 1-9.** Schematic of the DCET model, following<sup>32</sup>. (a) Energy levels in the model. Transitions from  $|L^*\rangle$  to  $|G\rangle$  are primarily radiative, whereas transitions from  $|D^*\rangle$  to  $|D\rangle$  are primarily nonradiative. (b) Diffusion on the parabolic potential surfaces for  $|L^*\rangle$  and  $|D\rangle$  across a sink at the energy-level crossing,  $Q^\ddagger$ , governs the fluorescence blinking.

conduction band levels, such as  $1P_e$  and  $1S_e$  undergoes light induced fluctuations. The line in the middle is the average value of corresponding electronic state. The thin jagged line within the shaded band represents the state energy randomly fluctuating with time. The electronic transition in the conduction band (CB) from the lowest-lying state,  $1S_e$ , to a higher-lying state,  $1P_e$ , may be in or out of resonance with a transition of a hole from the valence band (VB) to the band of trap states. When the two transitions are not in resonance, the QD has photoluminescence emission upon radiation. When the two transitions are in resonance, there is a continuous cycling from  $1S_e$  to  $1P_e$  and from the VB to the trap, as shown in Figure 1-10(a), followed by a relaxation from  $1P_e$  to  $1S_e$  and an Auger-assisted transition from the trap to the VB, as in Figure 1-10(b). This process is assumed to be much faster than the radiative relaxation, so the QD is dark.

## 1.7 QD-QD Interactions

Since collective optical behavior of small QD clusters is going to be studied, it is necessary to go over the possible interactions between single QDs when multiple singles are adjacent to each other. Researchers have observed QD-QD energy transfer in films<sup>45-47</sup>, linear chains<sup>48,49</sup>, and between single QDs<sup>50,51</sup>. QDs are theorized to couple through several means, the strongest of which occurs through electronic excitations that cause excitons to tunnel through multiple dots, resulting in electron transfer (Dexter transfer). In weakly coupled QD assemblies or arrays, dipole-dipole interactions allow QDs to communicate via resonance energy transfer (RET), including Förster resonant energy transfer. The summary of inter-QD couplings observed from previous steady-state studies is shown in Table 1-2. The possible mechanisms considered included FRET

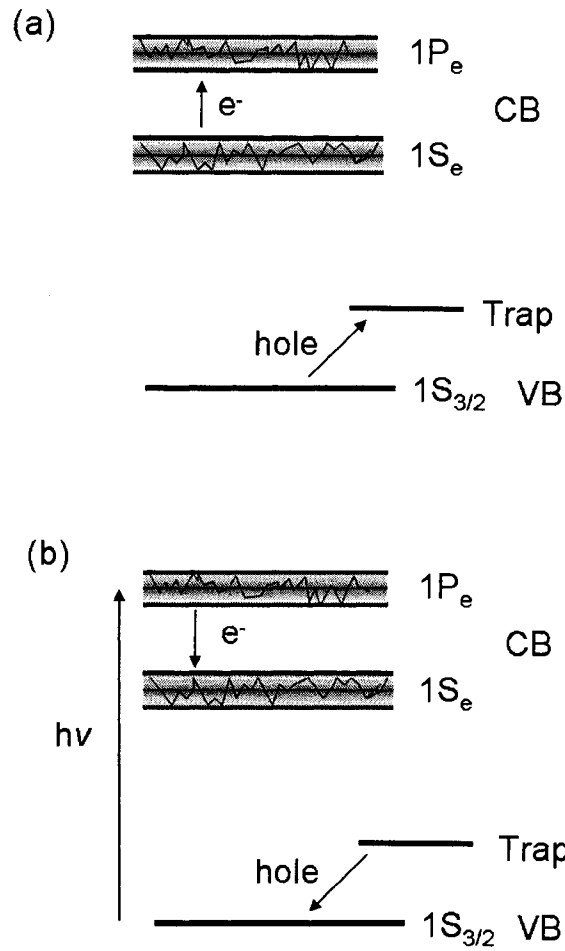


**Figure 1-10.** Schematic of the fluctuating electronic states model, following<sup>40, 42</sup> (a) Holes are trapped through the promotion of an electron in the conduction band (CB). (b) Auger-assisted detrapping mechanism.

exciton transfer, and the quantum confined Stark effect (QCSE) <sup>35</sup>. In the latter case, Stark shifts in absorption and emission spectra<sup>52-54</sup> are induced by built-in internal electric fields originating from surface charges<sup>54, 55</sup>. Each mechanism has its distinguishable characteristics

**Table 1-2.** Results comparing the situations of single QDs.  $\uparrow, \downarrow$  and  $\leftrightarrow$  mean increase, decrease, and no change, respectively. \*Valid for small QDs. \*\*No size limitation.

Parameter		UV-Visible Absorption		Fluorescence Emission			Fluorescence Lifetime
		$\lambda$	HMW	$\lambda$	HMW	Intensity	
Resonance	FRET <sup>48, 56</sup>	$\leftrightarrow$	$\leftrightarrow$	$\uparrow$	$\downarrow$	Band Edge $\downarrow$ Deep Trap $\uparrow$	$\downarrow$
Exchange	ED <sup>56</sup>	$\uparrow^*$	$\uparrow$	$\uparrow$	$\leftrightarrow$	Band Edge $\leftrightarrow$ Deep Trap $\leftrightarrow$	$\leftrightarrow$
	QCSE <sup>52, 53</sup>	$\uparrow^{**}$	$\uparrow$	$\uparrow$	$\uparrow$ <sup>54</sup>	-----	$\downarrow$ <sup>57</sup>

## 1.8 Fluorescence Blinking Data Analysis

### 1.8.1 Autocorrelation Analysis

Autocorrelation analysis is a technique of fluorescence correlation spectroscopy (FCS). Fluctuations in the fluorescence signal are quantified by temporal autocorrelation of the recorded intensity signal. In principle, this autocorrelation routine provides a measure for the self-similarity of a time signal and highlights characteristic time constants of underlying processes. In our experiments, the raw data measured will be arrival times of each photon. The arrival times can be represented as the number of counts recorded continuously during each consecutive time bin,  $\Delta t$ . This intensity

trajectory can be generated with any value of  $\Delta t$  not smaller than the time resolution. The autocorrelation function,  $g^{(2)}(\tau)$ , is given by the equation  $g^{(2)}(\tau) = \langle I(t)I(t+\tau) \rangle / \langle I(t) \rangle^2$ , where  $I(t)$  is the fluorescence intensity at time  $t$ , and  $\tau$  is the lagtime.  $g^{(2)}(\tau)$  decays with increasing  $\tau$  depending on the time scale at which the fluorescence signal fluctuates. The normalized experimental autocorrelation function,  $g^2(\tau)$ , is calculated from an intensity trajectory of  $N$  bins as:

$$g^2(\tau) = \frac{\left(\frac{1}{M-k}\right) \sum_{t=1}^{M-k} n(t)n(t+\tau)}{\left(\frac{1}{M-k}\right)^2 \sum_{t=1}^{M-k} n(t) \sum_{t=1}^{M-k} n(t+\tau)}$$

where  $M$  is the total number of sampling intervals per scan for each detector,  $k$  is the number of sampling intervals corresponding to lagtime  $\tau$ , and  $n(t)$  and  $n(t+\tau)$  are the number of photon counts accumulated at counting interval  $t$  and  $t+\tau$ .<sup>58</sup>

## 1.8.2 “On” / “Off” Time Density Distribution

The continuous probability densities,  $P[t_{\text{on}}]$  and  $P[t_{\text{off}}]$ , are generated by first setting an intensity threshold, typically 2 to  $3\sigma$  higher than the background noise level of a fluorescence trajectory. Photon counts above the threshold are treated as “on” states while those below the threshold are “off” states. Then the on/off histogram elements are weighted with nearest adjacent events.<sup>31</sup> The MatLab programs for calculating the threshold and probability densities are listed in Appendix A.

## 1.8.3 Photon Counting Histogram

Here, photon counting histogram is the analysis of intensity histogram of a fluorescence trajectory. The histogram may contain one or more peaks with varying widths, which reveals photophysical processes.<sup>59</sup> The MatLab program for calculating the photon counting histogram can be found in Appendix A.

#### **1.8.4 Atomic Force Microscope (AFM)**

The AFM is an exciting tool for the investigation of surfaces, which creates high-resolution images of a sample surface by scanning a sharp tip over the sample. The sharp tip is attached to a flexible spring lever, or cantilever, which bends in response to forces between the tip and sample. The AFM head provides optical correction of the laser beam path to track the movement of the probe while scanning under the fixed laser beam assembly. Images of the sample surface are created by raster-scanning the cantilever and tip across the surface while monitoring variations in the cantilever motion. The results of the cantilever measurement are recorded and can be displayed as false color images or as three-dimensional plots.

**Tapping Mode.** The tapping mode used in our experiments is probably the most useful imaging technique for a wide variety of samples. In this mode the cantilever is set into oscillation at the cantilever's resonant frequency. Then the cantilever is brought close to the sample until the tip briefly contacts ("taps") the sample surface at the bottom of each oscillation cycle. Because the cantilever only intermittently contacts the sample surface, frictional forces are virtually eliminated, dramatically reducing damage to the sample from imaging. The brief contact between the cantilever and sample reduces the

amplitude of the cantilever oscillation. During scanning, a feedback loop is used to adjust the position of the piezoelectric tube that moves the cantilever support to keep the cantilever amplitude constant. Again, a topographic map of the sample is created by recording the motion of the piezoelectric tube required to keep the amplitude constant.

**Phase Imaging.** As the probe lightly taps the surface, the amplitude of oscillation is reduced and the AFM uses this change in amplitude in order to track the surface topography. This is what we mean by in the tapping mode. In addition to its amplitude, the probe motion can be characterized by its phase relative to a driving oscillator. The phase signal changes when the probe encounters regions of different composition. Phase shifts are registered as bright and dark regions in phase images, comparable to the way height changes are indicated in height images. Phase images often show extraordinary contrast for many composite surfaces of technological and scientific interest.

## References:

1. Michalet X, Pinaud FF, Bentolila LA, Tsay JM, Doose S, Li JJ, Sundaresan G, Wu AM, Gambhir SS, Weiss S: Quantum dots for live cells, in vivo imaging, and diagnostics. *Science* **2005**, 307:538.
2. Alivisatos AP, Gu WW, Larabell C: Quantum dots as cellular probes. *Annual Review of Biomedical Engineering* **2005**, 7:55.
3. Medintz IL, Uyeda HT, Goldman ER, Mattoussi H: Quantum dot bioconjugates for imaging, labelling and sensing. *Nature Materials* **2005**, 4:435.
4. Nozik AJ: Quantum dot solar cells. *Physica E-Low-Dimensional Systems & Nanostructures* **2002**, 14:115.
5. Franceschetti A, An JM, Zunger A: Impact ionization can explain carrier multiplication in PbSe quantum dots. *Nano Letters* **2006**, 6:2191.
6. Schaller RD, Agranovich VM, Klimov VI: High-efficiency carrier multiplication through direct photogeneration of multi-excitons via virtual single-exciton states. *Nature Physics* **2005**, 1:189.
7. Vanmaekelbergh D, Liljeroth P: Electron-conducting quantum dot solids: novel materials based on colloidal semiconductor nanocrystals. *Chemical Society Reviews* **2005**, 34:299.
8. Bailey RE, Smith AM, Nie SM: Quantum dots in biology and medicine. *Physica E-Low-Dimensional Systems & Nanostructures* **2004**, 25:1.
9. Schaller RD, Petruska MA, Klimov VI: Effect of electronic structure on carrier multiplication efficiency: Comparative study of PbSe and CdSe nanocrystals. *Applied Physics Letters* **2005**, 87:253102.
10. Schaller RD, Sykora M, Pietryga JM, Klimov VI: Seven excitons at a cost of one: Redefining the limits for conversion efficiency of photons into charge carriers. *Nano Letters* **2006**, 6:424.
11. Kuno M, Fromm DP, Gallagher A, Nesbitt DJ, Micic OI, Nozik AJ: Fluorescence intermittency in single InP quantum dots. *Nano Letters* **2001**, 1:557.
12. Kuno M, Fromm DP, Hamann HF, Gallagher A, Nesbitt DJ: Nonexponential "blinking" kinetics of single CdSe quantum dots: A universal power law behavior. *Journal of Chemical Physics* **2000**, 112:3117.
13. Nirmal M, Dabbousi BO, Bawendi MG, Macklin JJ, Trautman JK, Harris TD, Brus LE: Fluorescence intermittency in single cadmium selenide nanocrystals. *Nature* **1996**, 383:802.
14. Zhang K, Chang HY, Fu AH, Alivisatos AP, Yang H: Continuous distribution of emission states from single CdSe/ZnS quantum dots. *Nano Letters* **2006**, 6:843.
15. Bukowski TJ, Simmons JH: *Critical reviews in Solid State and Materials Sciences* **2002**, 27:119.
16. Michalet XP, F.; Lacoste, T. D.; Dahan, M.; Bruchez, M. P.; Alivisatos, P.; Weiss, S: *Single Mol* **2001**, 2:261.
17. Dabbousi BO, RodriguezViejo J, Mikulec FV, Heine JR, Mattoussi H, Ober R, Jensen KF, Bawendi MG: (CdSe)ZnS core-shell quantum dots: Synthesis and characterization of a size series of highly luminescent nanocrystallites. *Journal of Physical Chemistry B* **1997**, 101:9463.

18. Murphy CJ: Optical sensing with quantum dots. *Analytical Chemistry* **2002**, 74:520A.
19. Nirmal M, Brus L: Luminescence photophysics in semiconductor nanocrystals. *Accounts of Chemical Research* **1999**, 32:407.
20. Murray CB, Norris DJ, Bawendi MG: Synthesis and Characterization of Nearly Monodisperse Cde (E = S, Se, Te) Semiconductor Nanocrystallites. *Journal of the American Chemical Society* **1993**, 115:8706.
21. Steigerwald ML, Brus LE: Semiconductor Crystallites - a Class of Large Molecules. *Accounts of Chemical Research* **1990**, 23:183.
22. Peng XG, Thessing J: In *Semiconductor Nanocrystals and Silicate Nanoparticles*. Volume 118; 2005: pp79-119.
23. Peng ZA, Peng XG: Formation of high-quality CdTe, CdSe, and CdS nanocrystals using CdO as precursor. *Journal of the American Chemical Society* **2001**, 123:183.
24. Qu LH, Peng ZA, Peng XG: Alternative routes toward high quality CdSe nanocrystals. *Nano Letters* **2001**, 1:333.
25. Peng ZA, Peng XG: Nearly monodisperse and shape-controlled CdSe nanocrystals via alternative routes: Nucleation and growth. *Journal of the American Chemical Society* **2002**, 124:3343.
26. Yu WW, Peng XG: Formation of high-quality CdS and other II-VI semiconductor nanocrystals in noncoordinating solvents: Tunable reactivity of monomers. *Angewandte Chemie-International Edition* **2002**, 41:2368.
27. Li JJ, Wang YA, Guo WZ, Keay JC, Mishima TD, Johnson MB, Peng XG: Large-scale synthesis of nearly monodisperse CdSe/CdS core/shell nanocrystals using air-stable reagents via successive ion layer adsorption and reaction. *Journal of the American Chemical Society* **2003**, 125:12567.
28. Efros AL, Rosen M: Random telegraph signal in the photoluminescence intensity of a single quantum dot. *Physical Review Letters* **1997**, 78:1110.
29. Koberling F, Mews A, Basche T: Oxygen-induced blinking of single CdSe nanocrystals. *Advanced Materials* **2001**, 13:672.
30. Shimizu KT, Neuhauser RG, Leatherdale CA, Empedocles SA, Woo WK, Bawendi MG: Blinking statistics in single semiconductor nanocrystal quantum dots. *Physical Review B* **2001**, 63:205316.
31. Kuno M, Fromm DP, Hamann HF, Gallagher A, Nesbitt DJ: "On"/"off" fluorescence intermittency of single semiconductor quantum dots. *Journal of Chemical Physics* **2001**, 115:1028.
32. Tang J, Marcus RA: Mechanisms of fluorescence blinking in semiconductor nanocrystal quantum dots. *Journal of Chemical Physics* **2005**, 123:054704.
33. Tang J, Marcus RA: Diffusion-controlled electron transfer processes and power-law statistics of fluorescence intermittency of nanoparticles. *Physical Review Letters* **2005**, 95:107401.
34. Verberk R, van Oijen AM, Orrit M: Simple model for the power-law blinking of single semiconductor nanocrystals. *Physical Review B* **2002**, 66:233202.
35. Empedocles SA, Bawendi MG: Quantum-confined stark effect in single CdSe nanocrystallite quantum dots. *Science* **1997**, 278:2114.

36. Neuhauser RG, Shimizu KT, Woo WK, Empedocles SA, Bawendi MG: Correlation between fluorescence intermittency and spectral diffusion in single semiconductor quantum dots. *Physical Review Letters* **2000**, 85:3301.
37. Turck V, Rodt S, Stier O, Heitz R, Engelhardt R, Pohl UW, Bimberg D, Steingruber R: Effect of random field fluctuations on excitonic transitions of individual CdSe quantum dots. *Physical Review B* **2000**, 61:9944.
38. Basche TK, S.; Brauchle, C.: *Nature (London)* **1995**, 373:132.
39. Kuno M, Fromm DP, Johnson ST, Gallagher A, Nesbitt DJ: Modeling distributed kinetics in isolated semiconductor quantum dots. *Physical Review B* **2003**, 67:125304.
40. Heyes CD, Kobitski AY, Breus VV, Nienhaus GU: Effect of the shell on the blinking statistics of core-shell quantum dots: A single-particle fluorescence study. *Physical Review B* **2007**, 75:125431.
41. Pelton M, Grier DG, Guyot-Sionnest P: Characterizing quantum-dot blinking using noise power spectra. *Applied Physics Letters* **2004**, 85:819.
42. Pelton M, Smith G, Scherer NF, Marcus RA: Evidence for a diffusion-controlled mechanism for fluorescence blinking of colloidal quantum dots. *Proceedings Of The National Academy Of Sciences Of The United States Of America* **2007**, 104:14249.
43. Frantsuzov PA, Marcus RA: Explanation of quantum dot blinking without long-lived trap hypothesis. **2005**, 72:155321.
44. Shim M, Shilov SV, Braiman MS, Guyot-Sionnest P: Long-lived delocalized electron states in quantum dots: A step-scan Fourier transform infrared study. *Journal Of Physical Chemistry B* **2000**, 104:1494.
45. Crooker SA, Hollingsworth JA, Tretiak S, Klimov VI: Spectrally resolved dynamics of energy transfer in quantum-dot assemblies: Towards engineered energy flows in artificial materials. *Physical Review Letters* **2002**, 89:186802.
46. Franzl T, Shavel A, Rogach AL, Gaponik N, Klar TA, Eychmuller A, Feldmann J: High-rate unidirectional energy transfer in directly assembled CdTe nanocrystal bilayers. *Small* **2005**, 1:392.
47. Kagan CR, Murray CB, Nirmal M, Bawendi MG: Electronic energy transfer in CdSe quantum dot solids. *Physical Review Letters* **1996**, 76:1517.
48. Tang ZY, Ozturk B, Wang Y, Kotov NA: Simple preparation strategy and one-dimensional energy transfer in CdTe nanoparticle chains. *Journal of Physical Chemistry B* **2004**, 108:6927.
49. Westenhoff S, Kotov NA: Quantum dot on a rope. *Journal Of The American Chemical Society* **2002**, 124:2448.
50. Biju V, Makita Y, Sonoda A, Yokoyama H, Baba Y, Ishikawa M: Temperature-sensitive photoluminescence of CdSe quantum dot clusters. *Journal of Physical Chemistry B* **2005**, 109:13899.
51. Unold T, Mueller K, Lienau C, Elsaesser T, Wieck AD: Optical control of excitons in a pair of quantum dots coupled by the dipole-dipole interaction. *Physical Review Letters* **2005**, 94:137404.
52. Je KC, Ju H, Treguer M, Cardinal T, Park SH: Local field-induced optical properties of Ag-coated CdS quantum dots. *Optics Express* **2006**, 14:7994.

53. Muller J, Lupton JM, Rogach AL, Feldmann J, Talapin DV, Weller H: Monitoring surface charge migration in the spectral dynamics of single CdSe/CdS nanodot/nanorod heterostructures. *Physical Review B* **2005**, 72:205339.
54. Turck V, Rodt S, Heitz R, Stier O, Strassburg M, Pohl UW, Bimberg D: Interplay of surface charges and excitons localized in CdSe/ZnSe quantum dots. *Physica E-Low-Dimensional Systems & Nanostructures* **2002**, 13:269.
55. Bogaart EW, van Lippen T, Haverkort JEM, Notzel R, Wolter JH: Coherent acoustic phonons in strain engineered InAs/GaAs quantum dot clusters. *Applied Physics Letters* **2006**, 88:143120.
56. Koole R, Liljeroth P, Donega CD, Vanmaekelbergh D, Meijerink A: Electronic coupling and exciton energy transfer in CdTe quantum-dot molecules. *Journal of the American Chemical Society* **2006**, 128:10436.
57. Bacher G, Weigand R, Seufert J, Kulakovskii VD, Gippius NA, Forchel A, Leonardi K, Hommel D: Biexciton versus exciton lifetime in a single semiconductor quantum dot. *Physical Review Letters* **1999**, 83:4417.
58. Jung JM, Van Orden A: Folding and unfolding kinetics of DNA hairpins in flowing solution by multiparameter fluorescence correlation spectroscopy. *Journal of Physical Chemistry B* **2005**, 109:3648.
59. Yip WTH, D. H.; Yu, J.; Vanden Bout, D. A.; Barbara, P. F.: *J Phys Chem A* **1998**, 102:7564.

## **Chapter 2**

# **Spatially Correlated Single Molecule Fluorescence Spectroscopy and Atomic Force Microscopy**

This chapter presents a direct method of correlating spectroscopic and topographical properties of individual nanoparticles in a fluorescence blinking study. Single molecule fluorescence spectroscopy is spatially correlated with atomic force microscopy (AFM). AFM tells the size and conformation difference between single QDs and QD clusters. Fluorescence spectroscopy collects and analyzes fluorescence blinking data from QDs. It has an extremely small probe region, making it possible to observe intensity fluctuation from single particles. The laser beam of the confocal microscope locally scattered from

the apex of the AFM tip is recorded as an image along with the topographical image. This image presents the position of the laser probe region. QDs occupying the probe region contribute most of the fluorescence. Polystyrene nanobeads are used as studying samples.

## 2.1 Introduction

In our study of fluorescence blinking of individual isolated nanometer-sized particles, it is of great importance to have an experimental technique that is able to characterize the relationship between the spectroscopic and topographical properties of the nanostructured materials. Near-field scanning optical microscopy (NSOM)<sup>1, 2</sup> and apertureless NSOM (ANSOM)<sup>3, 4</sup> are the techniques often used to obtain such information. However, both techniques have their fundamental limitations. For NSOM, it is difficult to fabricate aperture probes capable of characterizing accurately both optical and topographical properties. Besides that, both methods have the limitation that the probe might alter the spectroscopic properties of the sample<sup>5</sup>. Moreover, topographical artifacts are likely present in the optical images. An alternative method is to perform two separate measurements on the same area of the sample. Then the pattern of bright spots in the fluorescence image can be matched with the corresponding pattern in the topographical image. However, as the fluorescent features are getting smaller and smaller, or when nonfluorescent or fluorescence blinking species exist, it is difficult to identify the topographical image in the fluorescence image.

In this chapter, we introduce a direct and effective way to correlate the optical and topographical information. This method is used through the entire project. It is the spatially correlated single molecule fluorescence spectroscopy/atomic force microscopy (AFM) method, upgraded from previous study<sup>5</sup>. This technique is needed because of the large differences in spatial resolution of the optical and topographical imaging. AFM is used to tell the topographical difference, such as between single QDs and QD clusters, while the fluorescence spectroscopy is used to collect fluorescence blinking data. The laser probe region has an extremely small probe volume, in  $\mu\text{m}^3$  scale, making it possible to observe intensity fluctuations from single particles. AFM creates high-resolution images of a surface by scanning a sharp tip over the sample. When the AFM tip is scanning a sample area containing the focused laser spot, the locally scattered light from the apex of the tip is recorded as an image along with the topography, which shows the position of the laser probe region on the sample surface. This allows the AFM to quickly zoom in on the particles of interest. QDs occupying the probe region contribute most fluorescence signals collected. In this way AFM and fluorescence spectroscopy are spatially correlated.

## **2.2 Experimental Section**

### **2.2.1 Instrumentation**

Figure 2-1(a) displays a schematic diagram of the setup, which contains an AFM scanning head, a piezo driven *x-y*- scanning stage (Nanonics, Model NIS-30 SC-100/208, Isreal), and an inversed confocal optical microscope, partially enlarged in Figure 2-1(b). The AFM is a Digital Instruments Bioscope equipped with Nanoscope IIIa software and

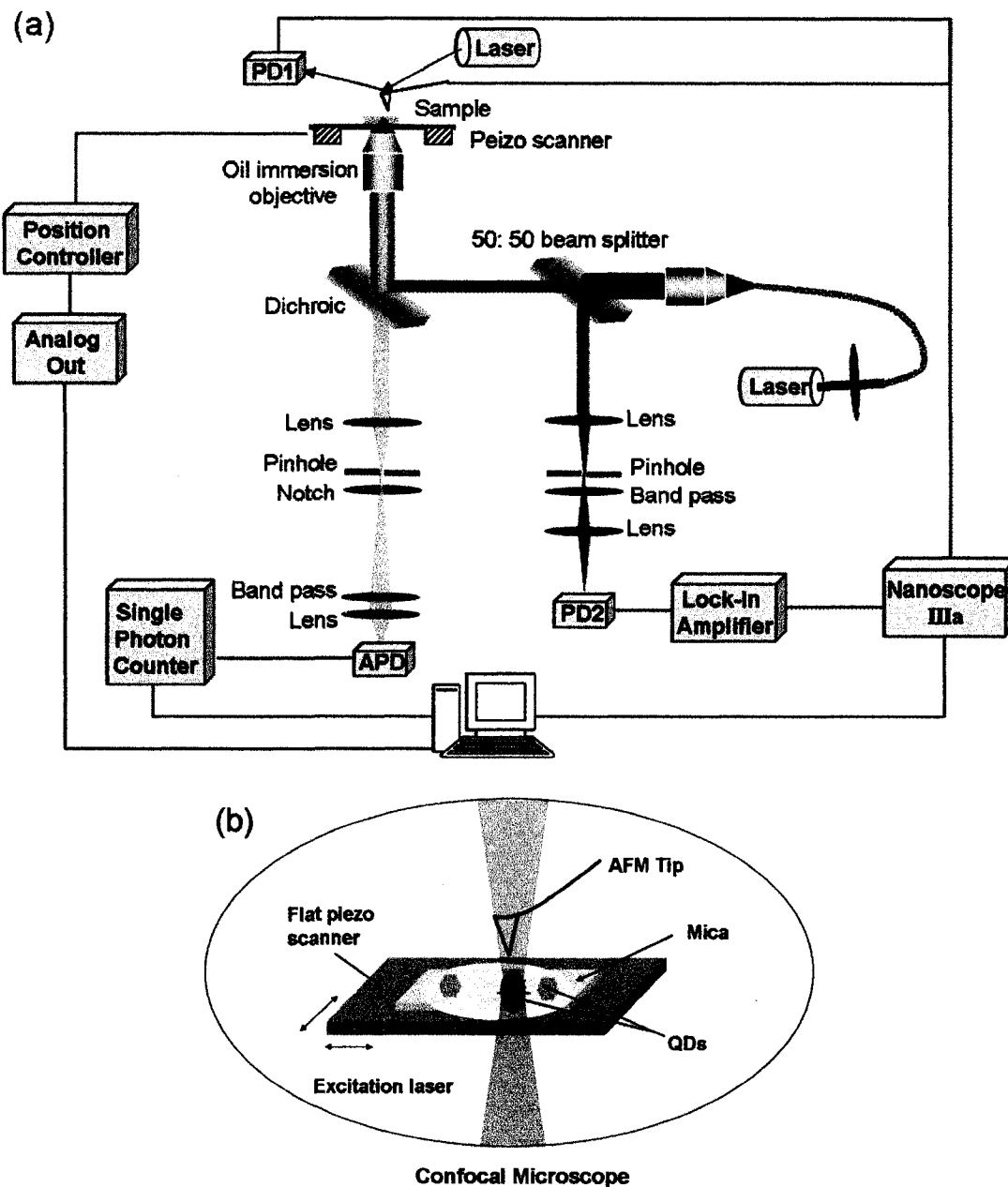


**Figure 2-1.** (a) Schematic diagram of the spatially correlated single molecule fluorescence spectroscopy and AFM. PD1, AFM feedback detector; PD2, Si photodiode detector; APD, avalanche photodiode detector. (b) Partially enlarged section of the AFM tip, the flat piezo scanning stage, and a sample substrate.

control electronics. It is operated in tapping mode using Olympus etched Si probes (Digital Instruments model OTESPA) with force constants of  $\sim 42$  N/m and resonance frequencies between 250 and 300 kHz. The scan rate is typically 1 Hz. A 488-nm CW air-cooled semiconductor laser (Novalux, INC, Protera laser) is used as the excitation source. The laser light passes a 488nm clean-up filter and is coupled into a single-mode optical fiber. The output of the fiber is then collimated by a 20 $\times$  microscope objective, directed through the rear port of the optical microscope, and reflected by a 50% reflective, 50% transmissive beam splitter into a 40 $\times$ , 1.3 NA oil immersion objective (Zeiss, Plan-Fluar). The microscope objective focuses the laser beam to a  $<1$ - $\mu$ m-diameter beam waist positioned at the top surface of the substrate mounted on the computer-controlled x, y, z piezo stage, which scans the substrate under the diffraction limited laser excitation spot.

Fluorescence from QDs is collected by the same objective. The fluorescence is transmitted through the long pass dichroic beam splitter, focused through a 50- $\mu$ m-diameter pinhole and a 488-nm holographic notch filter, and directed to another long pass dichroic beam splitter. The fluorescent light travels through an 11-mm-focal length aspheric lens, which focused the fluorescence onto a single photon counting avalanche photodiode detector (APD, EG&G Optoelectronics model SPCM-AQR-14, dark count rate  $\sim 50$  Hz). Signals from the APD are converted into TTL pulses and fed into a single photon counter mounted in a computer. A computer program monitors the fluorescence intensity vs. time.

Meanwhile, when the tip is scanning the focused laser beam, the laser light locally scattered from the apex of the tip is collected by the same objective. The backscattered laser light is reflected by the first dichroic beam splitter and the 50:50 beam splitter. With two 50-mm focal length lens, the reflected light is focused through a 100- $\mu\text{m}$ -diameter pinhole, a  $500 \pm 30$  nm band-pass filter (Omega), and onto an amplified Si photodiode detector (PD, ThorLabs model PDA55). The output of the Si photodiode detector is directed into a lock-in amplifier (Stanford Research Systems model SR844) referenced to the drive frequency of the AFM probe. The backscattered laser light possesses a frequency component identical to the drive frequency of the vibrating tip. By means of lock-in amplification, this locally scattered light can be distinguished from other backscattered light coming from far-field region. An analog-to-digital converter on board in the Nanoscope controller is used to record the output of the lock-in amplifier as a function of the AFM tip position. Then the AFM head will zoom to that part to find out the relative position of the tip and the focus laser beam. Two channels of the Nanoscope are employed. One channel is for recording the output of the lock-in amplifier as a function of the AFM tip position. This gives images of the laser excitation region. Another channel is used to record images of the sample topography by recording the output from the detector of AFM head.

### **2.2.2 Operation Methods**

Two experimental operation methods were used, schematically illustrated in Figure 2-2 and Figure 2-3, respectively. The one in Figure 2-2 is often performed for smaller fluorescent particles, such as small QD nanocrystals with a diameter no larger than 5 nm,

which are difficult to be visualized in AFM images of a bigger scanning area. Therefore, spatially correlated fluorescence microscopy helped to locate the positions of bright fluorescent features in the bigger area. The other method shown in Figure 2-3 is often used for bigger fluorescent particles, such as 40 nm diameter polystyrene nanobeads and bulky QD bioconjugates of 15-25 nm in diameter, which can be seen relative easily in AFM images of a bigger scanning area.

The method shown in Figure 2-2 has several steps as following. Step (a): The AFM tip is roughly aligned with the laser beam. This is done by scanning the AFM tip relative to a clear substrate over a surface area that includes the probe region. The point spread function of scattered light from the AFM tip is recorded, as shown in the lower part of Figure 2-2(a). The bright area in the image represents the position of the laser probe region on the substrate. Step (b): The AFM head is raised up, laser beam is blocked, and a mica substrate containing fluorescent features is placed onto the flat piezo scanner. The laser beam is focused onto the top surface of the sample and attenuated with neutral density filters. As the raster scanning the sample surface with the piezo stage relative to the microscope objective, a two-dimensional (2D) confocal image of the substrate is generated. Fluorescent features appear as bright diffraction limited spots. Step (c): To characterize the optical properties of a specific bright particle, such as the one in the white circle in Figure 2-2(b), the particle is first positioned right above the objective by adjusting the stage x and y positions, controlled by an analog output PC-plug-in board. Then, the PC plug-in photon counters are used to record the pulses from the APD. Step (d): The laser power is restored; AFM head is brought back and scans the sample. This

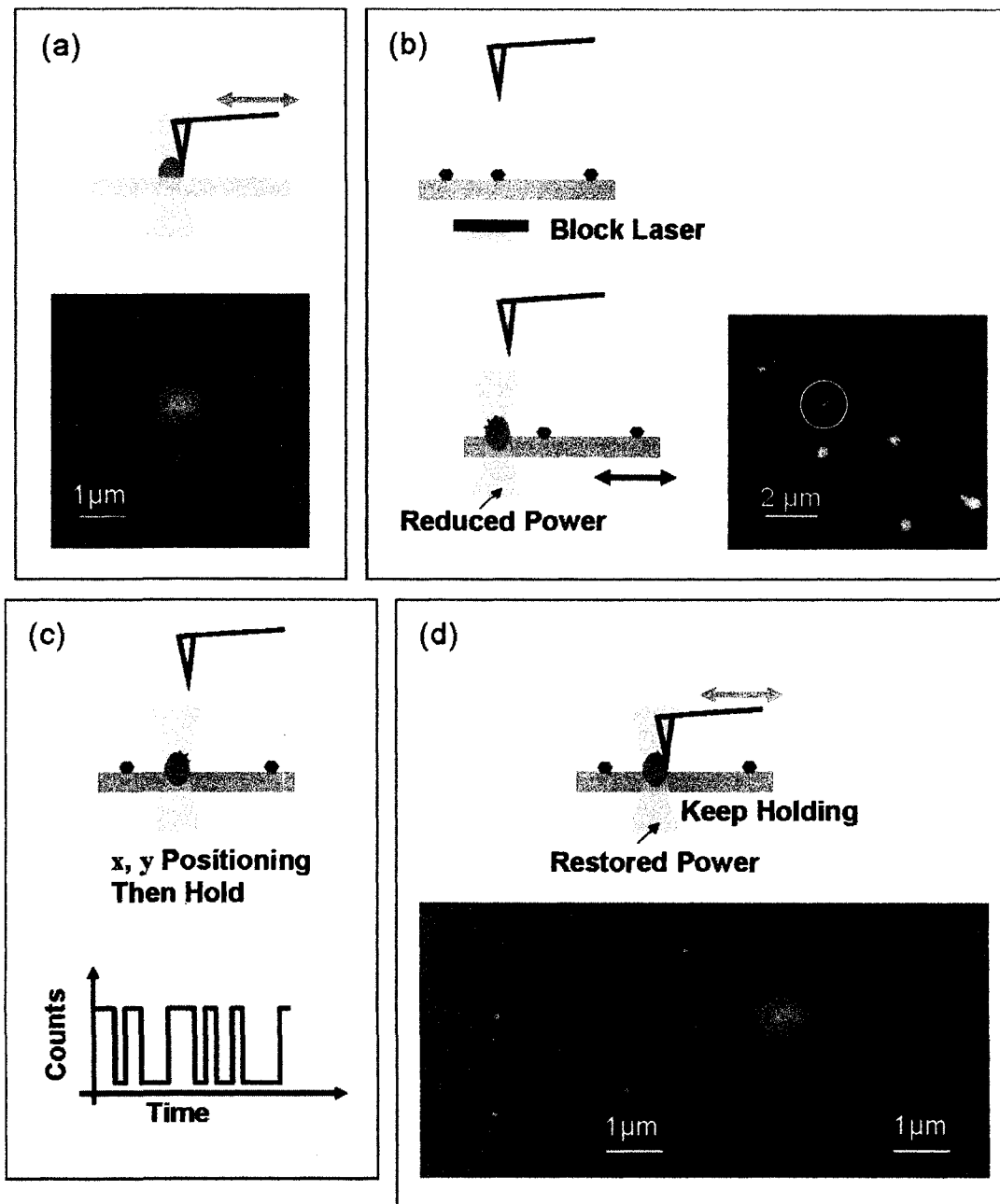


**Figure 2-2.** Schematic diagram of one experimental operation method for smaller fluorescent particles on substrates with (a), (b), (c) and (d) performing steps, in which the fluorescence microscopy in (b) helps to locate the particle positions.

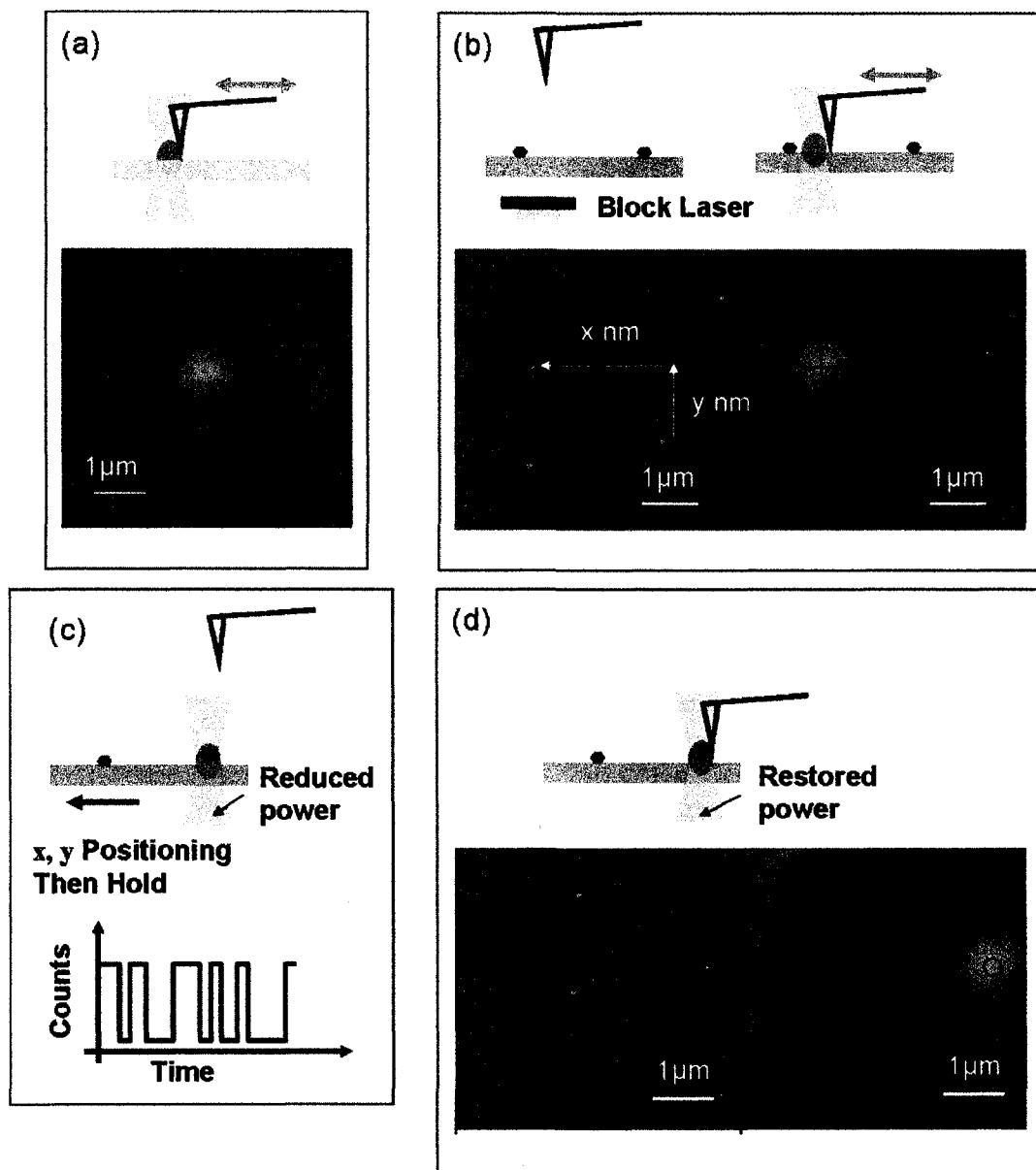


**Figure 2-3.** The other experimental operation method for bigger fluorescent particles on substrates, which can be seen in AFM images of bigger scanning area.

results in concurrent images of the laser illumination profile and the topography of the sample surface, which verifies the particle position relative to the probe region and visualizes the construction and size of the particle.

Figure 2-3 exhibits the other experimental operation method, which also has four steps, (a), (b), (c) and (d). Step (a) is exactly the same as that in Figure 2-2(a). The difference starts from step (b). Instead of scanning the flat piezo scanner, the AFM tip is brought back and scans the sample. As the AFM tip scanning the surface, images of the topography and the laser probe region are generated simultaneously. With the Nanoscope software, the position of the probe region can be marked in topographical image. The position of a desired spot relative to the mark can be measured and represented as x and y, such as the one in the black circle of Figure 2-3(b). Step (c): The particle is then moved into the probe volume by adjusting the scanning stage x and y positions. From experience, up (down) arrow is for positive (negative) y movement of the flat piezo scanner; left (right) arrow is for positive (negative) x movement of the scanner. Once the fluorescent feature is in the probe region, fluorescence trajectories are collected. Step (d): for the same purpose of Figure 2-2 (d), the AFM head is lower down and scans the substrate with the static scanning stage.

### **2.2.3 Sample Preparation**

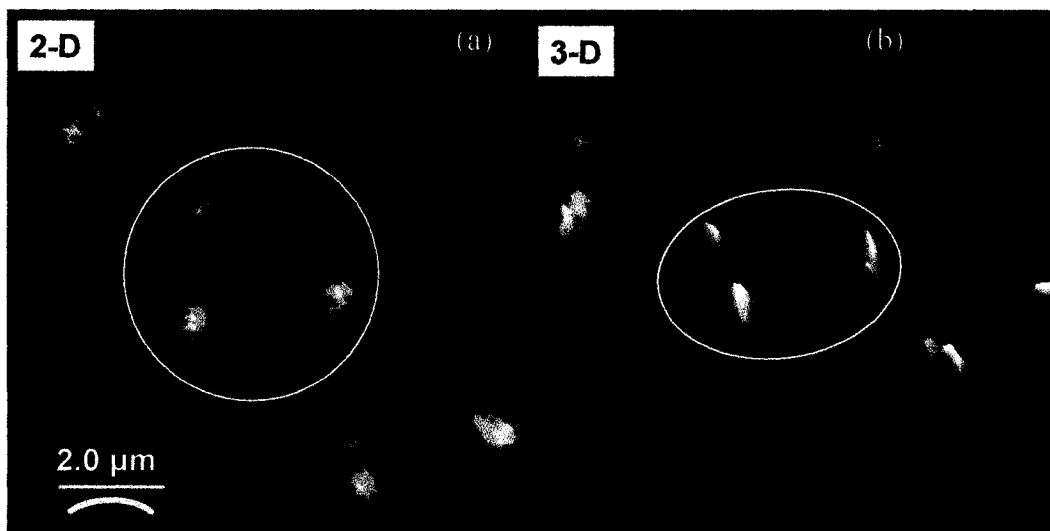
We have verified these experimental capabilities by analyzing individual fluorescent polymeric nanobeads. Samples of fluorescent nanobeads are prepared on 9.9-mm-diameter mica disks (SPI Supplies), freshly cleaved on one side, and mounted on 25 mm

× 25 mm glass cover slips (Fisher Scientific) with ultraviolet curing optical adhesive (Norland Products). A solution of 40-nm-diameter fluorescent polystyrene nanospheres (Orange FluoSpheres, 540- and 560-nm fluorescence excitation and emission maximums, Molecular Probes) at a concentration of 5% is sonicated for ~30 min prior to use. The nanospheres are then diluted to  $\sim 10^9$  particles/mL in ultrapure water. 20  $\mu\text{L}$  of 10 mM  $\text{MgCl}_2$  is deposited onto newly cleaved mica disks and allowed to incubate for 5min, which neutralizes the negative charges on mica surface and promotes the nanobeads distributing evenly since the beads also have negative charges. Then it is rinsed with deionized  $\text{H}_2\text{O}$  (electric resistivity  $>18\text{M}\Omega\cdot\text{cm}$ ) and dried with  $\text{N}_2$ . 10  $\mu\text{L}$  of the nanobeads solution is deposited onto the mica substrate and allowed to dry.

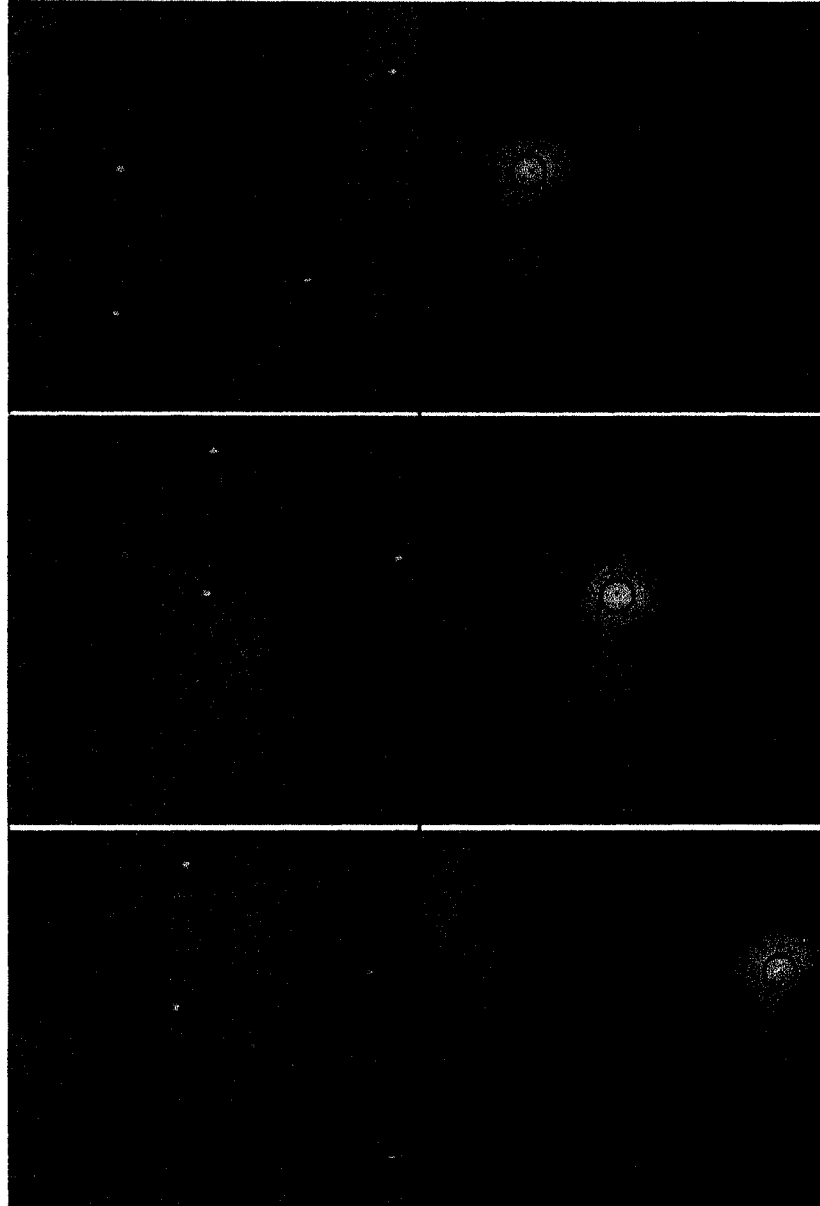
## 2.3 Results

Figure 2-4 shows a typical confocal image ( $9.8 \times 9.4 \mu\text{m}$ ) of the nanobeads on a mica plate, which are excited with the attenuated laser power ( $\sim 1 \mu\text{W}$ ). Each bright spot corresponds to the luminescence from either a single bead or a cluster of several beads. However, it is important to note that the smallest spot size ( $\sim 250\text{nm}$ ) is defined by the resolution of the confocal scanning optical microscope. The spots in the circle need to be characterized.

Figure 2-5 shows the concurrent  $5 \times 5 \mu\text{m}^2$  topographical (left) and probe region (right) images of the particles in the white circle of Figure 2-4. Only one of the nanospheres marked by the black circle occupies the laser probe region. If we collected the fluorescence photon counts at those three specific positions, respectively, the nanospheres



**Figure 2-4.** (a) 2-D confocal image of the  $3 \times 10^9$  Particles/mL, 40-nm diameter nanobeads on a mica plate. Each bright spot corresponds to the luminescence from beads on the substrate. (b) The 3-D image of the same area as (a), whose Z direction is fluorescence intensity or counts. The three bright spots in the white circle are particles to be characterized.



**Figure 2-5.** (a) are concurrent  $5 \times 5 \mu\text{m}^2$  topography (right) and scattered light (left) images from individual 40-nm diameter polystyrene beads dispersed on mica. Bead 1 is positioned near the central peak of the optical probe region. (b) and (c) were obtained from the same sample after positioning the sample stage until bead 2 and bead 3 were near the center of the probe region.

in the black circles in Figure 2-5(a), (b) and (c) would be responsible for most of the fluorescence signal, respectively. The other nanospheres do not occupy the central region of the excitation profile and, therefore, would not contribute significantly to the fluorescence signal. These preliminary studies confirm that we have the ability to correlate the optical and topographical properties of single nanometer-sized particles.

## **2.4 Conclusion**

In conclusion, we have described and demonstrated the spatially correlated single molecule fluorescence spectroscopy and AFM method. This technique is needed because of the large differences in spatial resolution of the optical and topographical imaging. In a typical experiment, simultaneous Tapping Mode<sup>TM</sup> AFM topography and scattered light images are recorded to identify particles of interest and measure their positions relative to the laser probe region of the optical microscope. The experimental applicability of the method is examined with fluorescent polystyrene nanobeads sample.

## References:

1. Bout DAV, Kerimo J, Higgins DA, Barbara PF: Near-field optical studies of thin-film mesostructured organic materials. *Accounts Of Chemical Research* **1997**, 30:204.
2. Dunn RC: Near-field scanning optical microscopy. *Chemical Reviews* **1999**, 99:2891.
3. Zenhausern F, Martin Y, Wickramasinghe HK: Scanning Interferometric Apertureless Microscopy - Optical Imaging At 10 Angstrom Resolution. *Science* **1995**, 269:1083.
4. Zenhausern F, Oboyle MP, Wickramasinghe HK: Apertureless Near-Field Optical Microscope. *Applied Physics Letters* **1994**, 65:1623.
5. Kolodny LA, Willard DM, Carillo LL, Nelson MW, Van Orden A: Spatially correlated fluorescence/AFM of individual nanosized particles and biomolecules. *Analytical Chemistry* **2001**, 73:1959.

## **Chapter 3**

# **Fluorescence Blinking of Bulky QD- bioconjugates**

In this chapter, we study the structures and fluorescence intermittency of single QD-bioconjugates and small ensembles of two or more isolated QD-bioconjugates by using the spatially correlated single molecule fluorescence spectroscopy and AFM method (See Chapter 2 for details). The individual QD-bioconjugates exhibited characteristic on- and off- fluorescence intermittency. Small clusters of QD-bioconjugates exhibit the prolonged multi-level blinking behavior, which is similar to that of the multiple noninteracting QD-bioconjugates probed simultaneously. Electronic interactions between the individual QDs in clusters might be very weak because the bulky protecting and functional layers on QD nanocrystals insulate the nanocrystals. Rolling off and

truncation in the probability density distribution of “on” times were observed under higher excitation power and in aged samples (stored more than one year). Higher laser power increases the rate of excitation, which in turn, enhances photoionization and makes it more likely for the fluorescent “on” state to become deactivated at higher excitation intensities. For aged QD-bioconjugates, it might be due to the derivation or changing of surface chemistry of the QD-bioconjugates with time.

### **3.1 Introduction**

Semiconductor QDs have been studied for many years to understand their unique, size tunable optical properties, and to investigate their potential applications in optoelectronic devices and biological imaging.<sup>1, 2</sup> In particular, much effort has been devoted to the phenomenon of fluorescence blinking of individual QDs<sup>3-5</sup>, introduced briefly in Chapter 1. Blinking is thought to occur when a photoexcited charge carrier formed in the core of the QD becomes trapped in a defect site on the QD surface. This leaves the QD in a non-fluorescent positive charged state. The fluorescence is reestablished when the trapped charge carrier recombines with the QD.

QDs can assemble into QD solids, thin films<sup>6</sup>, chains<sup>7</sup>, and clusters<sup>8</sup>. Electronic coupling between QDs, by way of Förster resonance energy transfer<sup>7, 9, 10</sup>, exciton transfer<sup>11</sup>, or photoinduced fluorescence enhancement (PFE)<sup>12-14</sup> has been observed. It is of interest to understand how such interactions affect, or are effected by, the fluorescence behavior of the individual QDs in the assemblies. Do the individual QDs blink independently, or can the blinking of one QD alter the behavior of neighboring QDs?

The former case appears to occur in solids doped with isolated QDs,<sup>15, 16</sup> whereas, the latter may occur in closed-packed QD films, in which the PFE effect has been observed.<sup>13</sup>

We seek to study the collective behavior of QDs in an assembly by characterizing the blinking of small ensembles containing two or more QDs. Such systems are large enough for multiple QDs to interact, but small enough so the blinking of the individual QDs is not obscured by ensemble averaging. In this chapter, we study individual QDs, small ensembles of isolated QDs, and QD clusters with the spatially correlated single molecule fluorescence spectroscopy and atomic force microscopy (AFM) (See Chapter 2 for details).

## **3.2 Experimental Section**

Instrumentation is the same as that in Chapter 2. A 650 nm short pass filter is used in front of the detector in this chapter to block the red light from the laser in AFM. QD-bioconjugates of QD565 streptavidin conjugates, QD605 biotin and QD605 streptavidin conjugates (Quantum Dot Corp.<sup>TM</sup>, now Invitrogen) are used in this study. QD565 and QD605 represent the QD samples with emission wavelengths around 565 nm and 605 nm, respectively. In the QD-bioconjugates, CdSe/ZnS core/shell QD crystals are surrounded by bulky polymeric and biomolecular coatings for passivation, good water solubility and functionality and insulation. Therefore the overall diameter of an individual QD-bioconjugate is as large as 15-25 nm. To compare the optical properties, especially blinking behavior, aged QD-bioconjugate samples are also studied. Aged samples mean that the samples have been stored for such a long time, such as more than one year, that

their surface chemistry may have been changed , possibly resulting in different optical behaviors.

QDs samples are prepared on (3-aminopropyl) triethoxysilane (APTES, Sigma) coated mica surface (AP-mica)<sup>17</sup>. Coating of the substrates is accomplished by placing 30  $\mu\text{L}$  of APTES on Teflon in a small plastic desiccator along with several newly-cleaved mica substrates and allowing the deposition to proceed at least for 2 hr., but at most overnight. To prepare samples of single isolated QDs, 60  $\mu\text{L}$  of 8 pM QD605 streptavidin conjugates in 0.1 $\times$ SSC (a solution of sodium chloride-sodium citrate in distilled/deionized water, Sigma) or 1 $\times$ PBS (phosphate buffer saline diluted with deionized water, Sigma) is applied onto an AP-mica substrate, allowed to incubate for 15 min, rinsed with 0.1 $\times$ SSC or 1 $\times$ PBS and deionized H<sub>2</sub>O, and dried in air. Individual isolated QDs and small QD clusters can both be found. The formation of small QD clusters might be due to multiple single QDs sitting together accidentally.

Aggregation of QDs is induced by specific biomolecular interactions between streptavidin and biotin, which is one of the strongest ( $K_a \approx 10^{13} \text{M}^{-1}$ ) found in nature. Equal volumes of 1 pM (before mixing) QD605 streptavidin conjugates and 1-50 pM (before mixing) QD605 biotin conjugates in 1 $\times$ TE buffer (10 mM Tris-HCl, 0.5 mM EDTA, pH 8, Sigma) are mixed and allowed to stand for 2 hr to overnight, resulting in QD clusters. The QD clusters solution is deposited onto the same AP- mica, allowed to incubate for 15 min, rinsed with 1 $\times$ TE and deionized H<sub>2</sub>O, and dried in air.

### **3.3 Fresh QD-bioconjugates**

#### **3.3.1 AFM Imaging of Isolated Single QDs and QD Clusters**

Figure 3-1 displays TappingMode and phase AFM images of single QDs and QD clusters. Well separated single QDs are dispersed on the substrate in Figure 3-1(a). In Figure 3-1(b), several interesting sizes and shapes of QD clusters are observed, including a linear structure that appears to contain five QDs in a chain. The QD clusters solution was prepared from a mixture of equal volumes (15  $\mu$ L) and concentrations (5 nM, before mixing) of QD605 streptavidin conjugates and QD605 biotin conjugates. Driven by interaction between streptavidin and biotin, aggregations of single QDs happened laterally, vertically, or randomly to form QD chains or blobs.

#### **3.3.2 Probing Individual QDs, Multiple Non-interacting QDs and Isolated QD Clusters**

Figure 3-2(a) shows the fluorescence trajectory segment (left) and the corresponding photon counting histogram (middle) of a QD605 streptavidin conjugate near the center of the laser probe region, which is marked with a black circle in the AFM topography image (right). The excitation intensity was always kept constant of 55.3 W/cm<sup>2</sup>, otherwise noticed. Two-state blinking is observed in the fluorescence time trace, consistent with previous studies on individual QDs<sup>3, 18</sup>. This two-state blinking is quantified using photon counting histogram (PCH) analysis (See Chapter 1 for details). The histogram is plotted according to the number of photons detected in each 10 msec counting interval of the multichannel scalar. Well-resolved peaks in the histogram confirm that the blinking occurs in a two-state manner. The time dependent properties of the blinking can be

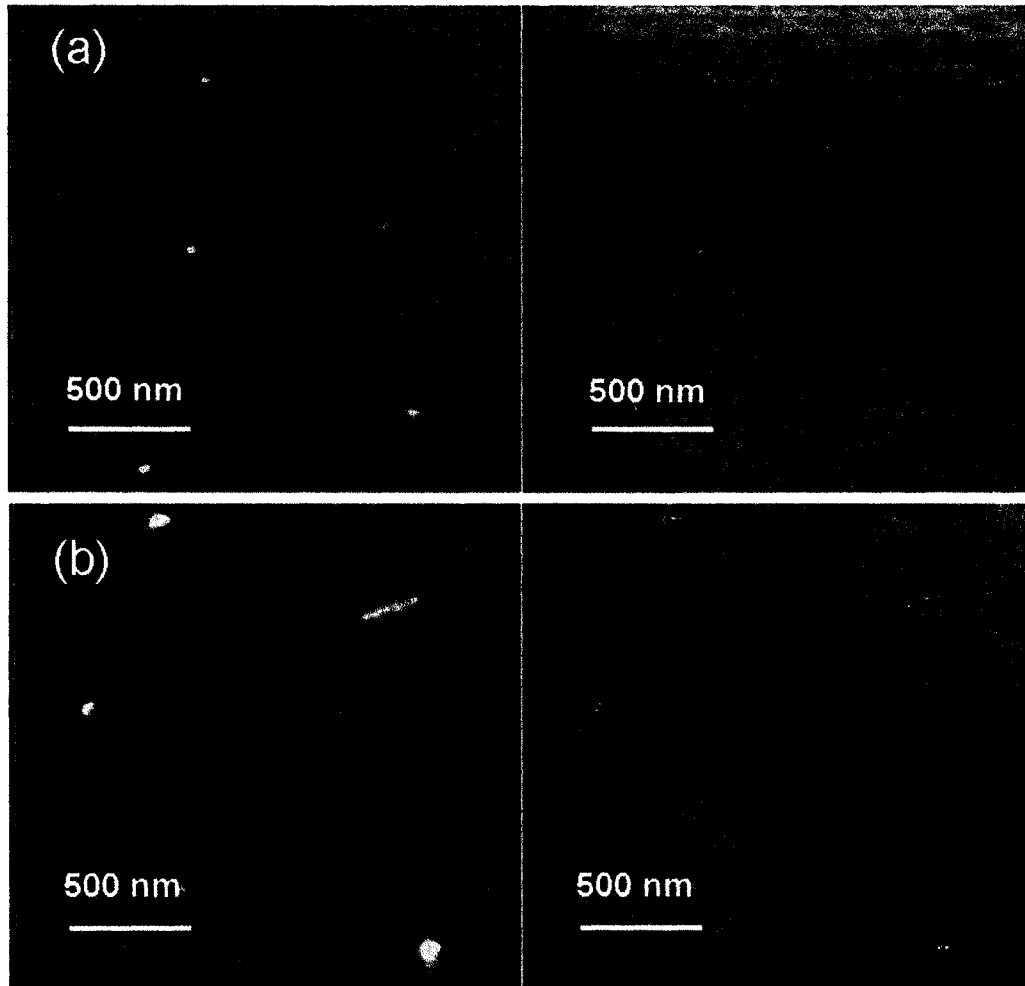


**Figure 3-1.** (a) TappingMode (left) and phase (right) AFM images of individual QD-bioconjugates. A sample of  $\sim 2.5$  nM of QD605 streptavidin conjugates was applied onto an AP-mica substrate. The height scale of the topographical image is 8 nm. (b) TappingMode (left) and phase (right) AFM images of QD clusters. A mixture of QD605 streptavidin conjugates and QD605 biotin conjugates was applied onto AP-mica substrate. The height scale of the topographical image is 15 nm.

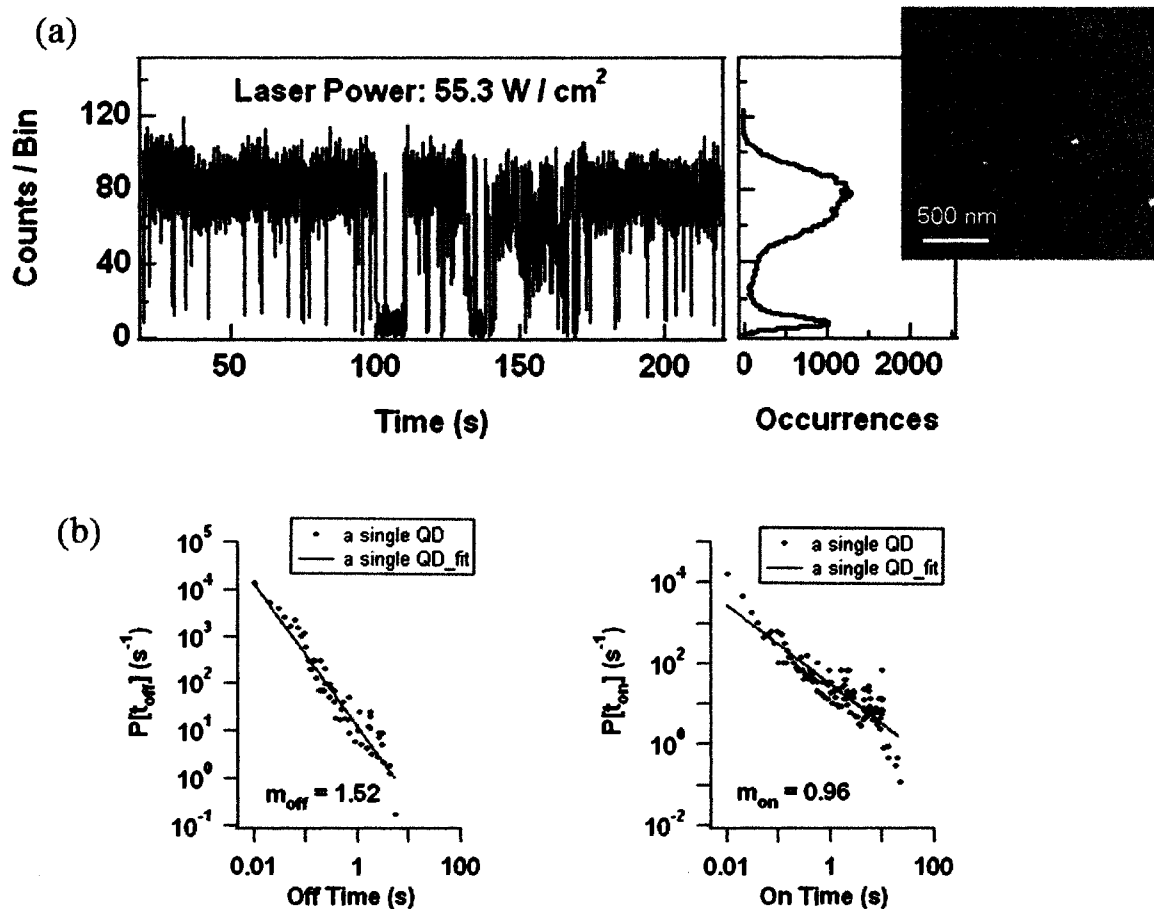


**Figure 3-2.** (a) Fluorescence trajectory segment (left) and the corresponding photon counting histogram (middle) of an QD605 streptavidin conjugate near the center of the optical probe region, which is marked with a black circle in the AFM topography image (right: height scale: 6 nm). The excitation intensity was 55.3 W/cm<sup>2</sup>.  $P[t]$  is proportional to  $t^{-m}$ . (b) “Off” (left) and “on” (right) time probability density distributions derived from the blinking time trace.

characterized by constructing on- and off-time probability density distributions, as shown in Figure 3-2(b). The probability density distributions display the power-law behavior, consistent with distributed on- and off- blinking kinetics<sup>3,4,18</sup>.

Figure 3-3(a) are the fluorescence trajectory segment (left) and the corresponding photon counting histogram (middle) of two isolated QD605 streptavidin conjugates near the center of the optical probe region, which are marked with a black circle in the AFM topography image (right). Figure 3-3(b) shows “off” (left) and “on” (right) probability density distributions derived from the blinking time trace. The larger apparent size of the QDs is due to the use of a blunt AFM probe tip at the time of these measurements. The fluorescence intensity time trace observed from this sample shows obvious three-level blinking that is confirmed by the photon counting histogram. The observed blinking pattern is consistent with two non-interacting QDs blinking independently. There is an off-state corresponding to both QDs blinking “off” simultaneously, an intermediate “on” state corresponding to one QD “on” and one QD “off”, and a second “on” state corresponding to both QDs blinking “on” simultaneously. The “on” and “off” probability density distributions exhibit the same power-law behavior as those of single QDs.

Figure 3-4(a) shows the fluorescence trajectory segment (left) and the corresponding photon counting histogram (middle) of an individual QD605 streptavidin conjugate cluster near the center of the probe region, which is marked with a black circle in the AFM topography image (right). The particle has a size and shape consistent with two QDs clustered together. From the fluorescence intensity time trace, and subsequent

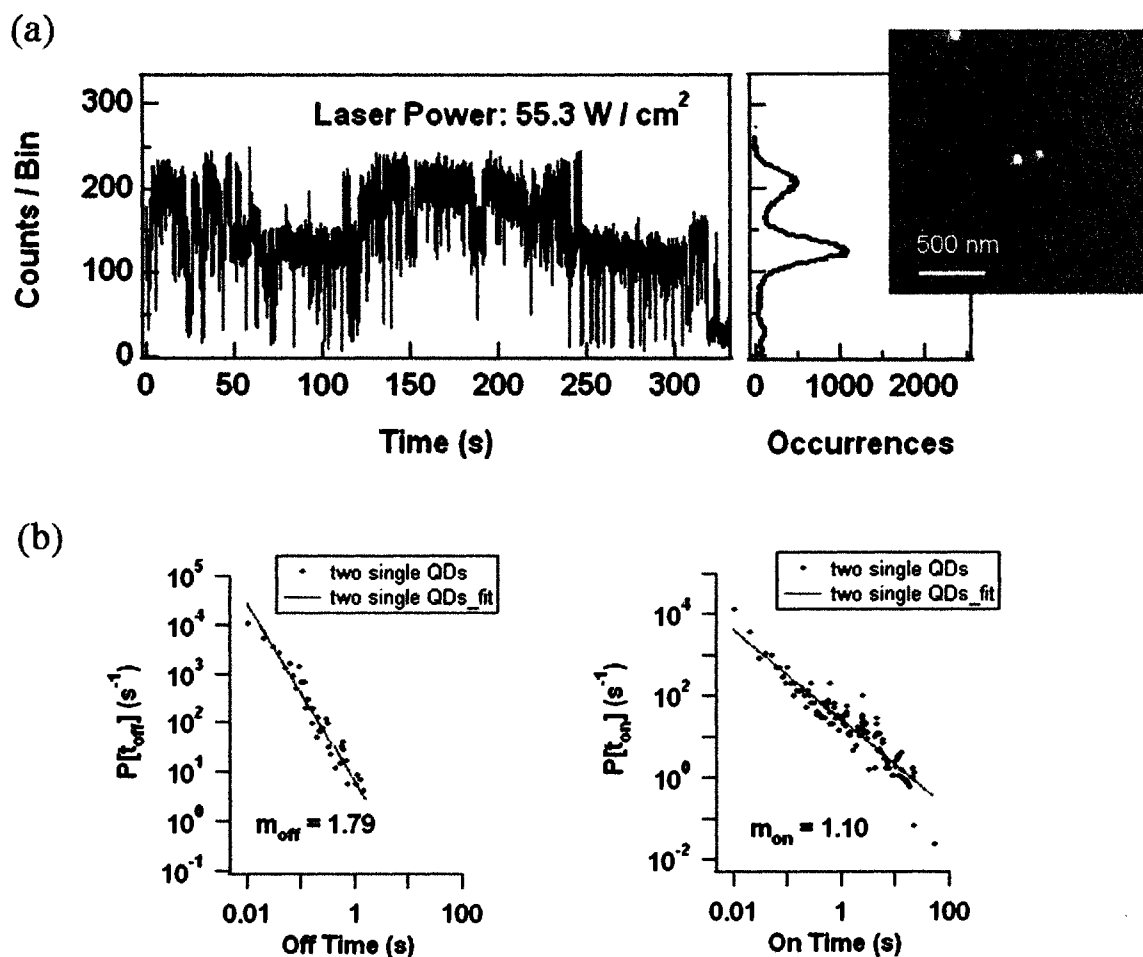


**Figure 3-3.** (a) Fluorescence trajectory segment (left) and the corresponding photon counting histogram (middle) of two isolated QD605 streptavidin conjugates near the center of the optical probe region, which are marked with a black circle in the AFM topography image (right: height scale: 6 nm). The excitation intensity was 55.3 W/cm<sup>2</sup>.  $P[t]$  is proportional to  $t^{-m}$ . (b) “Off” (left) and “on” (right) time probability density distributions derived from the blinking time trace.

photon counting histogram analysis, it appears that this cluster exhibits three-level blinking similar to the isolated non-interacting QDs discussed above. The emission intensities are lower, and there is a smaller intensity difference between the two “on” levels. This may point toward a small degree of energy transfer between the QDs. The “on” and “off” times probability density distributions shown in Figure 3-4(b) exhibit also a power law behavior.

It is hypothesized that if the QDs were close enough together to undergo efficient electronic energy transfer, they would behave as a single quantum system. This could cause a variety of effects that would be observable through analysis of the fluorescence intensity time trace. It could cause two-state blinking, due to efficient energy transfer of the excitation energy from a donor QD followed by emission of an acceptor QD, as in FRET. It could also result in faster blinking, due to more efficient charge transfer between electronically excited QDs and neighboring QDs. Finally, electron transfer between QDs could result in complete quenching of the QD fluorescence. Thus, comparisons between the fluorescence dynamics of multiple noninteracting QDs, and clusters containing an equivalent number of QDs will provide qualitative and quantitative information about the type and degree of energy transfer taking place.

As noted before, Quantum Dot Corporation encapsulates the QDs in an insulating polymeric material that is further modified with biomolecule functional groups. This may prevent the QD crystals from coming into close enough proximity to undergo efficient energy transfer when clustered together. Clusters formed from biotin and

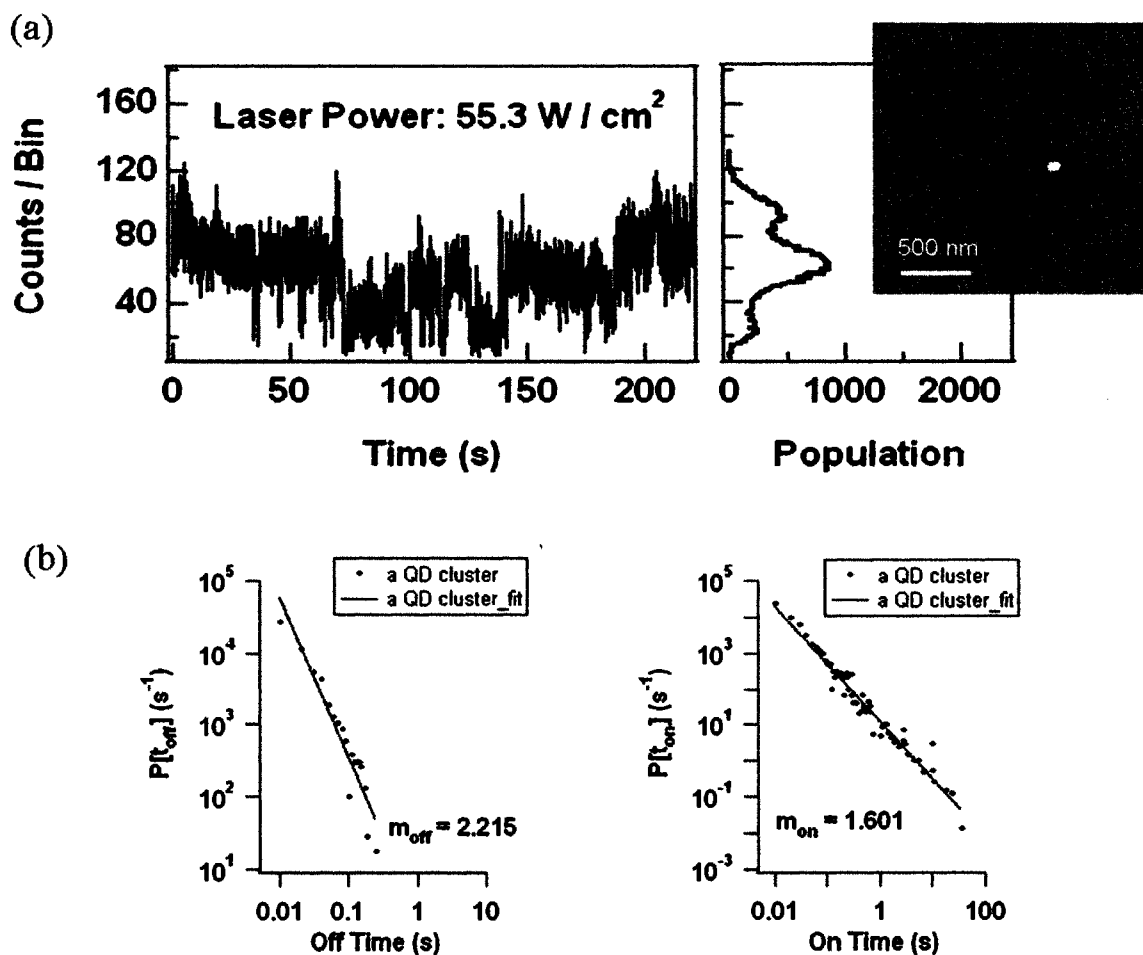


**Figure 3-4.** (a) Fluorescence trajectory segment (left) and the corresponding photon counting histogram (middle) of an individual QD605 streptavidin conjugate cluster near the center of the optical probe region, which is marked with a black circle in the AFM topography image (right: height scale: 6 nm). The excitation intensity was 55.3 W/cm<sup>2</sup>.  $P[t]$  is proportional to  $t^{-m}$ . (b) “Off” (left) and “on” (right) time probability density distributions derived from the blinking time trace.

streptavidin conjugated QDs from Quantum Dot Corporation exhibit no significant energy transfer. QD surface chemistry and the method of coupling QDs together to form clusters play critical roles in determining whether energy transfer takes place and the degree of energy transfer.

### **3.3.3 Auto Correlation Function (ACF) Analysis**

The time dependent properties of blinking can be characterized by the ACF analysis (See Chapter 1). ACFs of the single QD, multiple QDs and QD cluster are compared in Figure 3-5. Because of statistical limitations of data analysis, only early parts of the autocorrelation curves give qualitative information. All three ACFs show a slow variation in the fluorescence fluctuations, characteristic of prolonged on- and off- states of the particles. There does not appear to be a change in the blinking rate between the different QD systems. It is hypothesized that if the QDs were undergoing efficient electronic energy transfer, they would behave as a single quantum system. This could raise a noticeable difference through the autocorrelation analysis, which is clearly not the experimental outcome. Hence, there is no strong evidence that the QDs in the cluster are undergoing efficient electronic energy transfer. In general, we find this to be the case for both small and large QD clusters prepared from the QD-bioconjugates. For larger sized clusters, the fluorescence intensity time traces show continuous fluorescence, consistent with averaging of multiple QDs blinking independently (data not shown).

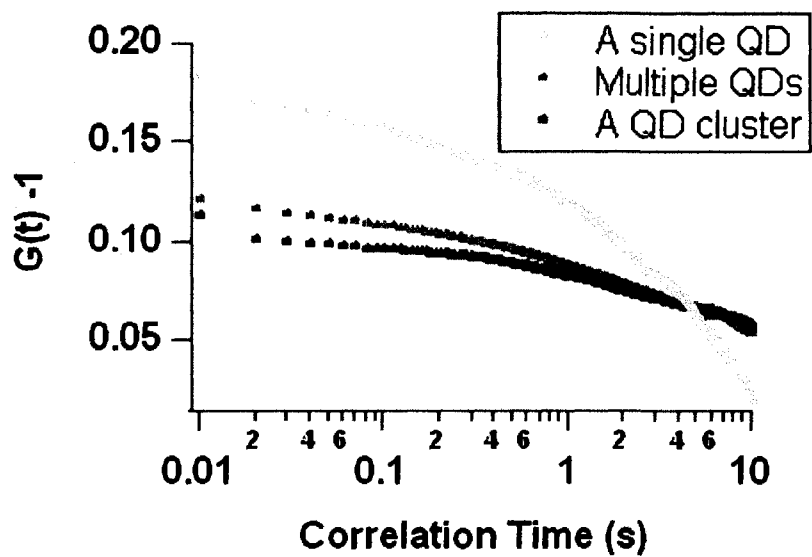


**Figure 3-5.** Autocorrelation functions of the individual QD, multiple QDs, and QD cluster derived from the fluorescence trajectories.

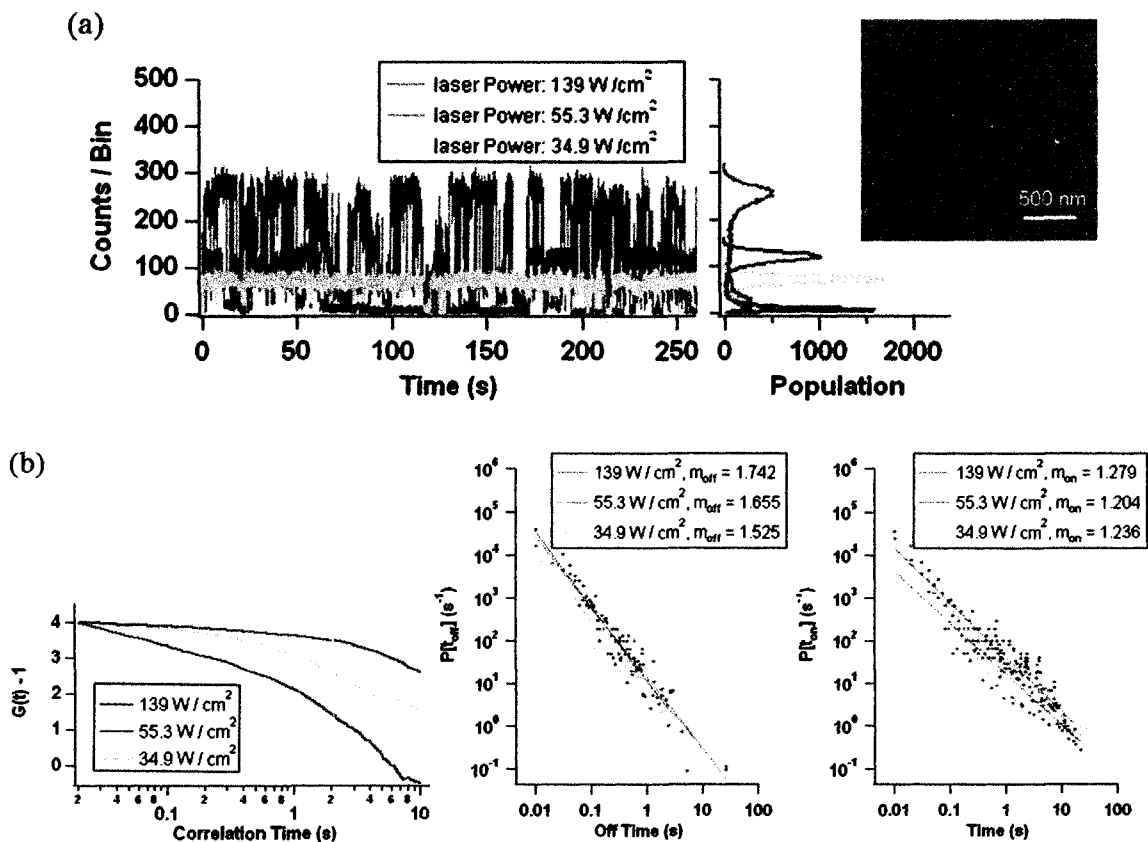
### **3.3.4 Probing Individual QDs with Different laser power**

Figure 3-6(a) shows the fluorescence trajectory segments (left) and the corresponding photon counting histograms (middle) of the same individual QD605 streptavidin conjugate probed at different excitation intensities (34.9 to 139 W/cm<sup>2</sup>), which is marked with a black circle in the AFM topography image (right). Figure 3-6(b) are derived autocorrelation functions (left), off- (middle) and on- (right) states probability density distributions. It is found that the intensity of the on-state increases with increasing laser power. Both on- and off- states follow the power law kinetics no matter the excitation power. The ACF analysis shows that the blinking becomes faster as the excitation intensity increases. We hypothesize that the higher laser power increases the rate of excitation, which in turn, enhances photoionization and makes it more likely for the fluorescent on state to become deactivated at higher excitation intensities.

## **3.4 Aged QD-bioconjugates Excited with High Power**

### **3.4.1 Topography/Blinking of One Single QD, Three Single QDs, a QD Chain, and a QD Blob.**

Figure 3-7 shows the fluorescence trajectories and the corresponding TappingMode AFM images of a single QD, three isolated single QDs, a QD chain, and a QD blob. For the aged QD samples, higher excitation power is necessary to obtain a reasonable signal to noise ratio. The excitation power used was 630-6300 W/cm<sup>2</sup>, higher than that for the fresh sample. In Figure 3-7(a), a single QD sitting in the probe region gave a neat two-level-blinking fluorescence trace. On the other hand the fluorescence trace shown in



**Figure 3-6.** (a) Fluorescence trajectory segments (left) and the corresponding photon counting histograms (middle) of the same QD605 streptavidin conjugate probing at different excitation power (34.9 to 139 W/cm<sup>2</sup>), which is marked with a black circle in the AFM topography image (right: height scale: 6 nm).  $P[t]$  is proportional to  $t^{-m}$ . (b) ACFs (left), “off” (middle) and “on” (right) time probability density distributions derived from the blinking time traces.

Figure 3-7(b) has several levels of “on” states, which is the result of occupation of the probe region by multiple single QDs. By accident, several single QD565 streptavidin conjugates were so close to each other that they formed a QD chain, which can be seen in the TappingMode image in Figure 3-7(c). To form QD clusters, equal volumes (50  $\mu$ L) of 1pM QD605 streptavidin conjugates and 50 pM QD605 biotin conjugates were placed together for 4 hr., which produced bigger QD clusters as the one shown in Figure 3-7(d). Blinking of the QD chain and blob display a different looking from that of isolated individual QDs. Instead of continuous long “on” periods, there are more consequent spikes in the trajectories.

### 3.4.2 On-/Off-time Probability Density Distributions

To get a glance at blinking kinetics of the above aged QD-bioconjugates, the on-time and off-time probability density distributions,  $P[t_{\text{on}}]$  and  $P[t_{\text{off}}]$ , of the corresponding fluorescence trajectories shown in Figure 3-7 were analyzed. Figure 3-8 shows the  $P[t_{\text{on}}]$  and  $P[t_{\text{off}}]$  of the single QD, multiple single QDs, QD chain, and QD blob. The dots represent experimental data and the solid lines are the fittings (orange for on-time distributions and blue for off-time distributions). It is well known that single QD blinking is governed by the inverse power law,  $P[t] \propto t^{-m}$ , where  $1 < m < 2$  in most cases<sup>19</sup>. However, on-time probability density distributions depend on excitation intensity<sup>20, 21</sup>, temperature<sup>20, 21</sup>, surface environments of QDs<sup>20</sup>, and the conduction of substrates<sup>22</sup>, which result in deviation of the distribution from the power-law. The deviation appears rolling off from the power law or cutoff of the power law. The DCET model (See Chapter 1 for details) proposed by J. Tang and R. A. Marcus gave a plausible explanation

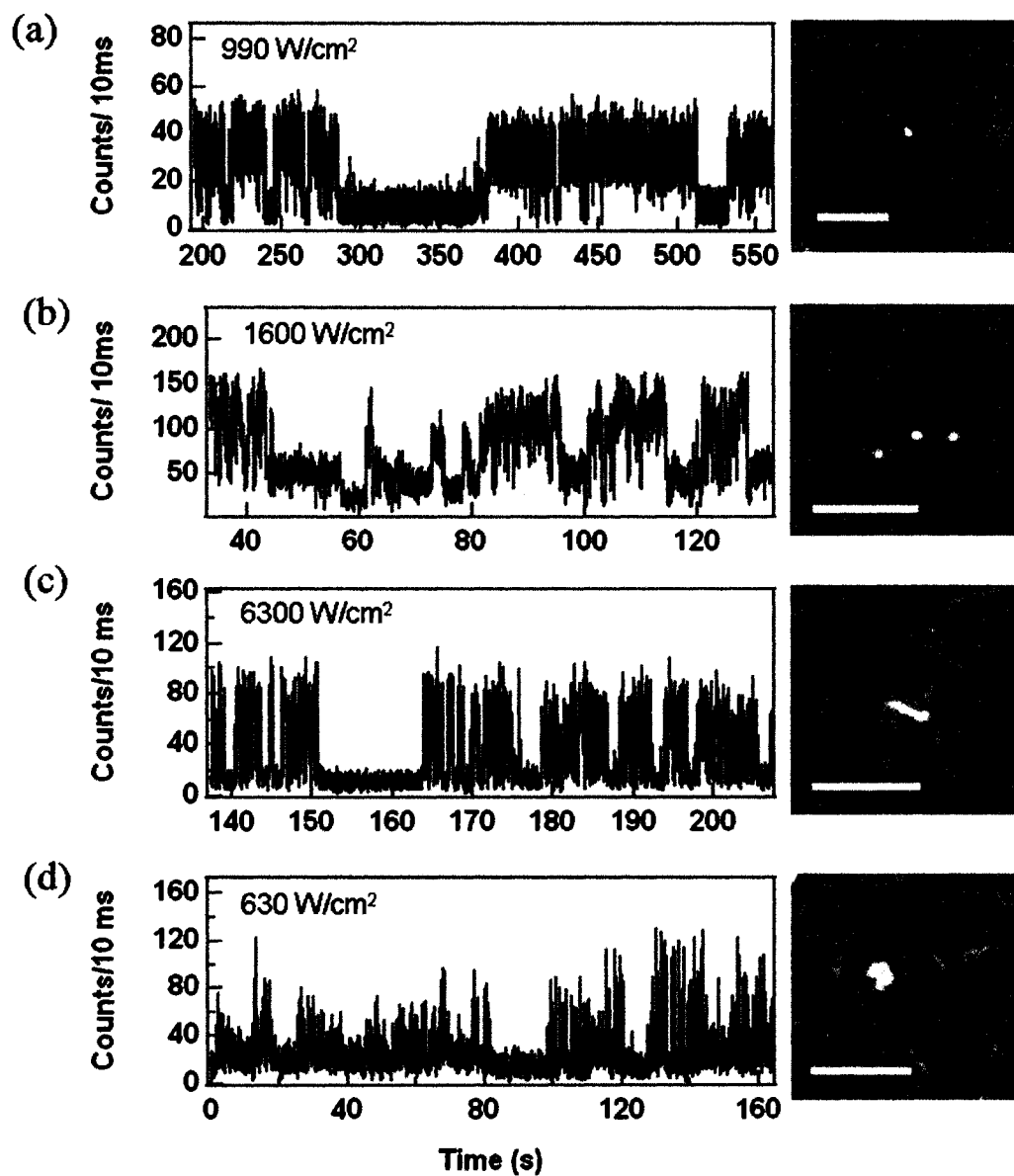


**Figure 3-7.** Fluorescence trajectories (left) and the corresponding TappingMode AFM images (right) of one isolated QD (a), three isolated QDs (b), a QD chain (d), and a QD blob (d). The scales of the white bars are 500 nm. The height scale of the topographical images is 10 nm.

to the deviation of  $P[t_{on}]^{21,23}$ . They claimed that at short time the power-law distribution had an exponent of  $-1/2$ , which changed to  $-3/2$  with an exponential bending tail and finally to a single exponential decay at a much longer time. Since the “on” durations of the QDs studied here are neither very short nor very long, we use the proposed Eq.(1) to fit the  $P[t_{on}]$  of the single QD, QD chain, and QD blob.

$$P[t_{on}] = At^{-m} \exp(-\Gamma t) \quad (1)$$

When  $\Gamma=0$ , Eq. (1) changes to the power law statistics, which is fitted to  $P[t_{on}]$  of the multiple single QDs.  $P[t_{off}]$  of the single QD, multiple single QDs, QD chain, and QD blob (in Figure 3-8) are all fitted with the power-law statistics,  $P[t] = 10^{-B} t^{-m}$ , resulting in straight line fittings. All of the fitting parameters are listed in Table 3-1, where parameters without uncertainty are held during fitting. The average “on” and “off” durations,  $\langle t_{on} \rangle$  and  $\langle t_{off} \rangle$ , of each QD system were also calculated by Eq. (2),

$$\langle t_{on/off} \rangle = \frac{\int_{0.01}^{t_{on/off}^{\max}} tP(t_{on/off})dt}{\int_{0.01}^{t_{on/off}^{\max}} P(t_{on/off})dt} \quad (2)$$

where  $t_{on/off}^{\max}$  is the maximum  $t_{on/off}$  observed in a given data set. Because we used 10 ms of bin size in data acquisition, the lower bound of the integration was chosen as  $0.01 \text{ s}^4$ . The multiple single QD system has the longest average on-state duration and shortest average off-state duration. This is because of the overlay of “on” times of several independent single QDs. If the number of single QD increased to infinite, blinking would not been seen. The average “on” times of the QD chain and QD blob are much shorter than those of individual QDs. In the single QD or multiple single QDs systems, the on-time distributions are either a straight line or a straight line with a short bending tail

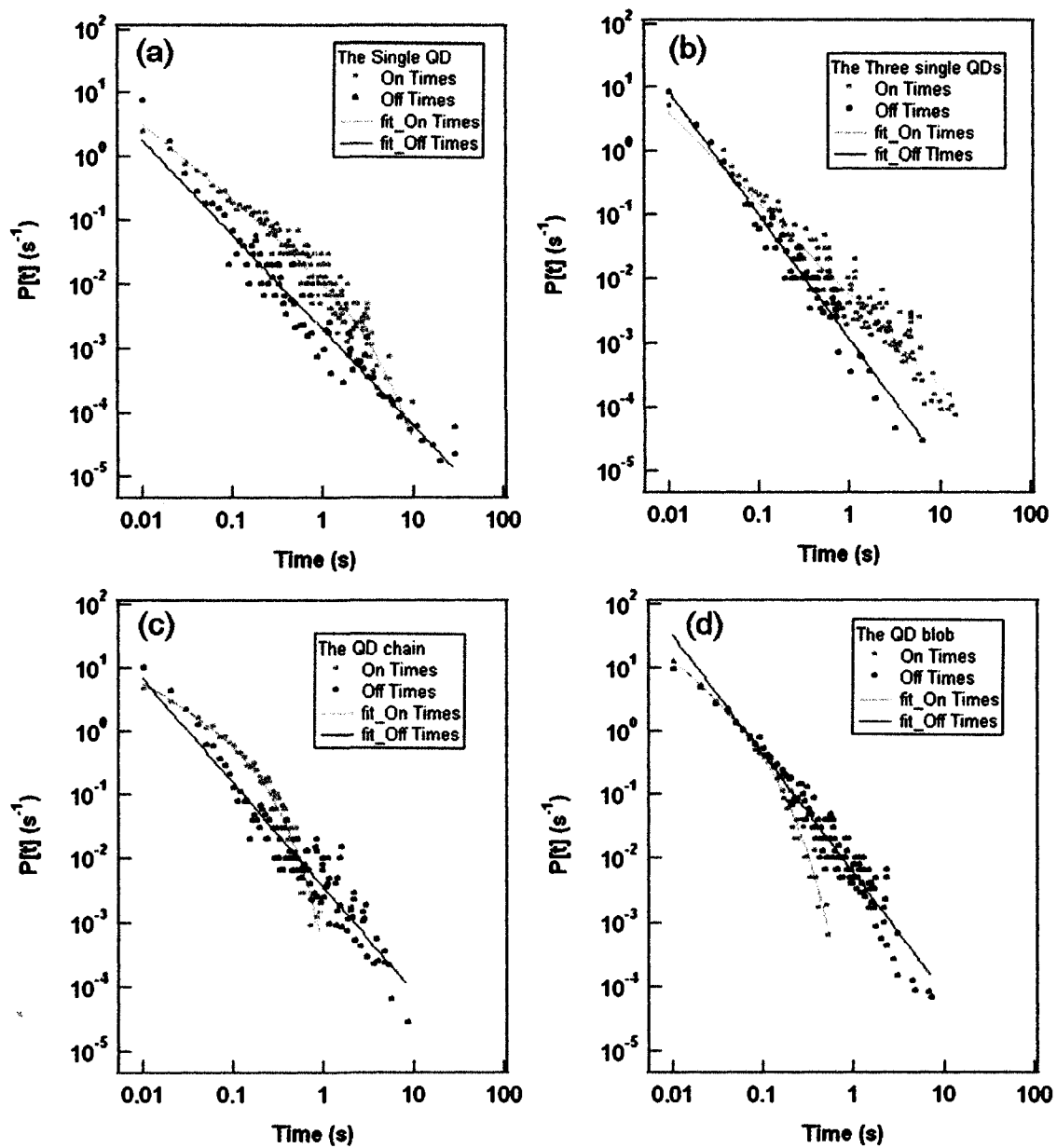


**Figure 3-8.** On-time (orange) and off-time (blue) probability density distributions of the single QD (a), the multiple single QDs (b), the QD chain (c), and the QD blob (d), whose fluorescence trajectories are shown in Figure 3-7. Dots represent the experimental data and solid lines show the fittings.

( $\Gamma_{\text{single}}=0.33(4)$ ) at the very end. In contrast, the  $P[t_{\text{on}}]$  of the QD chain and QD blob roll off much faster with  $\Gamma_{\text{chain}}=6.3(6)$  and  $\Gamma_{\text{blob}}=10.4(1.3)$ , respectively. The fast rolling off might be due to the higher excitation laser power and the interactions between single QDs in the clusters.

**Table 3-1.** Parameters from  $P[t]$  fitting.

System	Threshold	On Times					Off Times			
		$P[t_{\text{on}}]$			$t_{\text{on}}^{\text{max}}$ (s)	$\langle t_{\text{on}} \rangle$ (s)	$P[t_{\text{off}}]$		$t_{\text{off}}^{\text{max}}$ (s)	$\langle t_{\text{off}} \rangle$ (s)
		$A$	$m$	$\Gamma$			$B$	$m$		
1 QD	19	0.014(1)	1.17(6)	0.33(4)	9.870	0.3724	2.72(3)	1.49(4)	28.60	0.5581
3 QDs	33	0.0056(3)	1.43(4)	0	14.37	0.4897	2.94(5)	1.95(7)	6.270	0.0723
QD Chain	23	0.18(7)	0.8(1)	6.3(6)	0.900	0.0805	2.45(3)	1.63(5)	8.410	0.1855
QD Blob	31	0.08(5)	1.1(2)	10.4(1.3)	0.510	0.0447	2.23(3)	1.87(5)	7.160	0.0907

### 3.4.3 ACF Analysis

We also did ACF analysis for the four QD systems. Still, because of statistical limitations of data analysis, only early part of the autocorrelation curves giving qualitative information are shown in Figure 3-9. The ACF analysis further visualizes the differences. ACFs of the single QD and multiple single QDs are much flatter than those of QD clusters at shorter correlation times. The ACFs of the QD chain and QD blob decay fast from the minimum correlation time. By comparing fresh and aged samples, we propose that the changing of surface chemistry of the QD-bioconjugates with time, such as falling off of the bioconjugates and/or polymer coating from the QD surface, could bring closer the QD nanocrystals in clusters and facility the communications between the QDs, and result in the differences in the ACFs and  $P[t_{\text{on}}]$ .

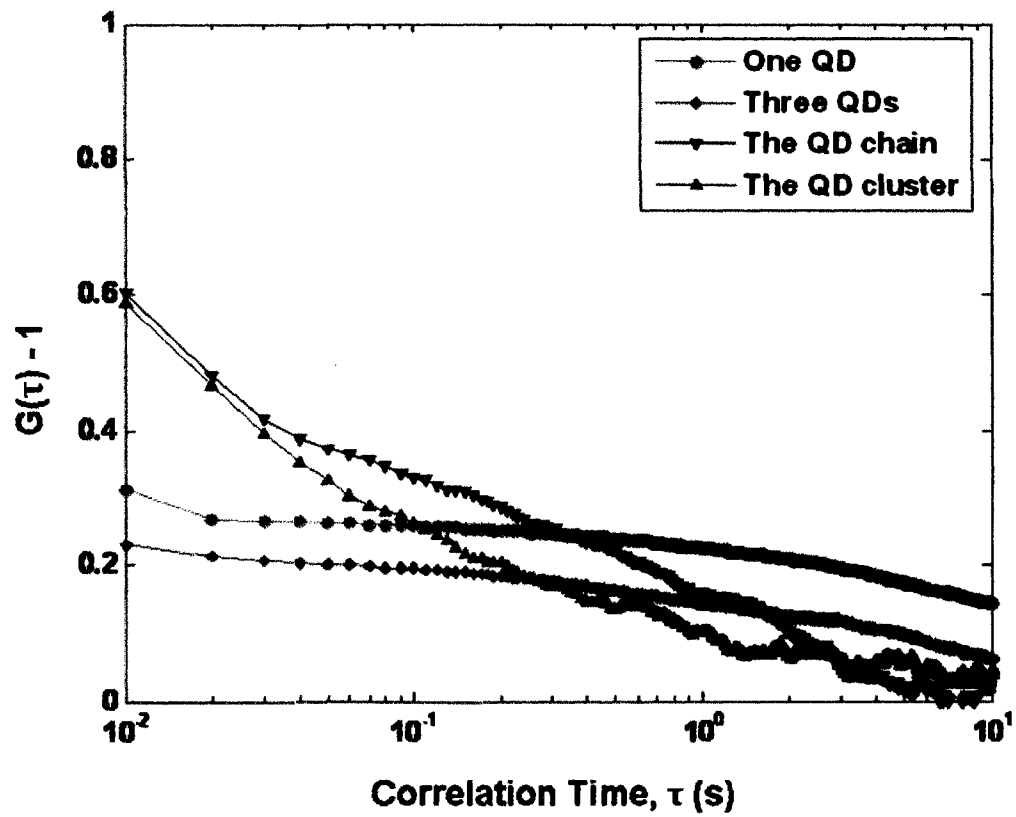


**Figure 3-9.** ACFs of the single QD, multiple QDs, QD chain, and QD blob shown in Figure 3-7.

### 3.5 Conclusion

We have studied the fluorescence blinking behavior of small clusters of QD-bioconjugates. Small clusters of fresh QD-bioconjugates present the prolonged multi-level blinking behavior, which is similar as that of multiple non-interacting fresh QD-bioconjugates probed simultaneously. We propose the electronic coupling between the neighboring QD-bioconjugates is very weak because the bulky protecting and functional layers on QD nanocrystals insulate the energy centers of nanocrystal cores. As the excitation intensity increases, blinking of individual QD-bioconjugates becomes faster. We hypothesize that the higher laser power increases the rate of excitation, which in turn, enhances photoionization and makes it more likely for the fluorescent “on” state to become deactivated at higher excitation intensities. Aged QD-bioconjugates are also studied and compared with the fresh samples. Fast rolling off in the probability density distribution of “on” times are observed. This might be due to the derivation or changing of surface chemistry of the aged QD-bioconjugates with time, such as the bioconjugates and/or protection coating ripping off, higher excitation laser power, and consequent closer interactions between neighboring QDs.

## References:

1. Alivisatos AP, Gu WW, Larabell C: Quantum dots as cellular probes. *Annual Review of Biomedical Engineering* **2005**, 7:55.
2. Klimov VI: Mechanisms for photogeneration and recombination of multiexcitons in semiconductor nanocrystals: Implications for lasing and solar energy conversion. *Journal of Physical Chemistry B* **2006**, 110:16827.
3. Kuno M, Fromm DP, Hamann HF, Gallagher A, Nesbitt DJ: Nonexponential "blinking" kinetics of single CdSe quantum dots: A universal power law behavior. *Journal of Chemical Physics* **2000**, 112:3117.
4. Kuno M, Fromm DP, Hamann HF, Gallagher A, Nesbitt DJ: "On"/"off" fluorescence intermittency of single semiconductor quantum dots. *Journal of Chemical Physics* **2001**, 115:1028.
5. Nirmal M, Dabbousi BO, Bawendi MG, Macklin JJ, Trautman JK, Harris TD, Brus LE: Fluorescence intermittency in single cadmium selenide nanocrystals. *Nature* **1996**, 383:802.
6. Crooker SA, Hollingsworth JA, Tretiak S, Klimov VI: Spectrally resolved dynamics of energy transfer in quantum-dot assemblies: Towards engineered energy flows in artificial materials. *Physical Review Letters* **2002**, 89:186802.
7. Tang ZY, Ozturk B, Wang Y, Kotov NA: Simple preparation strategy and one-dimensional energy transfer in CdTe nanoparticle chains. *Journal of Physical Chemistry B* **2004**, 108:6927.
8. Unold T, Mueller K, Lienau C, Elsaesser T, Wieck AD: Optical control of excitons in a pair of quantum dots coupled by the dipole-dipole interaction. *Physical Review Letters* **2005**, 94:137404.
9. Kagan CR, Murray CB, Nirmal M, Bawendi MG: Electronic energy transfer in CdSe quantum dot solids. *Physical Review Letters* **1996**, 76:1517.
10. Franzl T, Shavel A, Rogach AL, Gaponik N, Klar TA, Eychmuller A, Feldmann J: High-rate unidirectional energy transfer in directly assembled CdTe nanocrystal bilayers. *Small* **2005**, 1:392.
11. Koole R, Liljeroth P, Donega CD, Vanmaekelbergh D, Meijerink A: Electronic coupling and exciton energy transfer in CdTe quantum-dot molecules. *Journal of the American Chemical Society* **2006**, 128:10436.
12. Kimura J, Uematsu T, Maenosono S, Yamaguchi Y: Photoinduced fluorescence enhancement in CdSe/ZnS quantum dot submonolayers sandwiched between insulating layers: Influence of dot proximity. *Journal of Physical Chemistry B* **2004**, 108:13258.
13. Maenosono S: Monte-Carlo simulations of photoinduced fluorescence enhancement in semiconductor quantum dot arrays. *Chemical Physics Letters* **2005**, 405:182.
14. Maenosono S, Dushkin CD, Saita S, Yamaguchi Y: *Jpn J Appl Phys, Part 1* **2000**, 39:4006.
15. Chung IH, Bawendi MG: Relationship between single quantum-dot intermittency and fluorescence intensity decays from collections of dots. *Physical Review B* **2004**, 70:165304.

16. Pelton M, Grier DG, Guyot-Sionnest P: Characterizing quantum-dot blinking using noise power spectra. *Applied Physics Letters* **2004**, 85:819.
17. Kolodny LA, Willard DM, Carillo LL, Nelson MW, Van Orden A: Spatially correlated fluorescence/AFM of individual nanosized particles and biomolecules. *Analytical Chemistry* **2001**, 73:1959.
18. Kuno M, Fromm DP, Gallagher A, Nesbitt DJ, Micic OI, Nozik AJ: Fluorescence intermittency in single InP quantum dots. *Nano Letters* **2001**, 1:557.
19. Gomez DE, Califano M, Mulvaney P: Optical properties of single semiconductor nanocrystals. *Physical Chemistry Chemical Physics* **2006**, 8:4989.
20. Shimizu KT, Neuhauser RG, Leatherdale CA, Empedocles SA, Woo WK, Bawendi MG: Blinking statistics in single semiconductor nanocrystal quantum dots. *Physical Review B* **2001**, 63:205316.
21. Tang J, Marcus RA: Mechanisms of fluorescence blinking in semiconductor nanocrystal quantum dots. *Journal of Chemical Physics* **2005**, 123:054704.
22. Stefani FD, Knoll W, Kreiter M, Zhong X, Han MY: Quantification of photoinduced and spontaneous quantum-dot luminescence blinking. *Physical Review B* **2005**, 72:125304.
23. Tang J, Marcus RA: Diffusion-controlled electron transfer processes and power-law statistics of fluorescence intermittency of nanoparticles. *Physical Review Letters* **2005**, 95:107401.

## **Chapter 4**

# **Enhanced Blinking of Small Close-packed Clusters of QD Nanocrystals**

In this chapter, we study the structures and fluorescence intermittency of single CdSe/ZnS QD nanocrystals, ensembles of isolated QDs, and close-packed clusters containing two or more QDs by using the spatially correlated single molecule fluorescence spectroscopy and AFM method (See Chapter 2 for details). The individual QDs exhibit characteristic on- and off- fluorescence intermittency. When multiple isolated QDs are probed simultaneously, the fluorescence behavior is consistent with independent blinking of the particles. However, when small close-packed QD clusters are probed, the fluorescence intermittency becomes much more rapid and intense than can be explained by the independent blinking of multiple particles. This enhanced

blinking is suggested to occur when the QDs in the cluster become electronically coupled. The nature of this coupling is not known, though electrons trapped from QDs when they blink off may play a role by altering the electronic environment of neighboring QDs and enhancing their fluorescence properties.

## **4.1 Introduction**

We tried to study the collective behavior of QDs in an assembly by characterizing the blinking of small clusters containing two or more QDs. However, the QD-bioconjugates used in Chapter 3 have bulky insulators that block or weaken the communication between neighboring single QD-bioconjugates. In this chapter, small CdSe/ZnS core-shell QD nanocrystals are going to be studied with the correlated single molecule fluorescence spectroscopy and AFM method. In contrast to bulky QD-bioconjugates, these QD nanocrystals are expected to have strong communications, showing in fluorescence blinking behavior, when they are adjacent to each other.

## **4.2 Experimental Section**

The instrumentation in this section is the same as that in Chapter 2. The 650 nm short pass filter is still used in front of the detector as in Chapter 3. The QDs examined in this study are CdSe/ZnS core/shell colloidal nanoparticles capped with trioctylphosphine and trioctylphosphine oxide (TOP/TOPO) as stabilizing ligands. QD nanocrystal samples of green Evidots, yellow Evidots and red Evidots dissolved in toluene at  $\sim 70 \mu\text{M}$ ,  $40 \mu\text{M}$  and  $15 \mu\text{M}$ , respectively, are purchased from Evident Technologies (Evidots™,

Troy, NY). Figure 4-1 shows the TEM images\*, the size histograms and the photoluminescence (PL) spectra of the three QD samples. The green Evidots have an average diameter of 2.75 nm and emission wavelength of 540 nm. The sizes of the other QD samples are 3.96 nm and 5.38 nm, whose photoluminescence (PL) peaks are centered at 580 nm and 615 nm, respectively. It is obvious that these QD nanocrystals are much smaller than the QD-biocojugates studied in Chapter 3.

Small QD clusters are formed by treating ~1 mL of ~1 nM QDs diluted in hexane with a few microliters of methanol, and allowing the solution to stand for ~10-20 min. Methanol raises the polarity of the solvent, causing aggregation of the QDs by association of the hydrophobic ligands.<sup>1</sup> The degree of aggregation can be controlled by adjusting the QD and methanol concentrations and the incubation time. Following incubation, ~100  $\mu$ l of the solution are spin cast onto an AP-mica substrate to disperse the particles for subsequent fluorescence and AFM analysis in ambient air.

## 4.3 Observations

### 4.3.1 AFM Images of Single QDs and Small QD Clusters

Figure 4-2 shows AFM topography images of samples containing predominantly individual isolated QDs (Figure 4-2(a)) and small QD aggregates (Figure 4-2(b)) of green Evidots. The particles are analyzed to determine their *effective* volumes. The effective volume is larger than the true particle volume due to tip convolution artifacts, which also prevents us from resolving the individual QDs in the clusters. Volume histograms shown

---

\* By Dr. Ka Yee (Anna) Chick

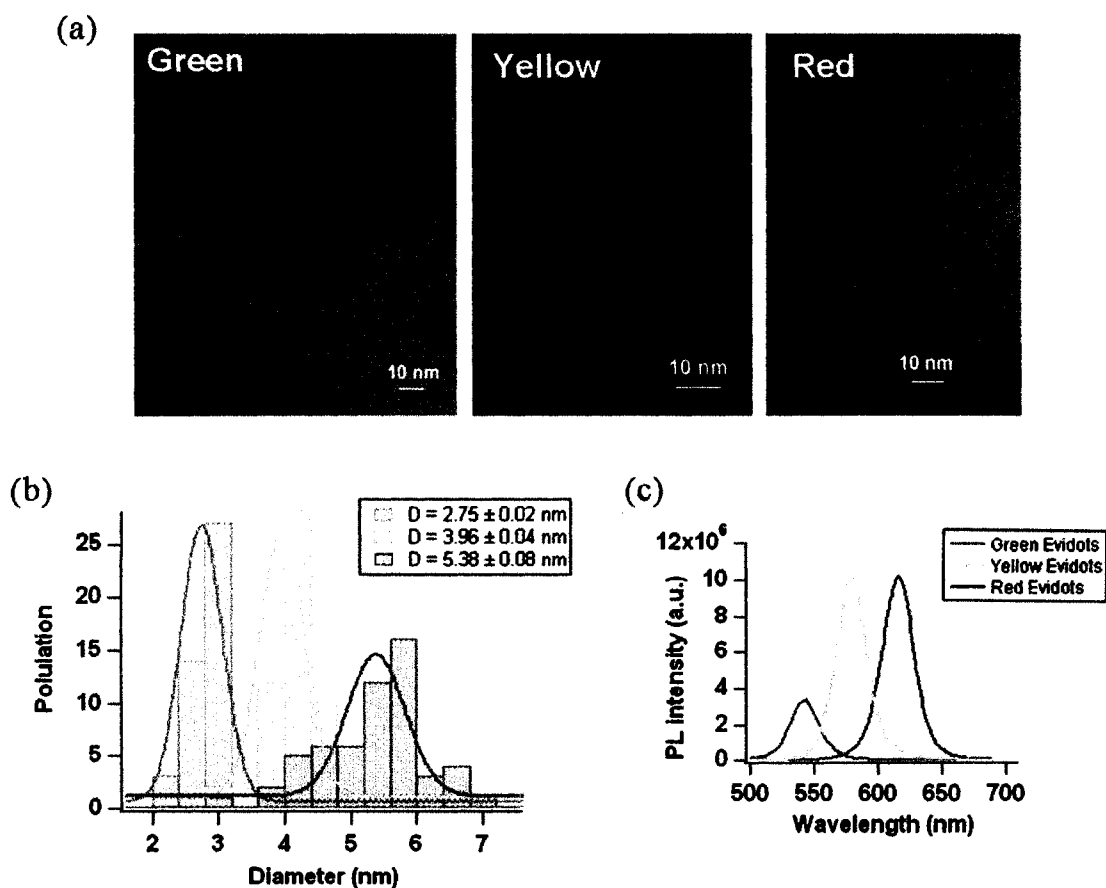


**Figure 4-1.** (a) TEM images of QD samples of green Evidots (left), yellow Evidots (middle) and red Evidots (right). (b) The size histograms from the TEM images of the three QD samples, with the average overall diameters of 2.75, 3.96 and 5.38 nm, respectively. (c) Photoluminescence (PL) spectra of the three QD samples, with the emission around 540, 580 and 615 nm, respectively.

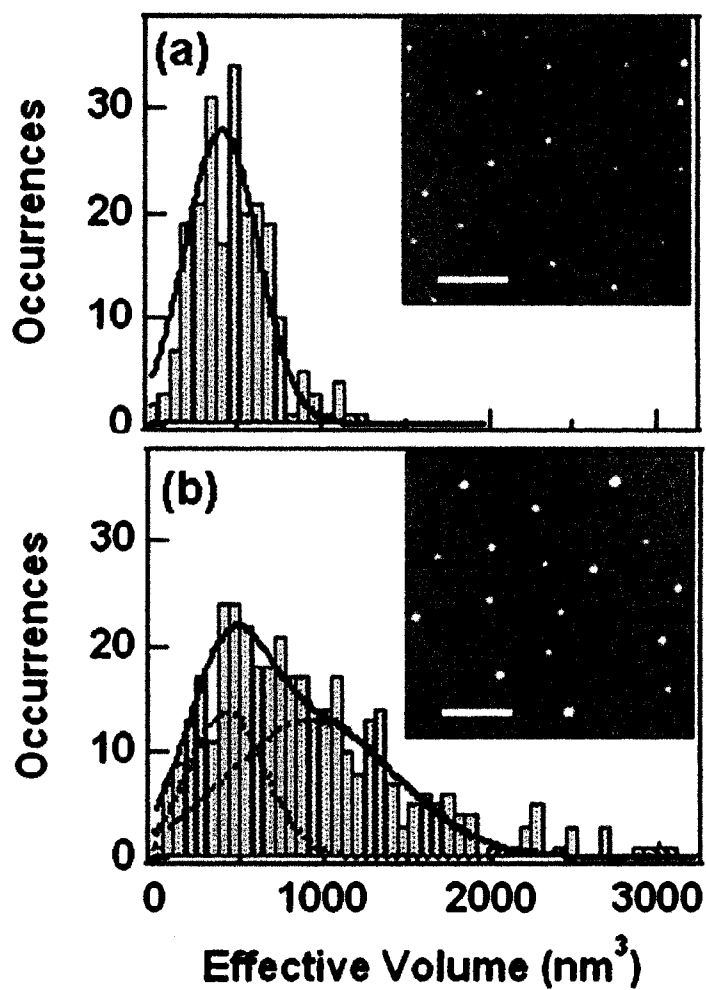


**Figure 4-2.** AFM topography images (inset) and effective volume histograms of (a) individual isolated Evidot QDs and (b) QD clusters on mica, imaged in ambient air. The scale bars on the AFM images are 500-nm and the z- height is 20-nm. The histograms were derived from four accumulated images each.

in Figure 4-2 are derived from equivalent sized images of four different sample regions. The histogram from the single QD sample shows a single size distribution, while in the sample of QD aggregates at least two sub-populations are present—one consistent with individual QDs and another showing QD clusters containing at least two QDs. Although there is considerable overlap between the two populations, it is found that particles with effective volumes larger than  $\sim 800\text{-nm}^3$  can be identified as QD clusters with  $> 90\%$  probability.

### **4.3.2 Probing Single QD Nanocrystals and Small QD Clusters**

Figure 4-3 shows fluorescence intensity trajectories observed for several different particles or groups of particles. The corresponding AFM topography images show the regions of the sample being probed by the optical microscope while the fluorescence trajectories are recorded. In Figure 4-3(a), we observed a single particle with an effective volume of  $282\text{-nm}^3$  in a sample of green Evidots that contained both single QDs and QD clusters. From the particle size, and the characteristic prolonged on- and off-times observed, we can identify this particle as an individual isolated QD. In the green Evidots sample containing predominantly individual isolated QDs, most of the fluorescent particles observed ( $>80\%$ ) exhibited similar prolonged on- and off-time behavior.

Figure 4-3(b) shows a larger particle identified in the same sample as the one shown in Figure 4-3(a). This particle had an effective volume of  $1380\text{-nm}^3$ , identifying it as an isolated QD cluster containing two or more QDs. The fluorescence trajectory of the QD cluster differs strikingly from that of the single QD. In the lower intensity regime (Figure

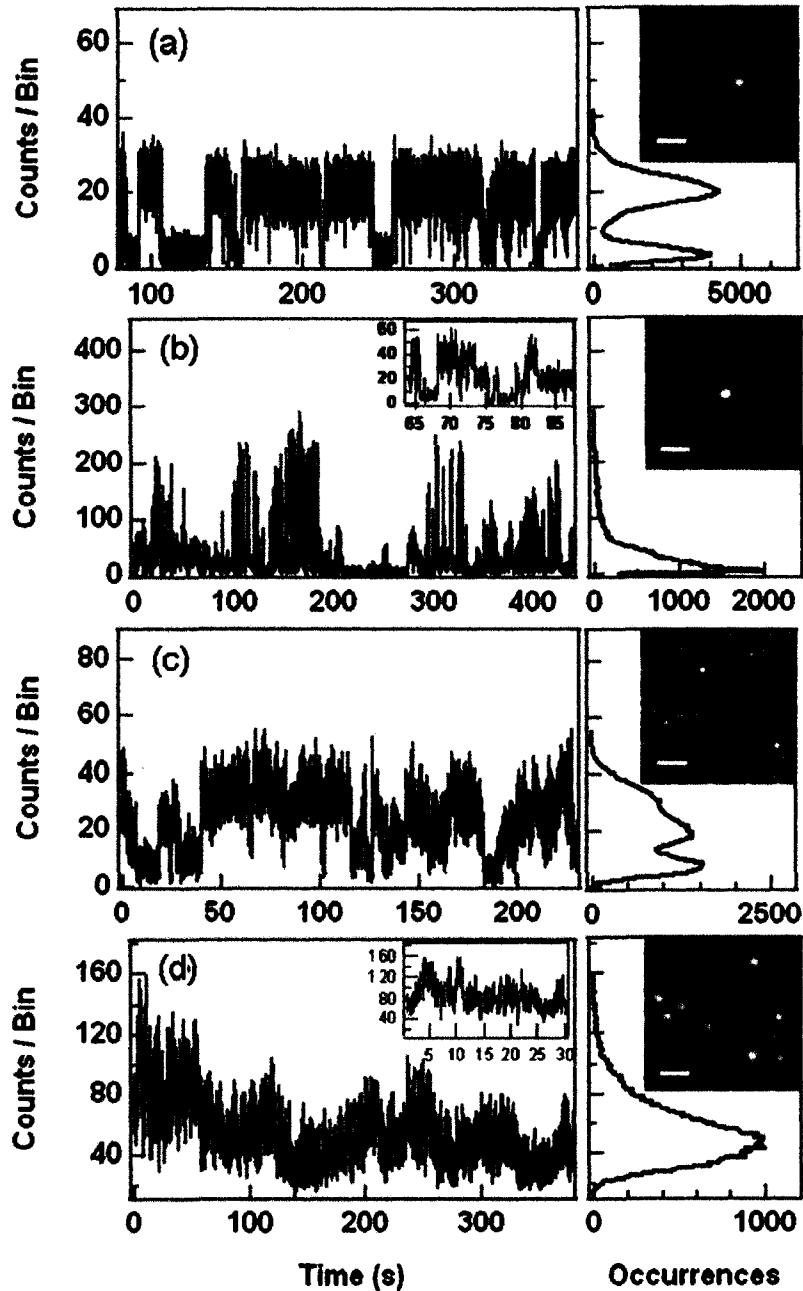


**Figure 4-3.** Fluorescence trajectory segments (left), photon count histograms (right), and AFM topography images (inset) of (a) a single QD, (b) a QD cluster, (c) three isolated QDs probed simultaneously, and (d) multiple isolated QDs in the same QD samples of green Evidots. The AFM images have scale bars of 98-nm and z-ranges of 8-nm.

4-3(b), inset), the fluorescence signal shows prolonged, multi-state blinking, characteristic of multiple QDs blinking independently. However, the fluorescence is dominated by extraordinary fast and intense blinking transitions, which we refer to as “enhanced” blinking.

To examine whether enhanced blinking could arise from the independent blinking of multiple QDs, we compared the fluorescence trajectories observed when two or more isolated QDs occupied the probe region of the optical microscope simultaneously. Samples that contained predominantly individual QDs were used. When three QDs were present (Figure 4-3(c)) in or near the optical probe region, the fluorescence trajectory showed prolonged, multi-state blinking, similar to the inset of Figure 4-3(b), but no enhanced blinking was observed. When up to nine QDs were probed (Figure 4-3(d)), the fluorescence trajectory showed strong fluctuations in the fluorescence intensity, but no abrupt on/off blinking transitions. This is precisely the behavior one would expect from multiple, non-interacting QDs blinking independently.

### **4.3.3 QD Size Dependence of the Enhanced Blinking**

Another experiment we did is the particle size dependence of the enhanced blinking. The enhanced blinking behavior has also been observed in medium-sized yellow Evidots (data not shown). However, QD clusters made of the biggest red Evidots did not exhibit the enhanced blinking. Instead, only prolonged, multi-state blinking showed up, similar to Figure 4-3(c) and (d). Figure 4-4 shows the fluorescence trajectory segments (left) and photon count histograms (right) of a single QD and a QD cluster in the same QD sample

of red Evidots. This is indicative that there are no strong interactions between these bigger QDs in a cluster, which has been seen in bulky QD-bioconjugates in Chapter 3. The “off” times of the single QD, shown in Figure 4-4(a), are short and rare. Base on this result, we propose that these red Evidots may have a thick, uniform ZnS passivating shell coated on the CdSe core, which subsequently blocks or weaken the interactions between adjacent single QDs, resulted from longer distance between the energy centers of single QDs.

## 4.4 Data Analysis

### 4.4.1. On/Off Times Probability Density Distributions

Figure 4-5 are the “on” and “off” times probability density distributions,  $P[t_{\text{on}}]$  and  $P[t_{\text{off}}]$ , of the single QD and the QD cluster shown in Figure 4-3(a) and (b). Both of the particles exhibit the power-law behavior<sup>2</sup>,  $P[t] \propto t^{-m}$ . Figure 4-6 summarizes the  $m_{\text{off}}$  and  $m_{\text{on}}$  from data fittings vs. the effective volumes from AFM measurements of 7 single QDs and 11 QD clusters, as the one from which the particles in Figures 4-3(a) and (b) are observed. The classifications are made based on the particle effective volume and the patterns of the fluorescence blinking. Single QDs show prolonged, two-state on/off blinking, while the small close-packed QD clusters show both prolonged multi-state blinking and enhanced blinking. Compared with single QDs, most of QD clusters have larger values of  $m_{\text{off}}$  and  $m_{\text{on}}$ , or steeper slope in the probability density distributions. This is because enhanced fluorescence blinking behavior of small QD clusters increases the relative populations of shorter “off” and “on” periods to the prolonged two-state blinking of single QDs.

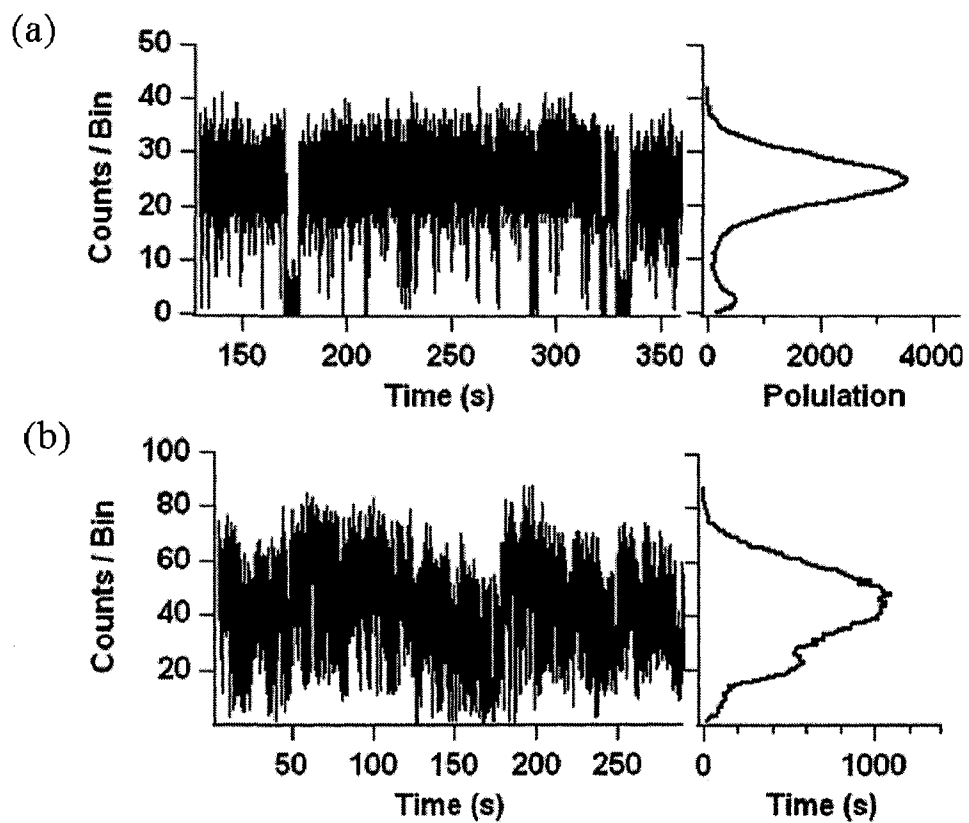


**Figure 4-4.** Fluorescence trajectory segments (left) and photon count histograms (right) of (a) a single QD with an effective volume of  $435 \text{ nm}^3$  and (b) a QD cluster with an effective volume of  $1098 \text{ nm}^3$ , in the same QD sample of red Evidots .

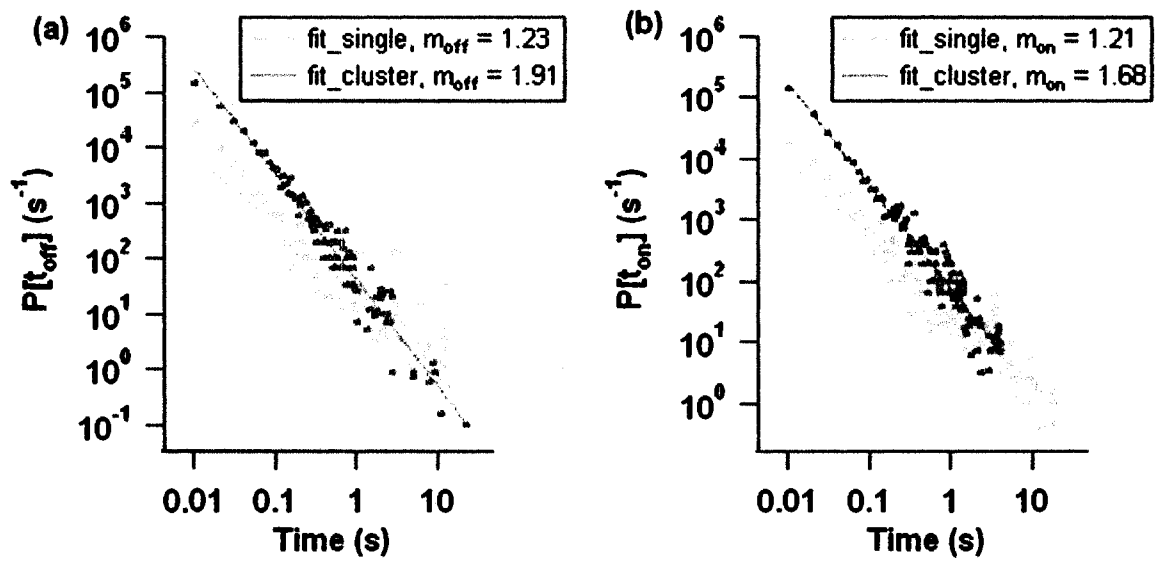


**Figure 4-5.** “off” (a) and “on” (b) time probability density distributions,  $P[t_{\text{off}}]$  and  $P[t_{\text{on}}]$ , derived from the single QD (orange) and the QD cluster (purple), shown in Figure 4-3.

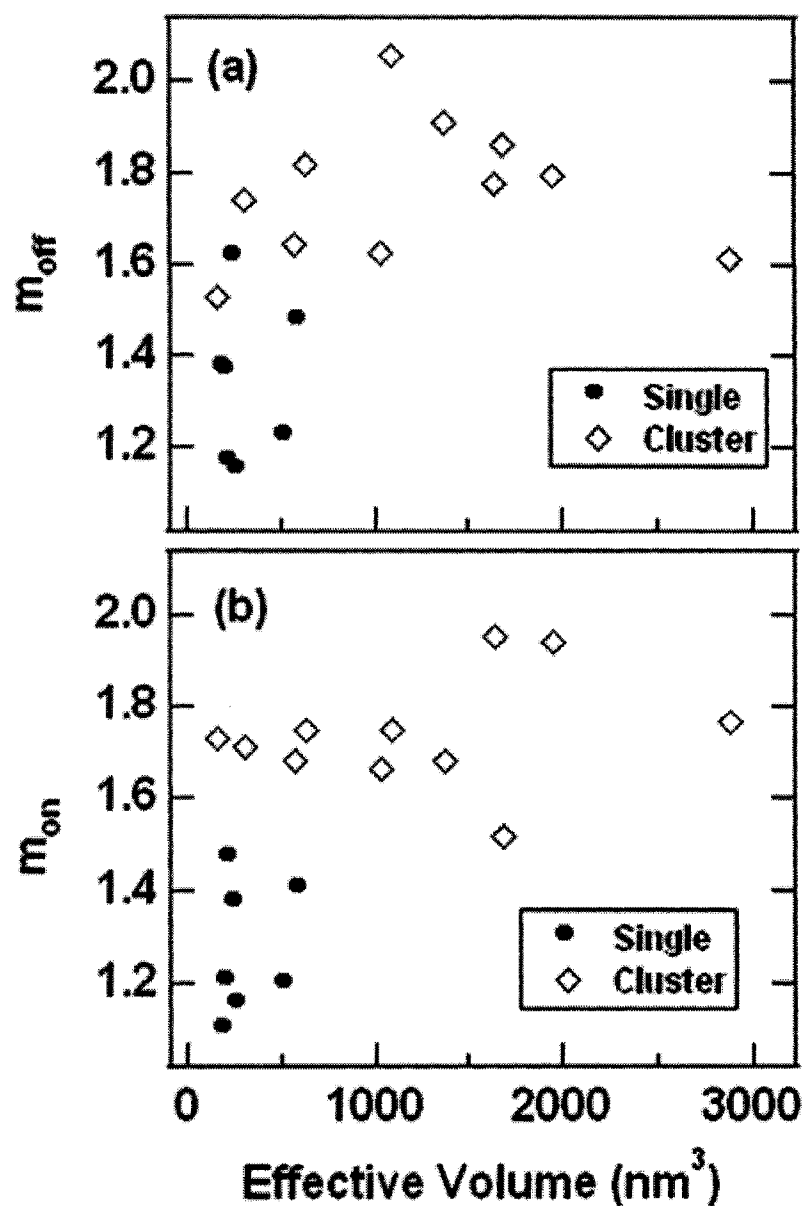


**Figure 4-6.**  $m_{\text{off}}$  and  $m_{\text{on}}$  of the power law vs. effective AFM volume for 18 particles in a QD sample of green Evidots containing a mixture of individual QDs and QD clusters. Black dots: single QDs showing slow two-state blinking; Diamonds: QD clusters showing both slow, multi-state blinking and enhanced blinking.

#### 4.4.2. Autocorrelation Analysis

We use autocorrelation analysis (See Chapter 1) of fluorescence trajectories to gain insight into the dynamics underlying the observed intensity fluctuations (Figure 4-7). For the single QD shown in Figure 4-3(a),  $g^{(2)}(\tau)$  varies slowly at shorter lagtimes due to the prolonged on- and off-time states (Figure 4-7, dash-dot line). Although the absolute decay time of the autocorrelation function depends on the observation time, as well as other factors,<sup>3,4</sup> the  $g^{(2)}(\tau)$  we measured exhibits a qualitative shape that is characteristic of individual isolated CdSe/ZnS core-shell QDs. When multiple independent particles are probed simultaneously (Figures 4-3(c) and (d)), the  $g^{(2)}(\tau)$ 's are qualitatively similar to that of the single QD. Fluorescence emission from multiple independent particles does not contribute to the decay of  $g^{(2)}(\tau)$  because the emitted photons from independent particles are not correlated in time. Only the photons emitted from the same particle are correlated. Thus, the underlying dynamics captured by  $g^{(2)}(\tau)$  characterizes the prolonged on- and off-times of the independent particles.

The autocorrelation function for the QD cluster (Figure 4-7, solid line) decays precipitously from the minimum lagtime. This behavior is fundamentally different from that of individual the isolated QDs. It shows that the rapid fluorescence intensity fluctuations observed in Figure 4-3(b) are correlated in time. This correlation function cannot be explained by the independent blinking of multiple QDs and suggests that the QDs in the cluster are not behaving as independent particles.

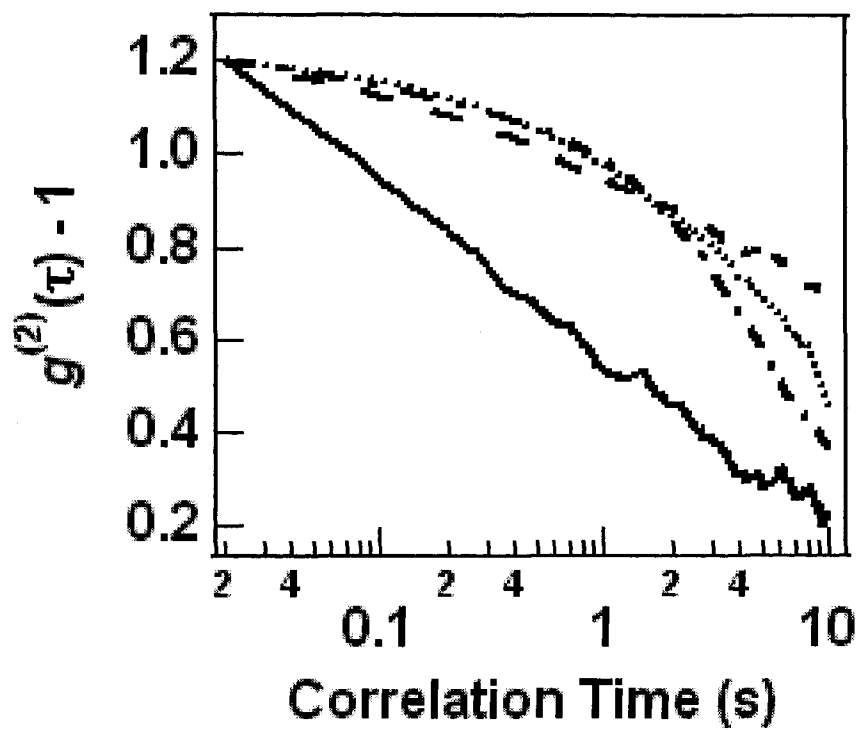


**Figure 4-7.** Normalized autocorrelation functions of the fluorescence trajectories shown in Figure 4-3. Dash-dot line: single QD; Solid line: QD cluster; Dot line: three isolated QDs; Dash line: multiple isolated QDs.

Figure 4-8 summarizes our fluorescence and AFM measurements of twenty-five particles observed from the same sample as the one described in Figures 4-3(a) and (b). The particles are classified into those showing prolonged, two-state or multi-state on- and off-blinking times (*i.e.* “normal blinking”), and those showing both normal blinking and enhanced blinking. The classifications are based on the fluorescence trajectory and autocorrelation function observed for each particle. Importantly, all particles with volumes greater than  $\sim 800 \text{ nm}^3$  exhibit enhanced blinking. The observed AFM image sizes characterize these particles as clusters containing at least two QDs. Hence, enhanced blinking is seen as a characteristic property of the QD clusters in our sample. The only particles that showed exclusively two-state blinking have effective volumes less than  $\sim 600 \text{ nm}^3$ , consistent with their identification as individual isolated QDs. A few of the enhanced blinking particles also have smaller effective volumes. These particles are thought to be smaller QD clusters that overlap with the single QD size distribution. Finally, some of the smaller particles showed multi-state blinking, but no enhanced blinking.

#### **4.4.3 Kinetics Analysis with a Hybrid MEM/NLS**

Enhanced blinking has been observed in small close-packed QD clusters, which shows a strikingly different autocorrelation function from that of single QDs. If physically meaningful parameters can be extracted from autocorrelation analysis of the blinking data, it might be interpreted in terms of the chemical kinetic rate constants of QDs coupling inside the QD clusters. However, the challenge is in identifying a detailed model of kinetics that accounts for all processes contributing to the autocorrelation

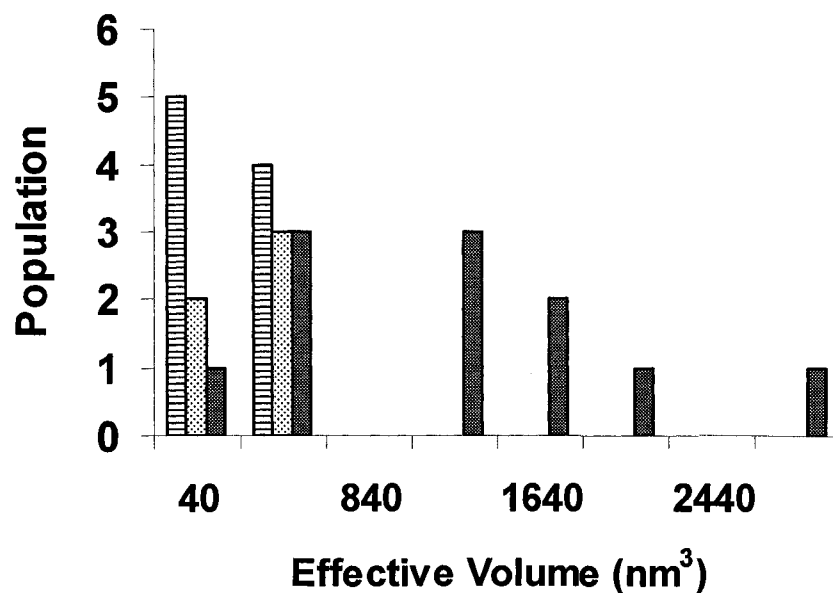


**Figure 4-8.** A bar graph histogram summarizing the blinking behavior of 25 particles in a sample of green Evidots containing a mixture of individual QDs and QD clusters, plotted vs. effective particle volume. Bars filled with horizontal lines represent particles showing exclusively two-state blinking. Bars filled with dots represent particles showing multi-state blinking with prolonged on- and off-times, but no enhanced blinking; particles showing both multi-state blinking and enhanced blinking are represented by mesh filled bars.

functions. Before such a model can be formulated, an accurate kinetic description must be obtained from the data. Fortunately, a hybrid maximum entropy method (MEM) and nonlinear-least-squares (NLS) algorithm<sup>5</sup>, programmed in a software package, so called as MemExp<sup>6</sup>, has been reported for describing accurate kinetic processes.

The software package, MemExp, accommodates kinetics measured at times  $t_i$  possessing positive and negative slopes and a slowly varying baseline, as shown in the following equation<sup>6</sup>:

$$F_i = D_0 \int_{-\infty}^{\infty} d \log \tau (g(\log \tau) - h(\log \tau)) e^{-t_i / \tau} + \sum_{k=0}^3 (b_k - c_k) (t_i / t_{\max})^k$$

where  $g(\log \tau)$  and  $h(\log \tau)$  are the lifetime distributions that correspond to decaying and rising kinetics, respectively, and a polynomial accounts for the baseline. A continuous description according to the MEM is used to guide a series of discrete NLS fits during which one exponential is added at a time. Thus, the hybrid algorithm provides an automated and objective approach to the multiple-minimum problem in NLS or ML when many kinetic processes are present. The MemExp algorithm is described in detailed in Ref. 6.

The normalized autocorrelation functions shown in Figure 4-7 of the single QD and QD cluster are analyzed with the MemExp program. Figure 4-9 shows the MemExp outputs of the corresponding fittings and lifetime distributions recovered from the fittings. Several differences are noticed from the recovered lifetime distributions in the number, the amplitudes and the time ranges of the kinetic processes. The single QD blinking has a broad peak around 10s in its recovered lifetime distribution, which is a missing kinetic

process in the QD cluster. There are more narrow kinetic peaks centered below 1s in the lifetime distribution recovered from the ACF of the QD cluster than the single QD. Moreover, the amplitudes in y axes of the lifetimes are much higher in the QD cluster. Seven fluorescence trajectories of normal blinking from single QDs and seven enhanced blinking from small QD clusters were analyzed with the MemExp program. Figure 4-10 summarizes the recovered lifetime distributions. It is clear that the differences observed are not an occasional case. They are common in all data analyzed. The peaks at the longer time range of the normal blinking are missing from the enhanced blinking. Instead, there are additional discrete kinetic processes with time range below 1s showing up in the enhanced blinking, whose amplitudes are much higher than those of normal blinking. Right now we do not know the meaning of those differences. However, it is likely that fluorescence blinking behavior of an individual QD is interfered while another one is close to it.

## **4.5 Discussion**

Our observations suggest that the QDs must be clustered together in close proximity for enhanced blinking to occur. Enhanced blinking is a transient phenomenon in which the QDs blink independently for part of the time, and then rapidly switch to an enhanced blinking state at other times. We believe this occurs when the photoexcited QDs in the cluster become electronically coupled. At present, we can only speculate as to the nature of this coupling. One possibility is that off blinking of one QD in the cluster produces an externally trapped electron that can interact with a neighboring QD. This trapped

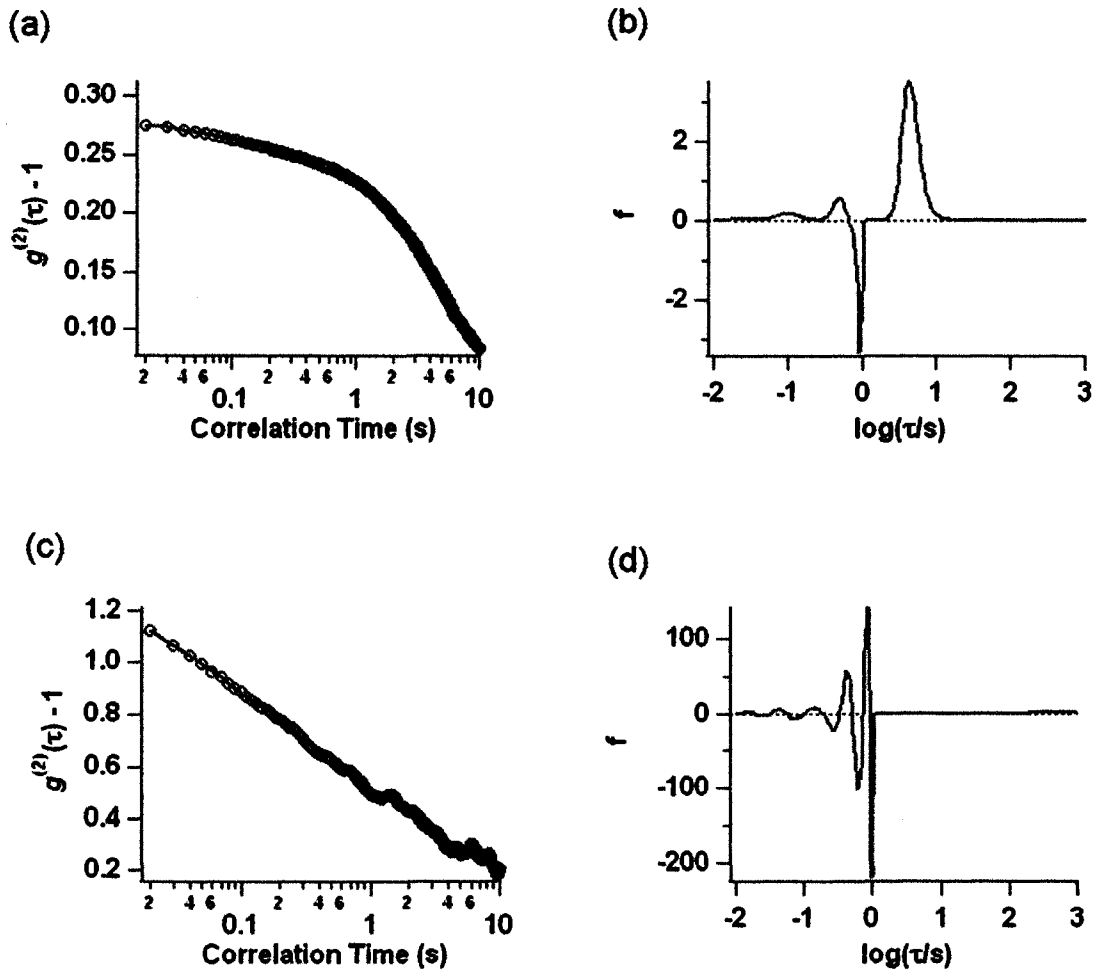


**Figure 4-9.** MemExp output. (a) Autocorrelation function of the *single QD* (black circles) shown in Figure 4-3 and the corresponding fitting (red solid); (b) Lifetime distribution recovered from the fitting in (a). (c) Autocorrelation function of the *QD cluster* (black circles) shown in Figure 4-3 and the corresponding fitting (red solid); (d) Lifetime distribution recovered from the fitting in (c).

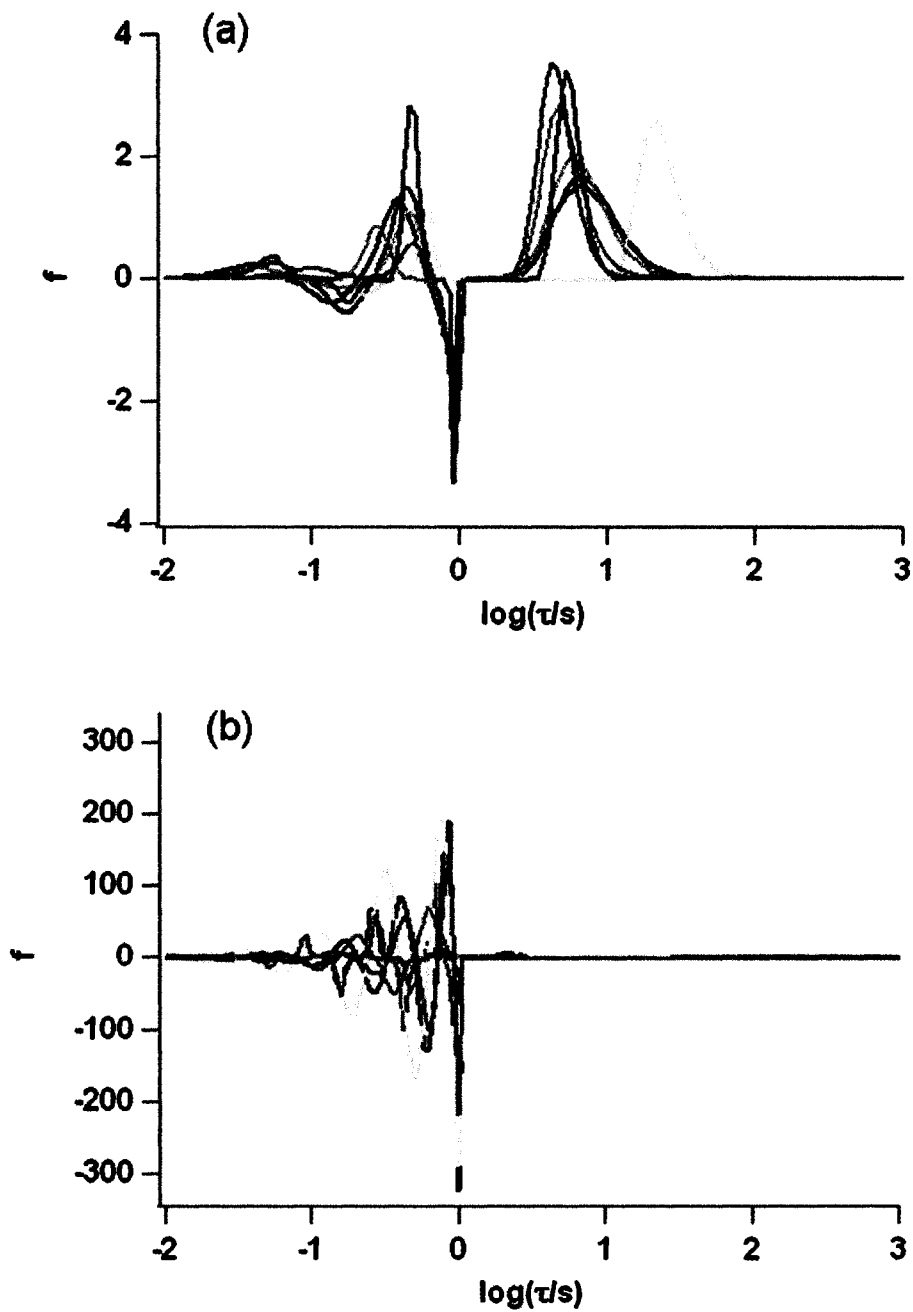


**Figure 4-10.** MemExp outcomes of the lifetime distributions recovered from the autocorrelation functions of (a) seven single QDs and (b) seven small close-packed QD clusters.

electron may alter the electronic environment of the neighboring QD in a way that enhances its fluorescence properties. The enhancement effect is transient, perhaps due to the mobility of the trapped electron, but it raises the average fluorescence intensity of the QDs over time. This could be the basis for the PFE phenomenon, which occurs in closed-packed QD films, and is believed to be caused by the build-up of trapped electrons upon continuous photoexcitation.<sup>7-10</sup> The trapped electrons enhance the fluorescence properties of the remaining neutral QDs in the film by some mechanism that is still not fully understood. Our experiment may be probing an analogous PFE process that occurs at the level of the individual QDs.

## **4.6 Conclusion**

In summary, individual, isolated QDs and QD clusters are analyzed using the correlated single molecule fluorescence spectroscopy and AFM. The individual QDs show characteristic prolonged on- and off- blinking times. The blinking behavior is additive when multiple isolated QDs are probed simultaneously. The QD clusters exhibit enhanced blinking that is believed to arise from collective interactions of the QDs in the cluster. One possible explanation for this observation could be that off state of one QD produces a trapped electron that can enhance the fluorescence properties of the neighboring QDs.

## References:

1. Murray CB, Norris DJ, Bawendi MG: Synthesis and Characterization of Nearly Monodisperse Cde (E = S, Se, Te) Semiconductor Nanocrystallites. *Journal of the American Chemical Society* **1993**, 115:8706.
2. Kuno M, Fromm DP, Hamann HF, Gallagher A, Nesbitt DJ: Nonexponential "blinking" kinetics of single CdSe quantum dots: A universal power law behavior. *Journal of Chemical Physics* **2000**, 112:3117.
3. Messin G, Hermier JP, Giacobino E, Desbiolles P, Dahan M: Bunching and antibunching in the fluorescence of semiconductor nanocrystals. *Optics Letters* **2001**, 26:1891.
4. Verberk R, Orrit M: Photon statistics in the fluorescence of single molecules and nanocrystals: Correlation functions versus distributions of on- and off-times. *Journal of Chemical Physics* **2003**, 119:2214.
5. Steinbach PJ, Ionescu R, Matthews CR: Analysis of kinetics using a hybrid maximum-entropy/nonlinear-least-squares method: Application to protein folding. *Biophysical Journal* **2002**, 82:2244.
6. <http://cmm.cit.nih.gov/memexp/doc/>
7. Kimura J, Uematsu T, Maenosono S, Yamaguchi Y: Photoinduced fluorescence enhancement in CdSe/ZnS quantum dot submonolayers sandwiched between insulating layers: Influence of dot proximity. *Journal of Physical Chemistry B* **2004**, 108:13258.
8. Maenosono S: Monte-Carlo simulations of photoinduced fluorescence enhancement in semiconductor quantum dot arrays. *Chemical Physics Letters* **2005**, 405:182.
9. Maenosono S, Dushkin CD, Saita S, Yamaguchi Y: *Jpn J Appl Phys, Part 1* **2000**, 39:4006.
10. Uematsu T, Maenosono S, Yamaguchi Y: Photoinduced fluorescence enhancement in CdSe/ZnS quantum dot monolayers: Influence of substrate. *Applied Physics Letters* **2006**, 89:031910.

## **Chapter 5**

# **Distinguishable Difference in PL between Enhanced and Normal Blinking**

We monitor the emission wavelength of the isolated small close-packed QD clusters possessing the enhanced blinking pattern observed in Chapter 4. The emission wavelength of the high intensity regime in the enhanced blinking is red shifted relative to that of the lower intensity regime. We propose that red-shifting in emission is one of the characteristics of electronic coupling within the QD clusters. The electronic coupling might be the temporal coupling of instant electric fields generated by charges on the single QDs composing the cluster when they are dark or charged. The instant net electric field drives charge carriers of the emitters away from trap states and decreases the confinement of the emitters, which results in red-shifted emission of high intensity

regime. Because both the temporal electric field and emitter are changing randomly, fast and intense fluorescence blinking is resulted.

## 5.1 Introduction

In the previous work, we observed enhanced fluorescence blinking pattern from isolated small close-packed QD clusters<sup>1</sup>, which is strikingly different from the blinking behaviors of individual QDs or multiple noninteracting single QDs. We speculated that the enhanced blinking pattern composed of noncoupled normal blinking and coupled enhanced blinking. As to how the single QDs interact with each other and what triggers the QD coupling, there are no clear answers yet, which need further investigations. Towards that direction, our first step is to monitor the fluorescence emission wavelength of the isolated small close-packed QD clusters. This idea is inspired by the spectral diffusion of single QDs<sup>2</sup> and the fact that the electronic coupling in several known phenomena do give the characteristic of photoluminescence (PL) shifting in ensemble measurements, such as fluorescence resonance energy transfer (FRET)<sup>3</sup>, quantum confined stark effect (QCSE)<sup>4</sup>, and Dexter electron transfer<sup>5</sup>. To detect and compare PL positions of independent and coupling fluorescence blinking of isolated QD clusters, the experimental setup with two synchronous detecting channels is employed. The total PL emission from a QD cluster is split equally first, then filtered and focused into two detectors. With different filters in the detecting pass, certain wavelength ranges can be extracted out of the total emission of the cluster. Surprisingly, a difference in emission position between normal and enhanced blinking is observed. When the enhanced

blinking in a fluorescence trace shows up, it is accompanied with a red-shifted emission position compared to that of the normal blinking.

## **5.2 Experimental Section**

### **5.2.1 Instrumentation**

Individual QDs and QD clusters are analyzed using the two-detector setup (See Figure 5-1) of the spatially correlated single molecule fluorescence spectroscopy/AFM method is used in this chapter to study fatherly the enhanced blinking of small close-packed clusters of the QD nanocrystals. Different from that in the single-detector setup (See Chapter 2 for details), in the two-detector setup, the collected fluorescence is focused onto two single photon counting avalanche photodiode detectors (APDs) (PerkinElmer Optoelectronics, model SPCM\_AQR\_14, Wellesley, MA). By changing the optical filters in front of the individual detectors, we can selectively detect emission photons of certain wavelength range. All particles studied in this chapter are, except mentioned, exposed to a laser illumination intensity of  $139\text{-W/cm}^2$  during fluorescence data acquisition.

### **5.2.2 Sample Preparation**

QD nanocrystals are yellow Evidots (See Chapter 4 for details) of 3.2 nm CdSe colloidal nanoparticles, capped with inorganic ZnS shell and trioctylphosphine/trioctylphosphine oxide (TOP/TOPO) as stabilizing ligands. QD samples dissolved in toluene at  $\sim 40\text{-}\mu\text{M}$  were purchased from Evident Technologies (Troy, NY). Small QD

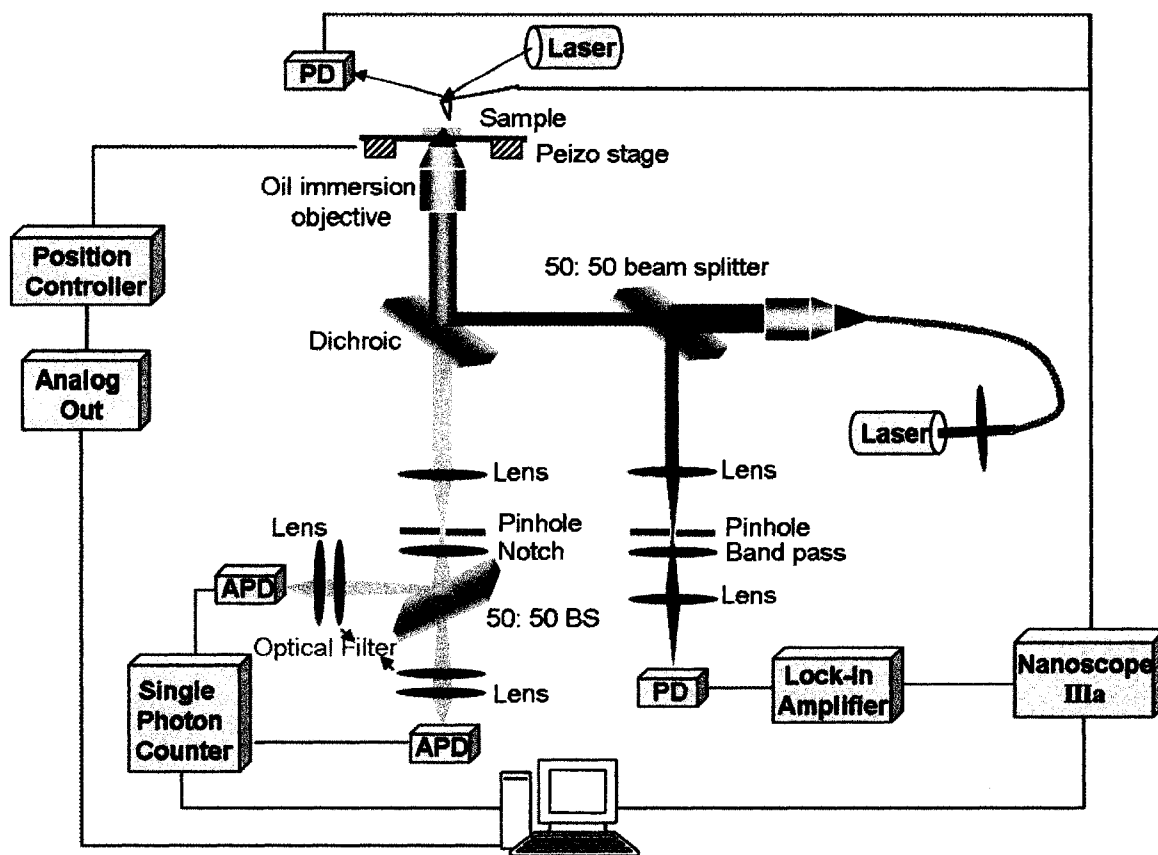


**Figure 5-1.** The two-detector setup of the spatially correlated single molecule fluorescence / AFM. PD1, AFM feedback detector; PD2, Si photodiode detector; APD, avalanche photodiode detector; BS, band pass filter.

clusters are formed by treating ~1-mL of ~0.3-nM QDs diluted in hexane with a few microliters of methanol, and allowing the solution to stand for ~15 min. Methanol raises the polarity of the solvent, causing aggregation of the QDs by association of the hydrophobic ligands.<sup>6</sup> The degree of aggregation can be controlled by adjusting the QD and methanol concentrations and the incubation time. Following incubation, ~100- $\mu$ l of the solution are spin cast onto a AP-mica cover slip to disperse the particles for subsequent fluorescence and AFM analysis in ambient air.

Figure 5-2 shows the PL spectrum of yellow Evidots from the ensemble measurement and the transmission spectra of optical filters in front of detectors involved in this study. The PL emission peak of the single QDs is centered at 580-nm, shown with a black dotted curve. The transmission spectra of the 650 nm short pass (SP), 605/40 nm band pass, 565/40 nm band pass and 590/40 nm band pass filters (BPs) are represented as black, blue, green and orange solid curves, respectively. In the two-detector experimental setup, one detecting channel is always modified with the 650 nm SP to collect photons of all wavelengths, while the other channel detects selectively the photons of a specific range of wavelength, which can pass through the narrower band pass filters of 605/40 nm, 565/40 nm or 590/40 nm BPs. As we can see, the 560/40 nm BP covers more than 50% of the PL emission spectrum of the single QDs on the shorter wavelength side or blue side, while the 605/40 nm BP monitors almost the rest of the spectrum of the longer wavelength or red side.

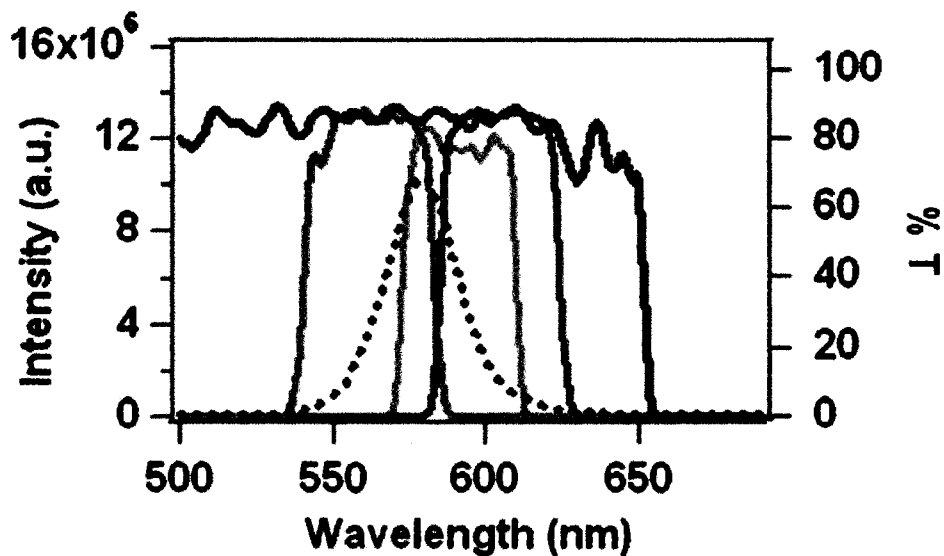


**Figure 5-2.** Black dotted line: PL spectrum of the single yellow Evidots, centered at 580 nm; Black solid line: transmission spectrum of the 650 nm short pass filter (SP); Blue: transmission spectrum of the 605/40 nm band pass filter (BP); Green: transmission spectrum of the 565/40 nm band pass filter (BP); Orange: transmission spectrum of the 590/40 nm band pass filter (BP).

## 5.3 Results and Observations

### 5.3.1 Emission Wavelength of the Small QD Clusters

The 605/40 nm BP and 650 nm SP filters were used to modify the synchronous detecting channels. The 650 nm SP monitored the total fluorescence signals while the 605/40 nm BP detected partial photons possessing longer wavelengths, as introduced in the Experimental Section. The approximate portion of photons in the longer wavelength range can be extracted out of the total emission by comparing fluorescence trajectories obtained from two channels side by side.

Figure 5-3 shows the experimental result of a small QD cluster exhibiting enhanced blinking pattern. Figure 5-3(a) is the entire fluorescence trajectory continuously collected for up to 800 s under the constant laser excitation. The black trace is collected from the detecting channel modified by the 650 nm SP, which contains the photons of all wavelengths. The blue trace represents the fluorescence signals collected by the other detecting channel modified by the 605/40 nm BP that allows only the photons of longer wavelengths to pass. Three facts are noticed from Figure 5-3(a). Firstly, the shapes or patterns of the fluorescence trajectories from the two detecting channels are similar before 200 s. In another word, the wavelength ranges of the majority of the photons, from both normal and enhanced blinking were within that of the 605/40 nm BP initially. Secondly, under continuous radiation, the discrepancy in the two fluorescence traces is getting bigger and bigger. Figure 5-3(b) and (c) are fluorescence trajectories segments and their corresponding photon counting histograms of the first (labeled with i) and the last (labeled with ii) 200 s of blinking traces shown in Figure 5-3(a), from which the

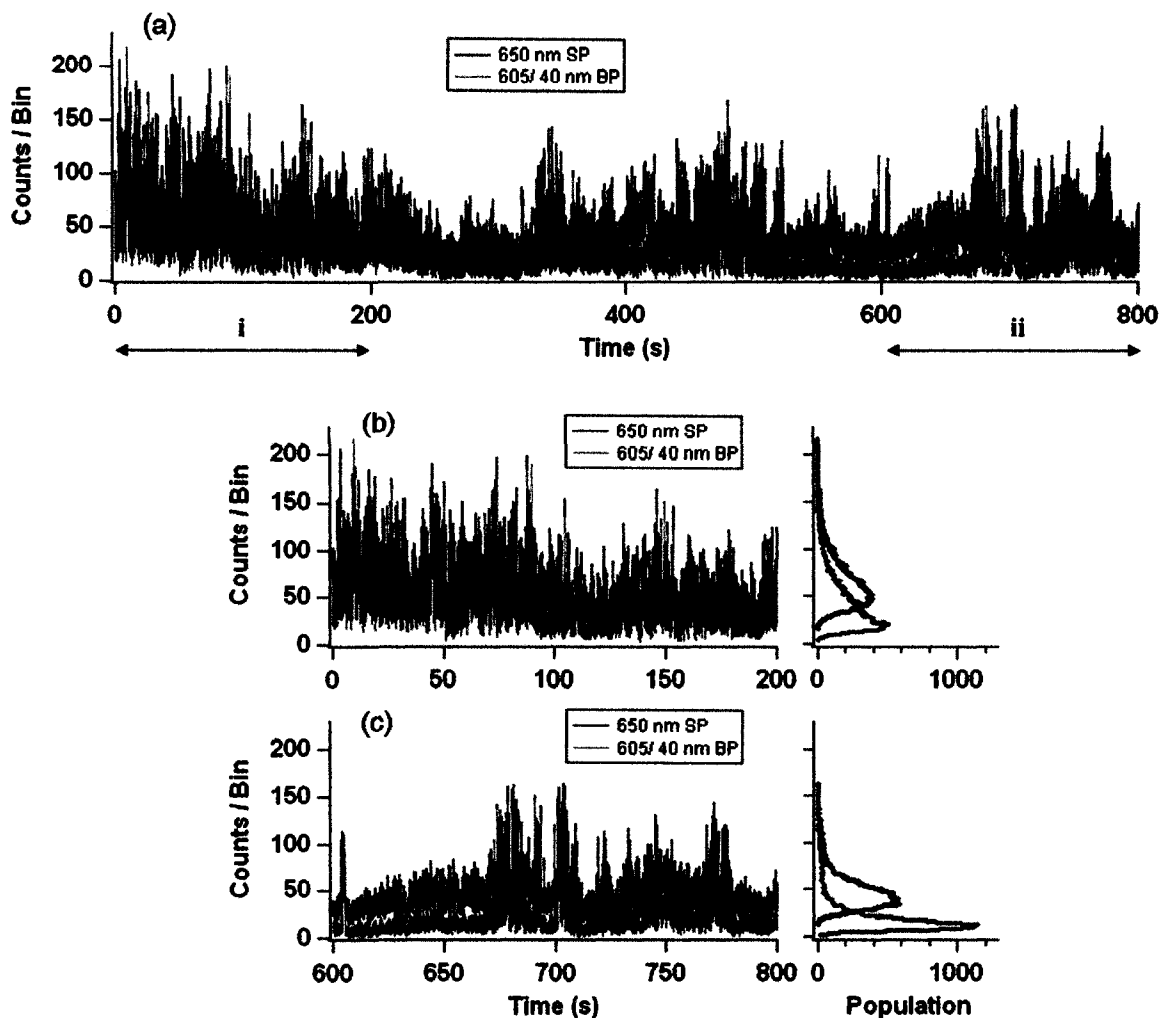


**Figure 5-3.** Fluorescence trajectories of a QD clusters under the constant laser excitation. Black: fluorescence signals in the 650 nm SP detecting channel; Blue: fluorescence signals in the 605/40 nm BP detecting channel. (a) The entire continuous fluorescence signals collected for up to 800 s. (b) The fluorescence trajectory segment (left) and the corresponding photon counting histogram (right) of part i in (a). (c) The fluorescence trajectory segment (left) and the corresponding photon counting histogram (right) of part ii in (a).

difference of blinking patterns from two detectors is further emphasized. Thirdly, distinguishable difference in fluorescence blinking trace between two detecting channels is observed, as shown in Figure 5-3(c). The fluorescence traces match with each other only at the regime of high fluorescence intensity (enhanced blinking)<sup>1</sup>. Most of the photons from enhanced blinking emission have wavelengths within the range of the 605/40 nm BP because what had been detected in both channels was very close. For the lower intensity regime (normal blinking)<sup>1</sup>, the fluorescence signals in the 650 nm SP channel are much higher than those in the 605/40 nm BP channel. Most of the photons from the normal blinking emission are blocked by the 605/40 nm BP. This suggests there is a difference in emission wavelength between the enhanced blinking and normal blinking.

The PL spectrum of the ensemble single QDs is centered at 580 nm. The emitted photons of the QD cluster in both normal blinking and enhanced blinking of the fluorescence trajectory were detected by the 605/40 nm BP initially, especially before 200 s in the blinking trace. This suggests that the PL emission of the QD cluster was red shifted relative to that of the ensemble single QDs. We speculate that Förster resonance energy transfer (FRET) was happening within the QD cluster, which resulted in the initial red shifted emission of the QD cluster. It has been reported that PL spectrum of ensemble single QDs shifts to shorter wavelength under continuous radiation, which is called bluing.<sup>7, 8</sup> Therefore, bluing might be the reason for the changing of blinking traces from Figure 5-3(b) to (c). If the two hypotheses were what really occurred in the QD cluster, the PL emission of the QD cluster in the enhanced blinking would have longer

wavelength range than that in the normal blinking, concluded with the aid of the two hypotheses. The hypothetic procedure would be as following. The QD cluster was one of those which had a red-shifted PL emission compared with that from the ensemble measurement of single QDs. Most of the emission was passed through the 605/40 nm BP and collected by the detector. While bluing was happening under continuous illumination, the cutting edge of the 605/40 nm BP on the shorter wavelength side would function as a filter to distinguish the normal and enhanced emission if there was a difference existing. Therefore, the enhanced emission had a longer emission wavelength relative to that of the normal emission. To verify the two hypotheses, further investigation was performed. Both hypotheses were proved to plausible.

### **5.3.2 Initial PL Positions of Isolated QD Clusters**

Here, PL emission of an isolated QD cluster is referred to the photons from its “on” states within a photon collecting window. Still, the 650 nm SP always monitors the total fluorescence signals in one detecting channel. The other detecting channel is modified either by the 605/40 nm BP to detect the photons within the longer wavelength range, or by the 565/40 nm BP to detect the photons of shorter wavelengths. The approximate portion of photons in a certain range of wavelengths can be extracted out of the total emission by comparing fluorescence trajectories obtained from the detecting channels.

A number of QD clusters have been examined. For those QD clusters which exhibit the enhanced blinking pattern, their PL emission wavelengths within the photon collecting windows are concluded into three groups, two of which are presented by their

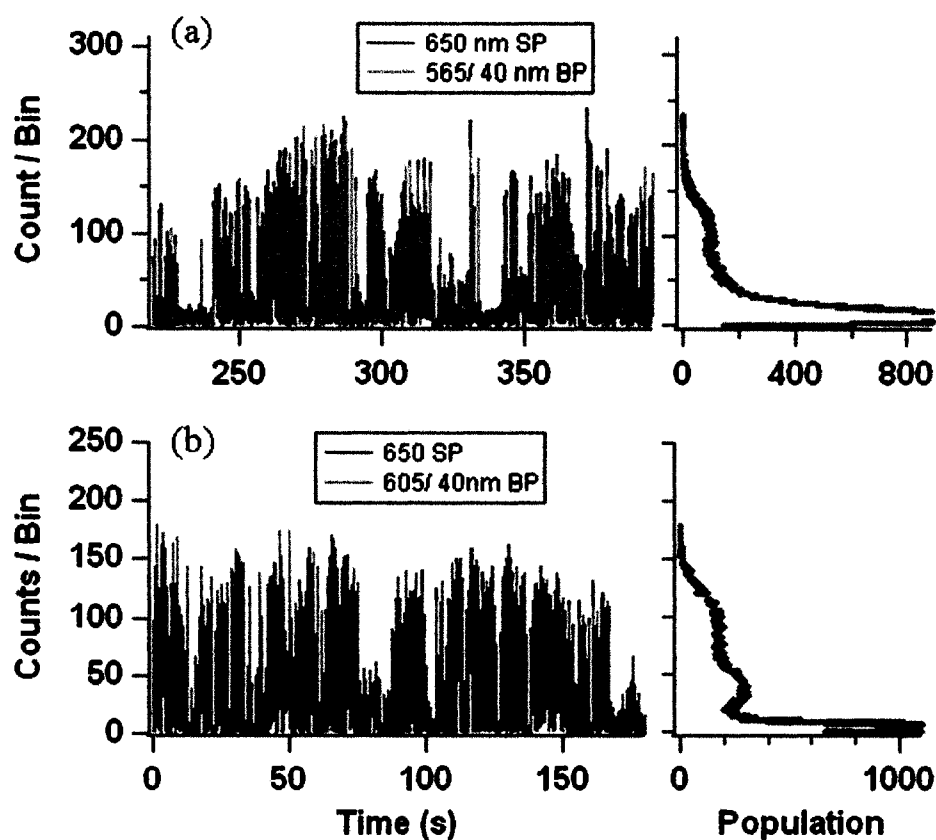


**Figure 5-4.** Fluorescence trajectory segments (left) and the corresponding photon counting histograms (right) of two different QD clusters in the same sample. Each panel representing a different QD cluster has two colored fluorescence traces and their photon counting histograms. Multiple colors help to distinguish fluorescence signals detected from different detecting channels modified with 650 nm SP (black) in one channel and either 565/40 nm BP (green) or 605/40 nm BP (blue) in the other channel.

typical examples in Figure 5-4(a) and (b), respectively. For each QD cluster there are two colored fluorescence traces and the corresponding photon counting histograms. Multiple colors help to distinguish fluorescence signals detected from two synchronous detecting channels modified with 650 nm SP (black) in one channel and either 605/40 nm BP (blue) or 565/40 nm BP (green) in the other channel. In Figure 5-4(a), with the combination of 650 nm SP and 565/40 nm BP, fluorescence signals from the two detecting channels matched each other perfectly, confirmed by the photon counting histogram. This type of QD clusters emitted photons, almost all of which passed through the 565/40 nm BP. This resulted in twin-like fluorescence trajectories and photon counting histograms for two different detecting channels. Figure 5-4(b) shows the second kind of QD clusters that emitted photons with longer wavelengths. The fluorescence trajectory from the channel modified by the 650 nm SP dovetailed with that from the other channel modified by the 605/40 nm BP. Most of the photons have the wavelengths which are covered by the 605/40 nm BP. The third group of the QD clusters have the PL emission wavelength range that contributes partially to both the 565/40 nm BP and 605/40 nm BP (data not shown).

Based on the types of QD clusters shown in Figure 5-4, we analyzed the photoluminescence emission positions and the particle effective volumes of 18 QD clusters, which are summarized in Figure 5-5. Black bars represent the same QD clusters as that shown in Figure 5-4(a). They emit fluorescence with shorter wavelength domination and most of the QD clusters have the effective volumes smaller than 1100 nm<sup>3</sup>. Gray bars represent the same QD clusters as that shown in Figure 5-4(b), whose

emission dominates the red side of the spectrum and effective volumes are bigger than  $1100 \text{ nm}^3$ . The result in Figure 5-5 agrees with FRET reported happening in 1-D homogeneous CdTe QD chains in the ensemble measurement<sup>9</sup>. FRET is triggered by the gradient of energy domain, which is characterized by the red shifted PL. The size distribution of homogeneous single QDs products in market today can be as low as 5%, which, however, is large enough to build up different energy domains in the QD chains or clusters close-packed with these single QDs. The more the single QDs forming the cluster, the bigger the chance it is that various QDs with different sizes are inside the cluster. Consequently, it is more likely to build up different energy domains inside the relatively bigger QD cluster, which facilitates FRET and results in the overall emission red shifting. An important point need to be mentioned here is that it seems FRET has nothing to do with the enhanced blinking because both types of QD clusters shown in Figure 5-4 exhibited the enhanced blinking pattern.

### **5.3.3 Bluing of Individual QDs and Small QD Clusters**

People have reported that under continuous radiation in air, photoluminescence from single QDs shifts to blue.<sup>7,8</sup> This is the result of increased confinement of QDs caused by photooxidation of outer layers of the QDs by  $\text{O}_2$  in air. Single QDs bluing is also observed in our study. Figure 5-6 shows the fluorescence trajectory of multiple isolated individual QDs near the probe region, which exhibits the multiple-level normal blinking. The laser was kept on through the entire data collecting period. Fluorescence signals were recorded right after the laser was turned on. To increase the bluing process, doubled excitation power of about  $280 \text{ W/cm}^2$  was used. Still, 650 nm SP was used in

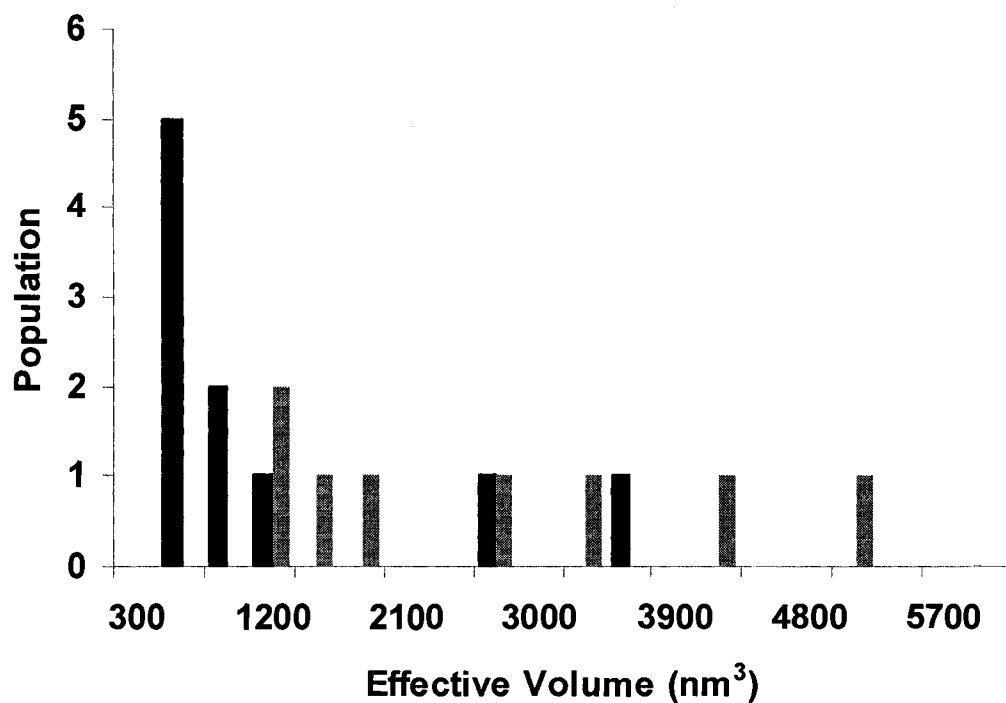


**Figure 5-5.** A bar graph histogram summarizing PL position of 18 QD clusters in the same sample, plotted vs. effective particle volume. Black bars represent QD clusters giving off the photons with the wavelength mainly in the range of 565/40 nm BP. Gray bars represent QD clusters giving off the photons with the wavelength mainly in the range of 605/40 nm BP.

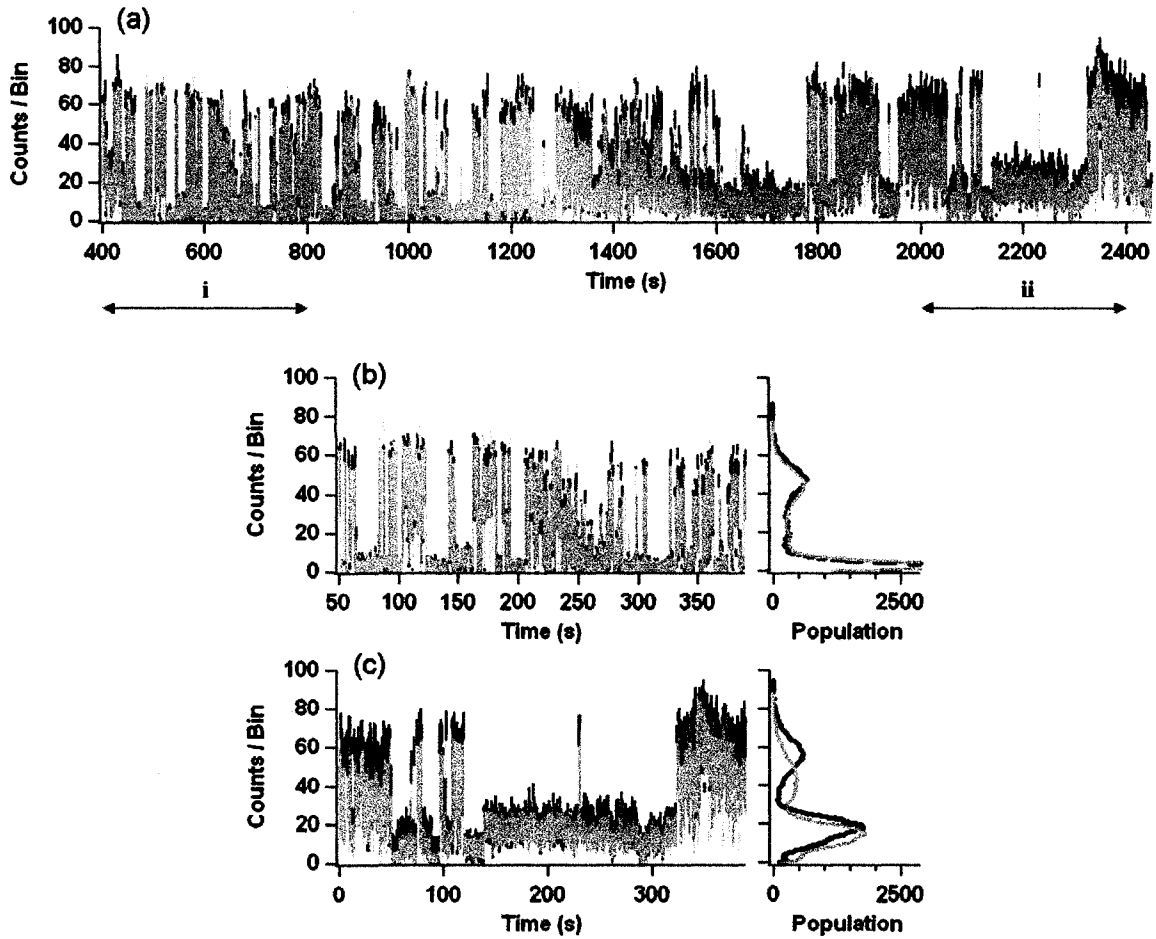


**Figure 5-6.** Fluorescence trajectories of multiple isolated single QDs, up to 3, near the probe region, under the excitation power of about  $280 \text{ W/cm}^2$ . To accelerate the bluing process, the double excitation power was used. Black: fluorescence signals in the 650 nm SP detecting channel; Orange: fluorescence signals in the 590/40 nm BP detecting channel. (a) The entire continuous fluorescence signals collected for up to 2500 s. (b) The fluorescence trajectory segment (left) and the corresponding photon counting histogram (right) of part i in (a). (c) The fluorescence trajectory segment (left) and the corresponding photon counting histogram (right) of part ii in (a).

one detecting channel to collect photons with all emission wavelengths. Since the emission of ensemble single QDs is centered at 580 nm, the other detecting channel was modified by the 590/40 nm BP (See Figure 5-2). It can be seen that the emission of both lower and higher intensity levels were shifting out of the 590/40 nm BP, which is very different from what has been shown in Figure 5-3.

We would also like to know whether the bluing phenomenon happens in isolated QD clusters and applies to both normal and enhanced blinking. Figure 5-7 shows several fluorescence trajectory segments and the corresponding photon counting histograms of the same QD cluster under continuous radiation with a constant excitation power of 139 W/cm<sup>2</sup>. Figure 5-7(a) is the detected signals of 400 s right after the laser was turned on and Figure 5-7(b) is the data of another 450 s after about 10 min continuous laser illumination. Still, the black trajectory represents data obtained from the detecting channel equipped with the 650 nm SP, while blue for the data obtained from the other detecting channel equipped with the 605/40 nm BP (See Figure 5-2 as a wavelength position reference). Under continuous laser radiation blue and black fluorescence traces shown in Figure 5-7(b) do not match as well as in Figure 5-7(a). The 650 nm SP detecting channel has almost the same fluorescence blinking signal, whereas both normal and enhanced blinking are diminishing from the 605/40 nm BP channel. This means emission wavelengths from the QD cluster shifted mainly out of the range of 605/40 nm BP upon excitation. To verify that fluorescence from the QD cluster was

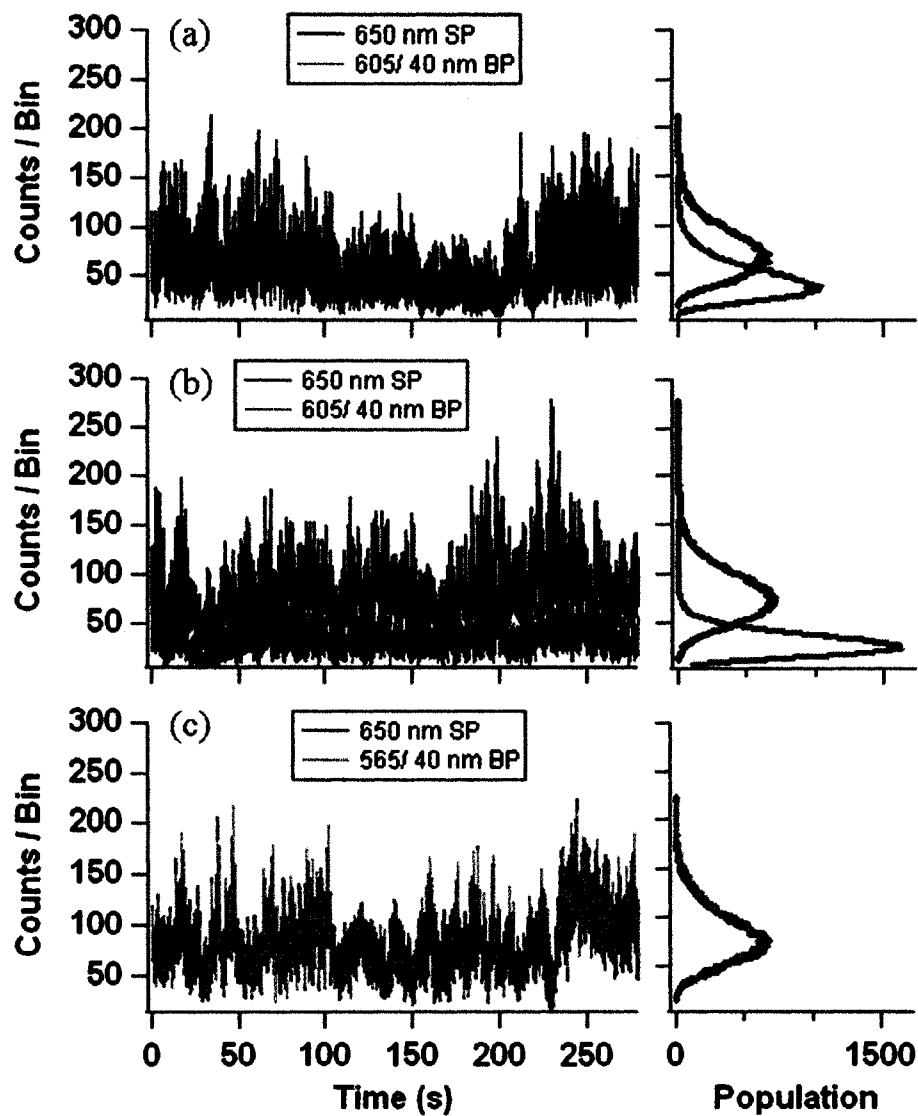


**Figure 5-7.** Fluorescence trajectory segments (left) and corresponding photon counting histograms (right) from the same QD cluster (a) right after, (b) after about 10 min, and (c) after about 20 min the laser was on. Black: the fluorescence signal obtained from the detecting channel equipped with the 650 nm short pass filter (SP). Blue: the fluorescence signal obtained from the channel equipped with the 605/40 nm band pass filter (BP). Green: the fluorescence signal obtained from the channel equipped with the 565/40 nm band pass filter (BP).

bluing, we replaced the 605/40 nm BP with the 565/40 nm BP in the detecting channel to continue to collect fluorescence signals, whose detected result is presented as green fluorescence trace in Figure 5-7(c). Clearly, fluorescence traces (containing both normal and enhanced blinking) detected by both photon detecting channels match each other perfectly, which implies that both normal and enhanced blinking in blinking traces of the QD cluster were bluing upon laser radiation. Most importantly, enhanced blinking pattern of the QD cluster was not interrupted while the emission of the cluster was blue-shifting. The bluing phenomenon was repeatedly observed from other QD clusters examined, which suggests bluing in QD clusters is not an occasional phenomenon.

## **5.4 Discussion**

The two assumptions of FRET and bluing are proved in the QD clusters possessing enhanced blinking. Moreover, the enhanced blinking happening in the QD clusters is not interrupted by FRET and bluing. Therefore the enhanced blinking has longer or red-shifted wavelength than that of normal blinking in the clusters. We also observed this difference repeatedly in several other QD clusters. However, the nature of this phenomenon is not clear. It can not be ruled out that this emission position difference happens only in a fraction of QD clusters possessing the enhanced fluorescence blinking pattern. However, it is the semblance of certain electronic coupling which results in the enhanced blinking and could drop a hint for the secret of enhanced blinking.

There are multiple emitters in a QD cluster exposed to light, whose number and role are varying with time. When individual single QDs inside the cluster act independently

or are coupled very weakly, PL of the QD cluster is the sum emission of the independent emitters at the moment, which gives the normal blinking of a multiple step style in the fluorescence trajectory. At a certain moment when conditions for electronic coupling are satisfied, strong electronic coupling is formed within the cluster, resulting in the enhanced blinking. This alters the representations of its detectable properties, such as the emission wavelength. When the union is broken, the enhanced blinking pattern switches back to normal blinking. In this study, we believe the change of emission wavelength before and after the electronic coupling, corresponding to normal and enhanced blinking is observed in this study. It has been mentioned in the introduction section that there are several existing electronic coupling mechanisms that give red-shifted PL spectrum, such as, FRET and Stark effect. Can the known mechanisms explain the red-shifted enhanced blinking?

We doubt that FRET is among the chief causes of enhanced blinking. In FRET, the total intensity of the cluster would not exceed the sum of the emission of the independent emitters in a QD cluster. This would not explain the appearance of spikes of the enhanced blinking in blinking traces, whose intensity is several times higher than that of the maximum “on” state of the normal blinking. Moreover, we observed enhanced blinking repeatedly in small homogeneous QD clusters, where FRET is not likely to happen strongly. Therefore, FRET is not crucial for triggering the enhanced blinking behavior of the QD clusters. As known, red shifted PL spectrum is one of the characteristics of QCSE.<sup>4, 10, 11</sup> People have reported that the existing of extra electronic potential from separated excitons enhanced the emission of nearby particles.<sup>12</sup> Based on

these two observations, we propose the following hypothetical model to explain the red-shifted enhanced blinking of the QD clusters.

The red-shifted enhanced blinking of a QD cluster is caused by the formation of emitter(s) affected by a temporal maximum oriented electronic field within the cluster. Before we dig into the details, let us trace back to the cause for single QD blinking a little bit. A well accepted mechanism for single QDs blinking is the forming and vanishing of extra charges in the QD core.<sup>13, 14</sup> It has been suggested a neutral QD is in its bright state and a charged in its dark state. The charged QD is created if one of the carriers is ejected into a trap state either in or near but outside the QD, leaving behind a counter charge in the QD. Subsequent photogenerated excitons recombine non-radiatively through Auger recombination, in which the excitons transfer their energy to the charge. Therefore, followed along with each “off” state in a blinking event, an electric field is produced, with the power  $\sim 10^5$  V/cm,<sup>4</sup> big enough to take effect on the nearby QDs. In a QD cluster, there are multiple individual single QDs, which are possible bright, dimmer or dark ones<sup>15-17</sup>. An electric field can be generated inside a QD cluster, which is contributed by the separated electron-hole pairs when fluorescence of single QDs turn off and/or charges in dark and dimmer QDs. Each single QD in a cluster is adjacent to several others, consequently, experiencing an instant net external electronic field produced by the nearby QDs. Instead of static, the electric field produced at any moment is varying, because number of emitters and role of single QDs inside a cluster are unfixed. For example, at one moment QD1 is an emitter and QD2 is one of the electric field generators, while at the other moment their parts can totally exchange. Even the instant

temporal electric field generated by the same single QD is not constant because of its varying charge density and distribution<sup>4</sup> or the fluctuation of electronic states<sup>18</sup>. As a result, the direction and power of the temporal net electric field produced in a QD cluster is varying with time.

We have suggested that instant temporal local maximum electric field can influence the nearby emitter(s) and give rise to the red-shift emission. But how is the electric field related to the enhanced blinking? It has been reported that the emission of QDs could be enhanced<sup>12</sup> or quenched<sup>19</sup> by an electric field produced from the blinking of other QDs<sup>12</sup> or applied external electric field<sup>19</sup>. In another word, an electric field can influence the going direction of the excited charges (electron or hole) upon excitation. Therefore, we suggest that besides spectral shifting, electric fields can also enhance the fluorescence blinking behavior. At one moment, the dark QDs produces a electric field that keeps the excited charges of its nearby emitters away from the trap, increases the possibilities of the emitters being bright in each photon collecting window, and enhances its emission. At another moment, a different temporal electric field can quench the fluorescence by decrease the frequency of this QD being bright. Different electric fields at different moments result in different degrees of fluorescence enhancing or quenching. Consequently, fast, intense changing of fluorescence emission of the QD cluster gives the enhanced blinking. The highest intensity might be due to the moment when the highest population of emitters is kept away from the trap states, which decreases the frequency of being dark and subsequently give the highest intensity.

## 5.5 Conclusion

In summary, distinguishable emission positions between normal and enhanced blinking in the fluorescence trajectory of a QD cluster has been observed in this study. The emission of enhanced blinking is red shifted relative to that of normal blinking. We propose electronic coupling might be responsible for it. The electronic coupling actually is the coupling of electric fields temporally generated by the single QDs composing the cluster when they are dark or charged. When the instant temporal net maximum electric field drive the excited charges of emitters inside the cluster away from the trap states, the possibilities of being dark of the emitter(s) decreases and the emitted photons in unit time increases, accompanied by red shifting emission. Because both the temporal electric field and emitters are changing randomly, fast and intense switching in fluorescence emission is resulted, which gives the enhanced blinking patten in the fluorescence trace of a QD cluster.

## References:

1. Yu M, Van Orden A: Enhanced fluorescence intermittency of CdSe-ZnS quantum-dot clusters. *Physical Review Letters* **2006**, 97:237402.
2. Gomez DE, Califano M, Mulvaney P: Optical properties of single semiconductor nanocrystals. *Physical Chemistry Chemical Physics* **2006**, 8:4989.
3. Willard DM, Mutschler T, Yu M, Jung J, Van Orden A: Directing energy flow through quantum dots: towards nanoscale sensing. *Analytical and Bioanalytical Chemistry* **2006**, 384:564.
4. Empedocles SA, Bawendi MG: Quantum-confined stark effect in single CdSe nanocrystallite quantum dots. *Science* **1997**, 278:2114.
5. Koole R, Liljeroth P, Donega CD, Vanmaekelbergh D, Meijerink A: Electronic coupling and exciton energy transfer in CdTe quantum-dot molecules. *Journal of the American Chemical Society* **2006**, 128:10436.
6. Murray CB, Norris DJ, Bawendi MG: Synthesis and Characterization of Nearly Monodisperse Cde (E = S, Se, Te) Semiconductor Nanocrystallites. *Journal of the American Chemical Society* **1993**, 115:8706.
7. van Sark W, Frederix P, Bol AA, Gerritsen HC, Meijerink A: Blueing, bleaching, and blinking of single CdSe/ZnS quantum dots. *Chemphyschem* **2002**, 3:871.
8. Ozasa K, Nemoto S, Maeda M, Hara M: Excitation-wavelength-dependent photoluminescence evolution of CdSe/ZnS nanoparticles. *Journal Of Applied Physics* **2007**, 101.
9. Tang ZY, Ozturk B, Wang Y, Kotov NA: Simple preparation strategy and one-dimensional energy transfer in CdTe nanoparticle chains. *Journal of Physical Chemistry B* **2004**, 108:6927.
10. Je KC, Ju H, Treguer M, Cardinal T, Park SH: Local field-induced optical properties of Ag-coated CdS quantum dots. *Optics Express* **2006**, 14:7994.
11. Muller J, Lupton JM, Rogach AL, Feldmann J, Talapin DV, Weller H: Monitoring surface charge migration in the spectral dynamics of single CdSe/CdS nanodot/nanorod heterostructures. *Physical Review B* **2005**, 72:205339.
12. Uematsu T, Maenosono S, Yamaguchi Y: Photoinduced fluorescence enhancement in CdSe/ZnS quantum dot monolayers: Influence of substrate. *Applied Physics Letters* **2006**, 89:031910.
13. Efros AL, Rosen M: Random telegraph signal in the photoluminescence intensity of a single quantum dot. *Physical Review Letters* **1997**, 78:1110.
14. Nozik AJ: Quantum dot solar cells. *Physica E-Low-Dimensional Systems & Nanostructures* **2002**, 14:115.
15. Sugisaki M, Ren HW, Nishi K, Masumoto Y: Fluorescence intermittency in self-assembled InP quantum dots. *Physical Review Letters* **2001**, 86:4883.
16. Ebenstein Y, Mokari T, Banin U: Fluorescence quantum yield of CdSe/ZnS nanocrystals investigated by correlated atomic-force and single-particle fluorescence microscopy. *Applied Physics Letters* **2002**, 80:4033.
17. Zhang K, Chang HY, Fu AH, Alivisatos AP, Yang H: Continuous distribution of emission states from single CdSe/ZnS quantum dots. *Nano Letters* **2006**, 6:843.
18. Pelton M, Smith G, Scherer NF, Marcus RA: Evidence for a diffusion-controlled mechanism for fluorescence blinking of colloidal quantum dots. *Proceedings Of*

*The National Academy Of Sciences Of The United States Of America* **2007**, 104:14249.

19. Huang HD, August; Nair, Gautham P.; Bulovic, Vladimir; Bawendi, Mounji G.: Bias-Induced Photoluminescence Quenching of Single Colloidal Quantum Dots Embedded in Organic Semiconductors. *Nano Lett* **2007**, 7:3781.

# **Chapter 6**

## **Environment Dependence of QDs**

### **Fluorescence Blinking**

The effect of surrounding atmosphere, on optical properties, especially fluorescence blinking behavior, of individual QDs and small close-packed QD clusters is studied in this chapter. The influence of ambient air and dry nitrogen are compared. In the dry nitrogen environment, on-state does not happen as often as that in ambient air. Its durations are also reduced significantly. Water and oxygen in ambient air play very important roles. Passivation by reversible absorption of H<sub>2</sub>O and irreversible oxidation of O<sub>2</sub> might be responsible for the photoluminescence enhancement of QD particles.

#### **6.1 Introduction**

In this section, we study the environmental effects, such as N<sub>2</sub> and ambient air, on optical properties especially the blinking behavior. It is known that optical properties of QDs are very sensitive to the surface chemistry because their big surface to volume ratio. Therefore, it is great important to investigate the effects of the adsorption of different gaseous analytes from the immediate surroundings onto the surface of QDs on their fluorescence blinking behavior.<sup>1-5</sup> A dramatic enhancement of the fluorescence intensity from single core-shell QDs has been observed upon sudden exposure to air from an evacuated surrounding.<sup>2</sup> Both the number of particles contributing to emission and the average emission intensity from a single particle increased. People also reported that fluorescence intensity measured assembly decreased under oxygen, which was rationalized by a shortening of the “on” times in fluorescence blinking.<sup>1</sup> According to the study from Nazzal *et al.*<sup>5</sup>, the adsorbed water molecules on the surface of QDs could enhance the fluorescence dramatically without causing any oxidation. The reported diversity of experimental data requires further exploration of influence of immediate surroundings on the fluorescence blinking process.

## **6.2 Experimental Section**

### **6.2.1 Instrumentation**

The single-detector setup (See Chapter 2 for details) is used in this chapter. The 650 nm short pass filter is placed in front of the detector. The apparatus is modified a bit to study the environment (N<sub>2</sub> and air) effects on the blinking behaviors. Figure 6-1 shows the schematic diagram of the setup. To create different atmospheres, the AFM head, the sample, and the flat XY scanning stage are mounted in a tightly sealed atmosphere

chamber with an optical window. A plastic hood functions as the atmosphere chamber to produce and maintain a specific environment. A hatch on the plastic hood controls the switch between different environments.

The procedure of alternating between atmospheres with the ambient air as a start is as the following. 1) The hatch is kept open, while a scanning confocal fluorescence image is recorded by raster scanning the sample through the probe region. 2) A fluorescent spot in the confocal image is positioned and held right above the probe region by x, y positioning function of the flat scanning stage. 3) A fluorescence time trace of the fluorescent spot is collected under the air atmosphere. 4) Block the laser, close the hatch, and purge dry N<sub>2</sub> at high flow rate into the plastic hood for at least 10 min. 5) Purge dry N<sub>2</sub> at low flow rate, perform a fine adjustment to the laser focusing and x, y positioning, and collect the fluorescence time trace again under the dry N<sub>2</sub> atmosphere. 6) Stop purging dry N<sub>2</sub>, open the hatch, readjust laser focusing, and lower the AFM tip to scan the spot. 7) Raise the AFM tip and collect fluorescence time trace under wet air atmosphere. 8) Repeat from step 5) but skip AFM scanning part for more fluorescence time traces collection under alternative atmospheres.

The procedure of alternating between atmospheres with the dry N<sub>2</sub> atmosphere as a start is as the following. 1) Close the hatch and purge dry N<sub>2</sub> at a high flow rate into the plastic hood for at least 10 min. 2) Purge dry N<sub>2</sub> at a low flow rate, perform a fine adjustment of the laser focusing and x, y positioning, and take a scanning confocal fluorescence image by raster scanning the sample through the probe region. 3) While the

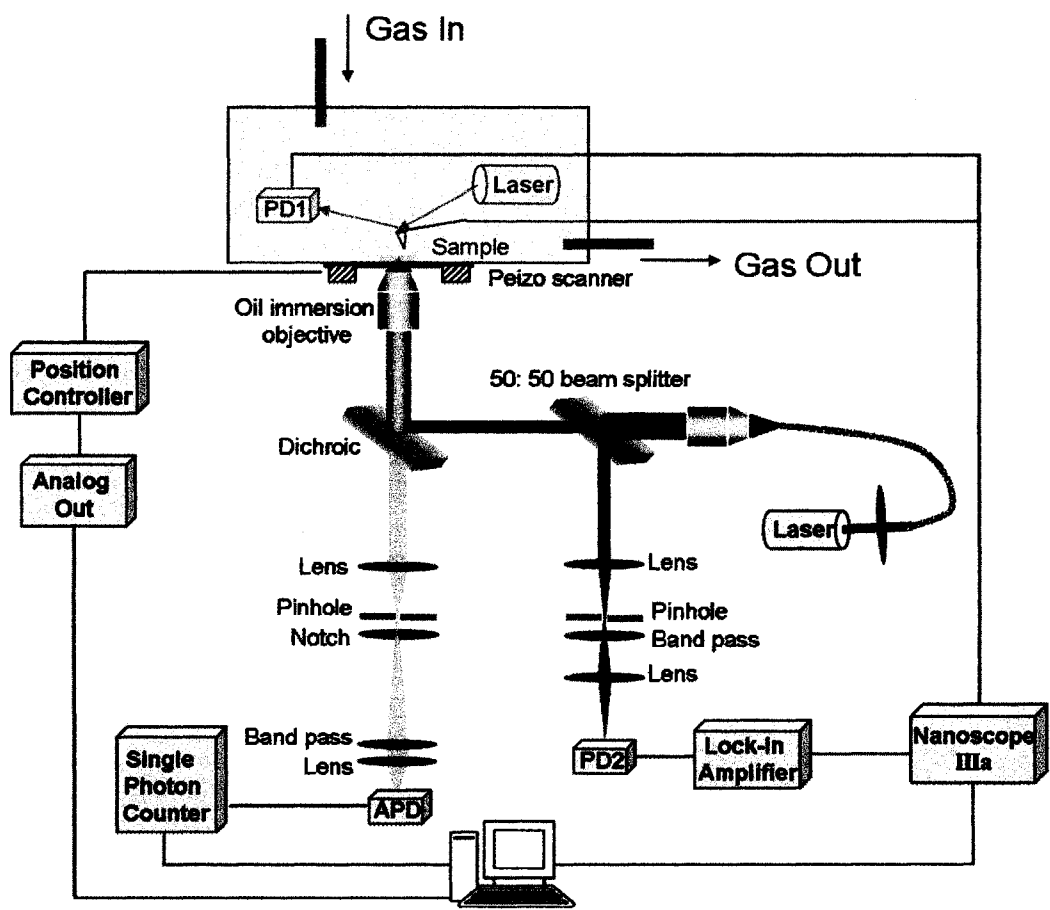


**Figure 6-1.** Schematic diagram of the gas hood modified single-detector correlation setup. PD1, AFM feedback detector; PD2, Si photodiode detector; APD, avalanche photodiode detector. Gray box: the plastic hood functioning as an atmosphere chamber.

dry N<sub>2</sub> is kept flowing, a fluorescent spot in the confocal image is positioned and held right above the probe region by x, y positioning function of the flat scanning stage. 4) A fluorescence time trace of the fluorescent spot is collected under the flowing dry N<sub>2</sub> atmosphere. 5) Stop purging dry N<sub>2</sub>, open the hatch, readjust laser focusing, and lower the AFM tip to scan the spot. 6) Raise the AFM tip and collect fluorescence time trace under the wet air atmosphere. 7) Repeat from step 1) but skip step 3) and the AFM scanning part for more fluorescence time traces collection under alternating atmospheres.

## 6.2.2 Sample Preparation

QD nanocrystals of yellow Evidots dissolved in toluene at ~40- $\mu$ M were purchased from Evident Technologies (Evidots™, Troy, NY). They are 3.96-nm CdSe colloidal nanoparticles, capped with inorganic ZnS shell and trioctylphosphine/trioctylphosphine oxide (TOP/TOPO) as stabilizing ligands (See Chapter 4 for details). Small QD clusters are formed by treating ~1-mL of ~0.4-nM QDs diluted in hexane with a few microliters of methanol, and allowing the solution to stand for ~10-20 min. Methanol raises the polarity of the solvent, causing aggregation of the QDs by association of the hydrophobic ligands.<sup>6</sup> The degree of aggregation can be controlled by adjusting the QD and methanol concentrations and the incubation time. Following incubation, ~100- $\mu$ l of the solution are spin cast onto a AP-mica cover slip (See chapter 2) to disperse the particles for subsequent fluorescence and AFM analysis.

## 6.3 Results and Discussion

Figure 6-2 shows the scanning confocal fluorescence images of individual QDs dispersed on AP-mica under atmospheres of ambient air and the dry nitrogen. The images were taken from the same area by raster scanning the sample through the excitation spot of the microscope and collecting the fluorescence (See chapter 2). The image under the atmosphere of ambient air, shown in Figure 6-2(a), was taken first, then followed by the measurement in dry N<sub>2</sub>, shown in Figure 6-2(b). The white circles mark the same QDs on two images. Minor shift of the image towards lower left is caused by the drifting of the flat piezo scanner. Compared to Figure 6-2(a), more bright QDs showed up in Figure 6-2(b). We doubt this is due to the effects of different immediate surroundings. Instead, the reported phenomenon, QD brightening<sup>7</sup>, provide a reasonable explanation. Under continuous radiation, photoluminescence of ensemble QDs is increasing initially because a fraction of dark QDs is switching on during the illumination. This is also observed in our study, as shown in Figure 6-3. Figure 6-3 shows the fluorescence time trace of a big QD blob illuminated continuously under ambient air. The big aggregation has an effective volume of  $1.5 \times 10^5 \text{ nm}^3$  and is obtained by increasing both solvent polarity and incubation time. Its effective volume is way bigger than those of small QD clusters exhibiting enhanced blinking behavior. There are many single QDs in the aggregate, thus the blinking patterns of single emitting units, such as individual QDs or small close-packed QD clusters, are covered by the averaging effect from the total emission of the huge aggregate. What can be seen in the fluorescence time trace is a whole “on” period with fluctuating intensities. Therefore, its optical behavior is similar with that of ensemble QDs. Before 150 s, the intensity is increasing, which is resulted from a dark fraction switching-on. After the intensity reaches a plateau, it

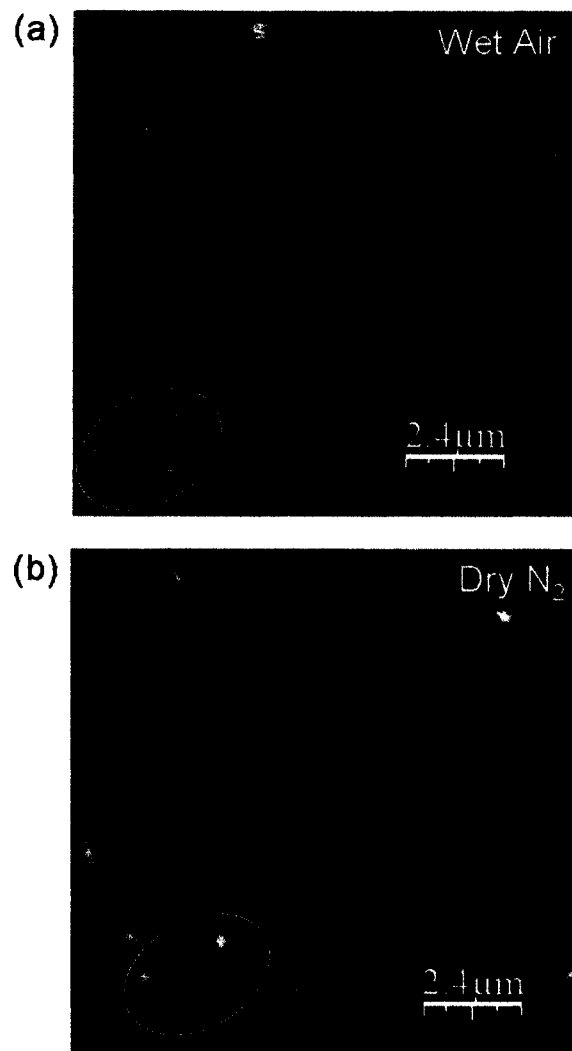


**Figure 6-2.** 2-D scanning confocal fluorescence images of isolated QD nanocrystals of yellow Evidots dispersed on AP-mica under (a) ambient air and (b) dry N<sub>2</sub>. The pictures were taken from the same area by raster scanning the sample through the excitation spot of the microscope and collecting the fluorescence. Image (a) was taken first, followed by image (b). The white circles mark the same QDs on both images.

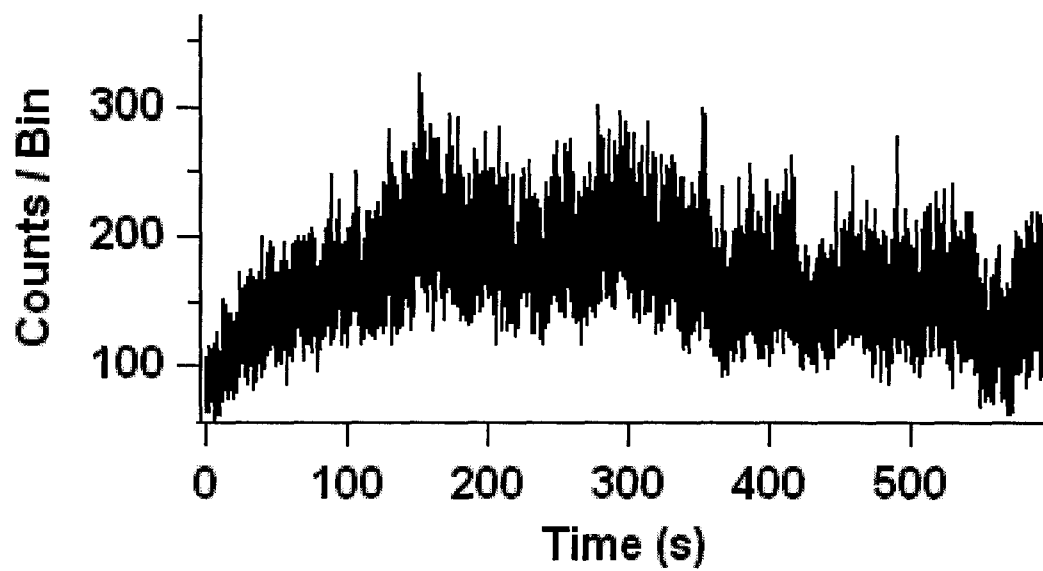


**Figure 6-3.** Fluorescence trajectory segment of a big QD blob under ambient air and constant illumination.

gradually decreases, which is the result of subsequent photobleaching. Therefore, QD brightening in Figure 6-2(b) compared to Figure 6-2(a) is not caused by the dry N<sub>2</sub> environment. In stead, it is the initial PL brightening under illumination. From the confocal fluorescence images, we could not observe obvious difference between dry N<sub>2</sub> and ambient air. The number and brightness of the QDs are almost the same in both immediate environments, if the PL brightening is not taken into account.

In the second set of experiments we have studied the influence of different atmospheres on blinking behaviors of individual single QDs and small QD clusters in single particle level. In Figure 6-4 the fluorescence trajectories of two individual QDs in the same sample on AP-mica are collected, where the samples were alternatively exposed to the atmospheres of ambient air and dry N<sub>2</sub>. The faster blinking pattern of the individual QDs is due to the elevated illumination power (See Chapter 3). It is seen that exposure to dry nitrogen leads to decreases of the population, durations and/or intensity of “on” times, which revert at least partially when the immediate environment is changed back to ambient air (See Figure 6-4(b)). Figure 6-5 shows the fluorescence trajectories of two small close-packed QD clusters in the same sample on AP-mica exposed alternatively to the dry nitrogen or ambient air. Similarly, dry nitrogen leads to decreases of the population and/or intensity of “on” times, especially the higher intensity regime of the enhanced blinking. As seen in Figure 6-5(a), the multi-state blinking of the normal blinking at lower intensity regime appears as usual, whereas the population of enhanced blinking increases dramatically only when the surrounding atmosphere is changed to ambient air.

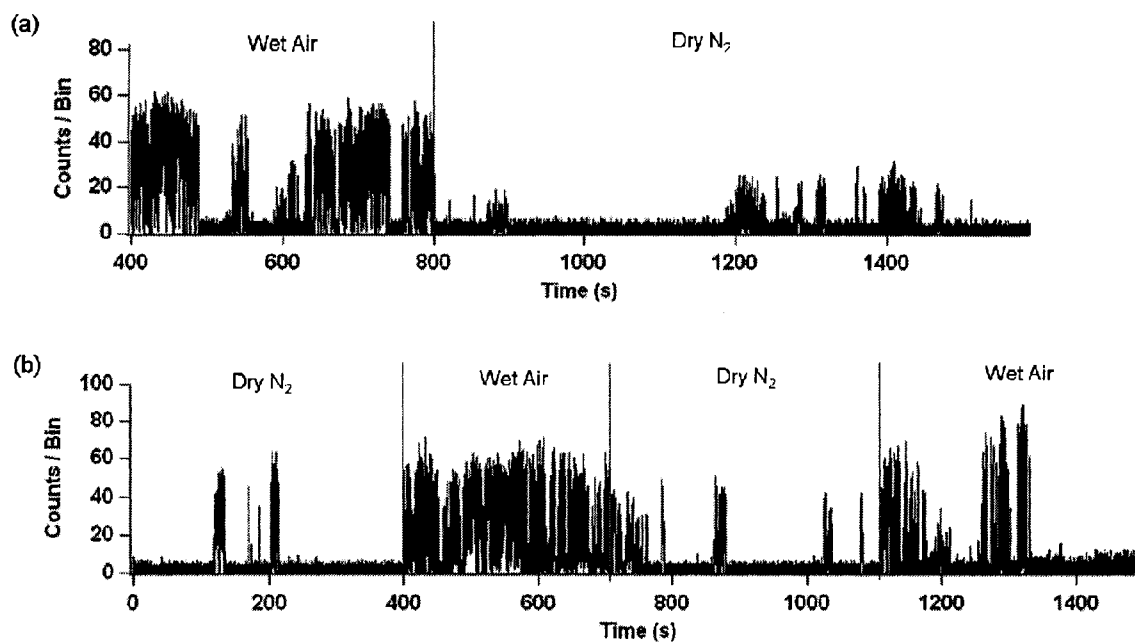


**Figure 6-4.** Fluorescence trajectories of two single nanocrystals in the same sample on AP-mica (excitation intensity  $\sim 280 \text{ W/cm}^2$ , time bin = 10ms) under alternative atmospheres of ambient air and dry N<sub>2</sub>.

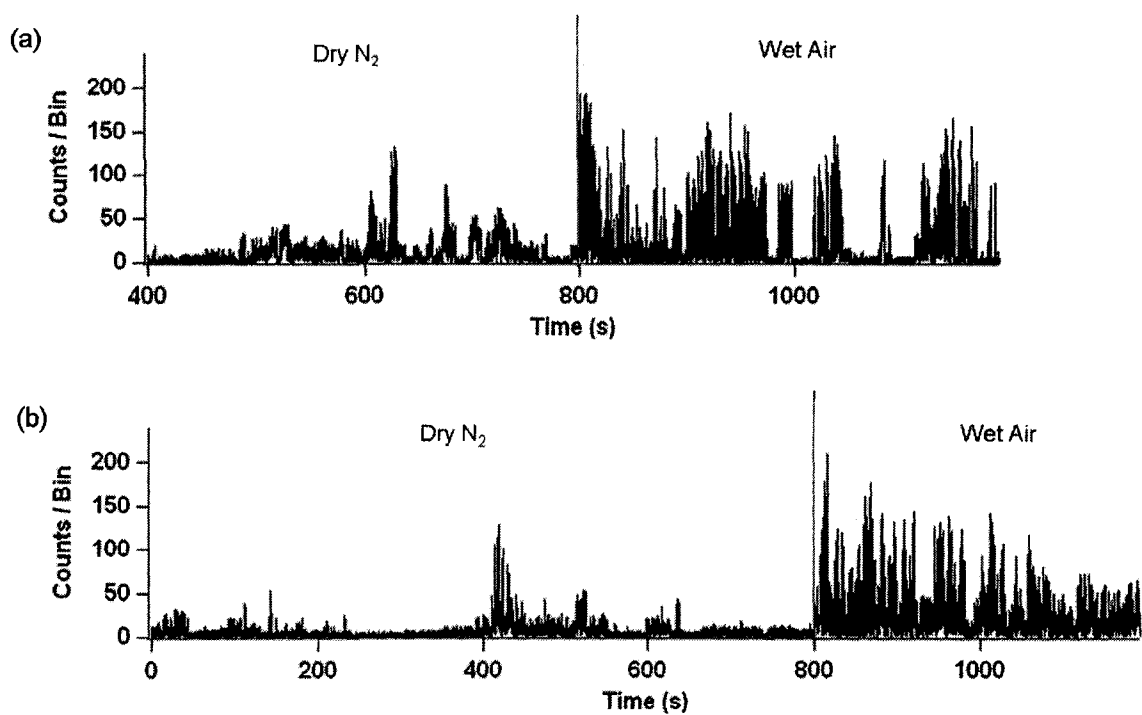


**Figure 6-5.** Fluorescence trajectories of two QD clusters in the same sample on AP-mica (excitation intensity  $\sim 280 \text{ W/cm}^2$ , time bin = 10ms) under alternative atmospheres of ambient air and dry N<sub>2</sub>.

Several scenarios have been discussed on how the fluorescence blinking behavior of QDs can be influenced by the surrounding environments<sup>1,2,7,8</sup>. Fluorescence blinking of QDs is very sensitive to their own surface chemistry and the chemistry in contact with or nearby them. We propose that H<sub>2</sub>O and O<sub>2</sub> molecules in ambient air atmosphere modify the surface chemistry in both reversible and irreversible ways, which increase the PL of individual particles. Oxidation of the exposing area of particles (single QDs or small QD clusters) by oxygen under radiation produces a protecting or passivation layer and consequently increases the PL of the particles, which is an irreversible process. The absorption of H<sub>2</sub>O in the wet air onto the surfaces of QD particles works also as a passivation for electron trap states on the QD surfaces, because H<sub>2</sub>O is an electron-rich agent. This process is reversible, which only take effects when H<sub>2</sub>O is present in the atmosphere surrounding the QD particles.

## 6.4 Conclusion

We have studied and compared the influence of surrounding atmospheres of dry nitrogen and ambient air on optical properties, especially fluorescence blinking behavior, of individual QDs and small close-packed QD clusters. Our results show that dry nitrogen environment decreases the population, intensity and/or durations of “on” times, comparing to ambient air atmosphere. The PL enhancement of QD particles by ambient air may potentially be explained by the passivation with reversible absorption of H<sub>2</sub>O and irreversible oxidation of O<sub>2</sub>.

## References:

1. Koberling F, Mews A, Basche T: Oxygen-induced blinking of single CdSe nanocrystals. *Advanced Materials* **2001**, 13:672.
2. Muller J, Lupton JM, Rogach AL, Feldmann J, Talapin DV, Weller H: Air-induced fluorescence bursts from single semiconductor nanocrystals. *Applied Physics Letters* **2004**, 85:381.
3. van Sark W, Frederix P, Bol AA, Gerritsen HC, Meijerink A: Blueing, bleaching, and blinking of single CdSe/ZnS quantum dots. *Chemphyschem* **2002**, 3:871.
4. van Sark W, Frederix P, Van den Heuvel DJ, Gerritsen HC, Bol AA, van Lingen JNJ, Donega CD, Meijerink A: Photooxidation and photobleaching of single CdSe/ZnS quantum dots probed by room-temperature time-resolved spectroscopy. *Journal of Physical Chemistry B* **2001**, 105:8281.
5. Nazzal AY, Wang XY, Qu LH, Yu W, Wang YJ, Peng XG, Xiao M: Environmental effects on photoluminescence of highly luminescent CdSe and CdSe/ZnS core/shell nanocrystals in polymer thin films. *Journal of Physical Chemistry B* **2004**, 108:5507.
6. Murray CB, Norris DJ, Bawendi MG: Synthesis and Characterization of Nearly Monodisperse Cde (E = S, Se, Te) Semiconductor Nanocrystallites. *Journal of the American Chemical Society* **1993**, 115:8706.
7. Lee SF, Osborne MA: Photodynamics of a single quantum dot: Fluorescence activation, enhancement, intermittency, and decay. *Journal Of The American Chemical Society* **2007**, 129:8936.
8. Shu GW, Lee WZ, Shu IJ, Shen JL, Lin JCA, Chang WH, Ruaan RC, Chou WC: Photoluminescence of colloidal CdSe/ZnS quantum dots under oxygen atmosphere. *Ieee Transactions on Nanotechnology* **2005**, 4:632.

# Chapter 7

## Surface Dependence of QDs Fluorescence

### Blinking

In this chapter we study the influence of substrates on optical properties individual QDs and small close-packed QD clusters. Both CTAB- and  $Mg^{2+}$ -mica substrates quench the fluorescence of single QDs and QD clusters on the substrates, which might be due to the dissociation of electron hole pairs of excited QDs by the electron attractive sites in CTAB molecules and  $Mg^{2+}$  ions.

#### 7.1 Introduction

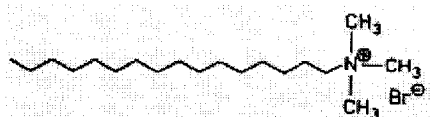
The commonly suggested tunneling ionization model of single QD blinking<sup>1</sup>, which implies that electron tunneling to/from external states, has been challenged

experimentally<sup>2-4</sup>. It was found that power law distributed blinking was insensitive of inorganic shell coating thickness<sup>2</sup>, the environment (in solution or immobilized on substrates)<sup>3,4</sup>. However, the dielectric constant of the contacting substrate did affect the stability of charge separation.<sup>5</sup> As the polarity of matrix got higher, the population of long “off” times increased. It has been reported and discussed how electron and hole conducting substrates affect optical behaviors of QDs.<sup>6</sup> In order to investigate the influence of the dielectric environment on the photoluminescence blinking of small QD clusters, experiments will be performed on substrates of different dielectric constants.

## 7.2 Experimental Section

Instrumentation is the same as Chapter 2. A 650 short pass filter is used in front of the detector in the study of this chapter. In this study different single QD nanocrystals from two companies were used. QD1 are 2.75 nm green Evidots dissolved in toluene at ~70  $\mu\text{M}$  from Evident Technologies (Evidot<sup>TM</sup>, Troy, NY). They are CdSe colloidal nanoparticles, capped with inorganic ZnS shell and trioctylphosphine/trioctylphosphine oxide (TOP/TOPO) as stabilizing ligands. QD2 are from NN-Labs (NN-Labs, LLC, Fayetteville, AR), which have absorption wavelength of 528 nm and emission wavelength of 549 nm. They are CdSe colloidal nanoparticles, capped with inorganic ZnS shell and mercaptoundecanoic acid (MUA) as stabilizing ligands. 1mL of 10 mM QD2 dissolved in water is the stock solution.

Mica surfaces are modified by either cetyltrimethylammoniumbromide (CTAB) or  $\text{Mg}^{2+}$ .



Cetyltrimethylammoniumbromide (CTAB)

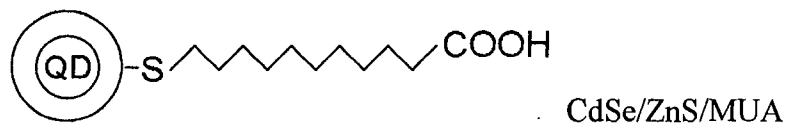
Three samples are prepared. Sample A: individual QDs of QD1 are spin cast onto CTAB-mica. Sample B: small close-packed clusters of QD1 from the same samples are spin cast onto CTAB-mica and AP-mica, respectively. Sample C: individual QDs of QD2 are immobilized onto  $Mg^{2+}$ -mica.

To prepare sample A, the following steps are performed. 1) Apply 200  $\mu$ l of 0.1 w% CTAB diluted in Millipore  $H_2O$  onto newly cleaved mica. 2) Place the mica substrate into a sealed 75% humidity chamber (Containing saturated NaCl solution) for 2 hr. 3) Rinse the mica surface with Millipore  $H_2O$  and blow dry with air. Now CTAB-mica is obtained. 4) 100  $\mu$ l of 70 nM individual QDs of QD1 diluted in hexane are spin cast onto CTAB-mica to disperse the particles for subsequent fluorescence and AFM analysis in air atmosphere. Newly cleaved mica has excess negative charge on the surface. The head part of a CTAB molecule has the positive charge and can attach to the negatively charged mica surface when they are in contact. The polycarbon chain tail grabs QD particles.

To prepare sample B, the preparation of CTAB-mica is the same as what has been mentioned above. Small close-packed clusters of QD1 are prepared by treating  $\sim$ 1 mL of several nanomolar single QDs diluted in hexane with a few microliters of methanol, and allowing the solution to stand for  $\sim$ 10-20 min. Then  $\sim$ 100  $\mu$ l of the solution are spin cast

onto a CTAB-mica cover slip to disperse the particles for subsequent fluorescence and AFM analysis in air atmosphere.

To prepare sample C, the procedure is as following. 1) Apply 30  $\mu\text{l}$  of 10 mM  $\text{MgCl}_2$  on a newly-cleaved mica cover slip and wait for 5 min. 2) Rinse with Millipore  $\text{H}_2\text{O}$  and blow dry with air. Now the  $\text{Mg}^{2+}$ -mica surface is formed. 3) Apply 80  $\mu\text{l}$  of 10 pM single QD2 diluted in water on  $\text{Mg}^{2+}$ -mica and wait for 10 min. 4) Rinse the mica surface with Millipore  $\text{H}_2\text{O}$  and blow dry with air for subsequent fluorescence and AFM analysis in air atmosphere. After treated with  $\text{Mg}^{2+}$ , the mica surface has excess positive charges, which can interact with the carboxyl groups of MUA molecules on QDs and consequently immobilize the QDs



### 7.3 Results and Discussion

In this study, the surface coverage densities of sample A, B and C are elevated and high enough that there is at least one particle in the probe region at any time. In this way, we can compare the effect of surface substrate on optical properties of single QDs and small QD clusters. For AFM images, lots of particles of individual QDs are observed on modified mica surfaces of sample A and C. However, fluorescence signals in the fluorescence confocal images are very weak. The same results are also observed in the sample of small QD clusters on CTAB-mica substrates, which are different from what has been observed in the sample of small QD clusters on AP-mica substrates. Figure 7-1

shows the 3-D scanning confocal fluorescence images of small close-packed QD clusters in the sample B dispersed on CATB-mica (a) and AP-mica (b). The pictures were taken by raster scanning the sample through the excitation spot of the microscope and collecting the fluorescence. There are lots of fluorescence signals from QD clusters on AP-mica, which, however, are quenched on CATB-mica.

We observed that both CTAB molecules and  $Mg^{2+}$  ions quench the fluorescence of single QDs and small QD clusters. This might be explained as following. Positive charge centers of CTAB molecules and  $Mg^{2+}$  ions function as electron sinks. Excited electrons of QD excitons are dissociated from the holes by electron traps or sinks of CTAB molecules and  $Mg^{2+}$  ions on mica substrates. Therefore fluorescence is extinguished by the excess charges in QDs themselves.

## 7.4 Conclusion

We have studied the influence of substrates on optical properties of individual QDs and small close-packed QD clusters. Both CTAB- and  $Mg^{2+}$ -mica substrates quench the fluorescence of single QDs and QD clusters, which is due to the dissociation of electron hole pairs of excited QDs by the electron attractive sites in CTAB molecules and  $Mg^{2+}$  ions.

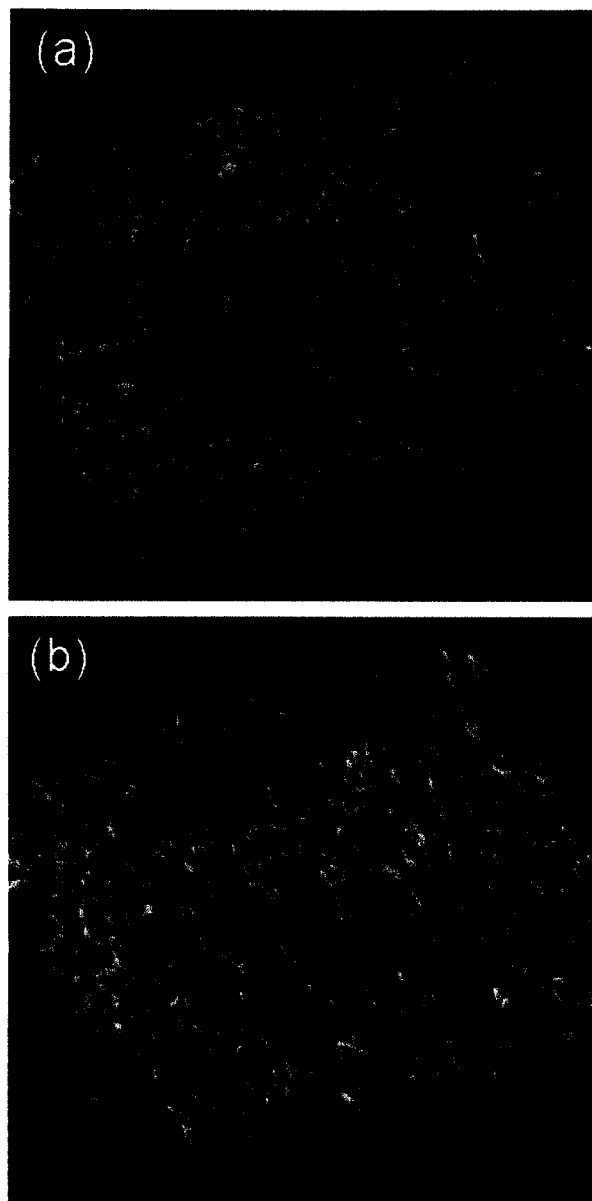


**Figure 7-1.** 3-D scanning confocal fluorescence images of small close-packed QD clusters of sample B dispersed on CATB-mica (a) and AP-mica (b). The pictures were taken by raster scanning the sample through the excitation spot of the microscope and collecting the fluorescence.

## References:

1. Kuno M, Fromm DP, Johnson ST, Gallagher A, Nesbitt DJ: Modeling distributed kinetics in isolated semiconductor quantum dots. *Physical Review B* **2003**, 67:125304.
2. Heyes CD, Kobitski AY, Breus VV, Nienhaus GU: Effect of the shell on the blinking statistics of core-shell quantum dots: A single-particle fluorescence study. *Physical Review B* **2007**, 75:125431.
3. Pelton M, Grier DG, Guyot-Sionnest P: Characterizing quantum-dot blinking using noise power spectra. *Applied Physics Letters* **2004**, 85:819.
4. Stefani FD, Knoll W, Kreiter M, Zhong X, Han MY: Quantification of photoinduced and spontaneous quantum-dot luminescence blinking. *Physical Review B* **2005**, 72:125304.
5. Issac A, von Borczyskowski C, Cichos F: Correlation between photoluminescence intermittency of CdSe quantum dots and self-trapped states in dielectric media. *Physical Review B* **2005**, 71:161302.
6. Huang HD, August; Nair, Gautham P.; Bulovic, Vladimir; Bawendi, Mounqi G.: Bias-Induced Photoluminescence Quenching of Single Colloidal Quantum Dots Embedded in Organic Semiconductors. *Nano Lett* **2007**, 7:3781.

## **Chapter 8**

### **Conclusions and Future Work**

As nanotechnology is growing, nanomaterials start to emerge on the stage and catch people's eyes because of their novel optical, optoelectronic, and mechanical properties. Semiconductor QDs are one of the significant members of nanomaterials. Fluorescence blinking is an intrinsic optical characteristic of QDs. There are two purposes to study the cooperative fluorescence blinking behavior of small QD clusters. Fundamentally, fluorescence blinking of QDs is not fully understood yet. Studying the interactions between neighboring QDs can help to exploit QD blinking. Practically, small QD clusters are potential building blocks of advanced devices of nanotechnology. Examining the cooperative blinking behavior of the small building blocks is beneficial for fabricating the QD devices and understanding the coupling manners between these individual quantum units.

It is hypothesized if the QDs were close enough to undergo efficient energy transfer, they would behave as a single quantum system. This could cause a variety of observable effects through data analysis. By using the spatially correlated single molecule fluorescence spectroscopy and AFM method, we have compared the fluorescence blinking behaviors of individual QDs and small QD clusters containing two or more QDs. QD commercial products from two companies were used, bulky QD-bioconjugates with high quantum yield from Qdot™ and small QD nanocrystals from Evident™. Fluorescence blinking behaviors of the individual QD-bioconjugates (from Qdot™) and their small QD clusters are similar to each other. This is because the bulky protecting and functional layers on the QDs surface insulate the QDs and block the possible communications between QDs in the clusters. However, blinking behaviors of the small single QD nanocrystals (from Evident™) and their small QD clusters are strikingly different. Fluorescence intermittency of the QD clusters become much more rapid and intense than can be explained by the independent blinking of multiple particles. This enhanced blinking is suggested to occur when the QDs in the clusters become electronically coupled. The nature of this coupling is not known.

We further monitored the emission wavelength of the close-packed QD clusters in single particle level and observed the difference between normal blinking and enhanced blinking. When the enhanced blinking in a fluorescence time trace showed up, it was accompanied with red-shifted emission compared to that of the normal blinking. Therefore it is proposed that the electronic coupling happening inside the QD clusters,

has a characteristic of red shifted emission. The electronic coupling might be the temporal coupling of instant electric fields generated by charges on the single QDs composing the cluster when they are dark or charged. The instant net maximum electric field could enhance the emission and decrease the confinement of the small QD clusters. Because both the temporal electric fields and emitters would be changing randomly with time, fast and intense fluorescence blinking is resulted.

We have also studied the influence of dry nitrogen and wet air on fluorescence blinking behavior of the small QD nanocrystals. Dry nitrogen decreases the population, intensity and/or durations of “on” times. The influence of substrates on optical properties of the QD nanocrystals was investigated, too. Both CTAB- and  $Mg^{2+}$ -mica substrates quench the fluorescence of single QDs and QD clusters, which is due to the dissociation of electron hole pairs of excited QDs by the electron attractive sites in CTAB molecules and  $Mg^{2+}$  ions. What we have studied is just a beginning. More aspects regarding to QD fluorescence blinking are of great interest to dig into.

## **8.1 Altering Capping Ligands**

We have been using methanol to make QD clusters by increasing the polarity of solvent. The inter particle distance would be 1 to 2 length of TOPO ligands, 0.7-1.4 nm<sup>1</sup>. People have investigated the dependence of optical properties of QDs on coating ligands.<sup>2</sup> To study the ligand effects on fluorescence blinking of small QD clusters we can exchange TOPO coating with aliphatic dithiols by ligands replacement<sup>3</sup>. This choice is made because the inter particle distance can be adjusted to the same as that in the QD

clusters coated with TOPO/TOP, while the bonding sites of thiols on QDs are potent electron donor<sup>4</sup> which give better passivation to surface trap states on QD surface than phosphate bonding sites in the TOPO ligands. The procedure to alter capping ligands is as the following. TOPO/TOP capped QDs obtained from the synthesis (See chapter 1 for details) are recapped with allylamine (AA) by a ligands exchange. Subsequently, aliphatic dithiols (i.e., 1, 8 octanedithiol) are used to cross-link the QDs<sup>5</sup>. By accurately varying the concentrations of the cross-linker in the QD dispersions, we would be able to control the fraction of QD clusters with a certain size.

## 8.2 Altering Inter Particle Distances of QD Clusters

Short molecules of hydrazine ( $N_2H_4$ ), with inter-N distance of 0.145 nm, were utilized to enhance coupling of QD films.<sup>6,7</sup> Replacing the TOPO ligands between QDs in QD clusters with hydrazine can increase the charge carrier mobility by reducing the inter-dot spacing while retaining relatively highly passivated surfaces.<sup>7</sup> To prepare hydrazine spacing QD clusters on mica, TOPO spacing QD clusters, prepared as usual, are first spin cast on AP-mica. Subsequently, the attached QD clusters are chemically treated by soaking the substrate in 1M hydrazine in acetonitrile for 20-24h<sup>7</sup>. One necessary control exp for AFM measurement is soaking blank AP-mica in 1M hydrazine in acetonitrile for 20-24h, followed by AFM scanning.

In Emission lifetime measurements of hydrazine coupled QD clusters, normal blinking would have longer decay time than TOPO coated clusters. This is because hydrazine, analogous to primary amines, is a strong Lewis base with lone pairs of

electrons that can saturate dangling bonds at QD surfaces<sup>8</sup>. In contrast to normal blinking, emission of enhanced blinking would have dramatically reduced lifetime. This is due to enriched electronically coupling in QD clusters by hydrazine shortening inter particle distance.

### **8.3 Altering Shell Thickness**

The shell of the core-shell QD system has two main provinces. The first is to passivate core surface dangling bonds, which confines the e- and hole wave functions away from the surface, thereby increasing the QY. The second is to facilitate chemical modification without affecting the optical properties of the core. Systematical investigation has been taken to learn the effect of the shell on the blinking dynamics of individual QDs.<sup>9</sup> It was found that there were not systematic effects of the shell thickness on the QD blinking statistics. The lack of dependence suggests that tunneling to an external trap is not the primary mechanism responsible for single QD blinking.

However this study is not in conflict with the possibility of electron tunneling between QDs when QD cores are close together<sup>5</sup>. We suggested the enhanced blinking of small CdSe/ZnS QD cluster might be caused by the electronic coupling between QDs. It is not clear whether the enhanced blinking was dominated by communications between only core-core 2-quantum or by core-shell-core 3-quantum systems. CdSe/ZnS/CdSe multiple quantum systems have been studied assembly<sup>10, 11</sup>. It was provided that the inner and outer CdSe layers could be coupled by tunneling of excitons through the ZnS barrier.<sup>11</sup> Moreover, electronically coupling or decoupling between CdSe layers could be

controlled by alteration of the thickness of the ZnS barrier layer.<sup>10</sup> Therefore, systematic variation of the shell thickness may be promising to gain further insight into electronic coupling in the QD clusters. We can choose the same CdSe cores upon varying the thickness of the ZnS capping layer<sup>9</sup> to prepare small QD cluster. Since single QD blinking was not very sensitive to the shell thickness, the emission lifetime of normal blinking in a QD cluster would always be the same. In the contrast to normal blinking, enhanced blinking would have dependent lifetime on the variation of the shell thickness.

## **8.4 Altering QD Clusters Shapes**

QD chains have been prepared by a simple self-assembly method.<sup>12</sup> We can use the similar method to prepare short one dimensional QD aggregates to investigate the blinking differences between round and linear QD clusters. First, thioglycolic acid recoated QDs<sup>3</sup> are partially stripped off the stabilizers by washing in methanol and separated from solution. Secondly, stabilizer depleted QDs are redissolved in basic solution and kept in a refrigerator at 4°C for 2 - 4 weeks depending on how long the chain is needed. Partial removal of thioglycolic acid from the QD surface leads to the decrease of the surface charge. The mutual electrostatic repulsion of NPs is reduced, and the dipole-dipole attraction manifests itself in the formation of the NP chains.

## **8.5 Altering the Single Quantum Units by Using Small Quantum Rods (QRs)**

Quantum rods (QRs) have recently attracted considerable attention<sup>13-16</sup> because of their advantages over spherical QDs. For example, color control is achievable by tuning the rod diameter which governs the band gap energy.<sup>17</sup> The Stokes shift is strongly dependent on the aspect ratio (length/diameter) of the rod.<sup>18</sup> QRs are brighter single molecule probes compared to QDs.<sup>16</sup> Emitted light from QRs is linearly polarized along the c-axis of the crystallites and the degree of polarization is dependent on the aspect ratio of the NCs.<sup>19</sup> The elongation of QRs also makes them better conductors than spherical NCs.<sup>20</sup> However, there are very limited reports describing blinking behavior of QRs<sup>21</sup>. Wang et al. reported that, just like QDs, “off” time probability distributions of QRs also obey power law behavior and “on” time probability distributions fit well a truncated power law, where the crossover time is linearly dependent on the QR aspect ratio. It would be very interesting to study the blinking behavior of small QR clusters.

## **8.6 Influence of Gold Nanoparticles**

Photoluminescence of QDs on nanostructured gold surfaces is modified because of a complex interplay of enhancing and quenching physicochemical processes.<sup>22-26</sup> Luminescence of QDs are related to gold substrates roughness<sup>22</sup> and the distance between QDs and gold substrates<sup>25</sup>, or particles<sup>26</sup>. Furthermore, the duration of “on” time could be increased to a point where the frequency of blinking events appreciably diminishes.<sup>22</sup> It would be very interesting to study the influence of Au nanoparticles on the blinking behavior of small QD clusters.

The experiment can be performed by placing a gold nanoparticle modified AFM tip in the vicinity of a small QD cluster dispersed on substrates. First, fluorescence time traces are collected as usually from small QDs clusters spin cast on AP mica<sup>27</sup>. Second, the gold nanoparticle modified AFM tip<sup>28</sup> is lower down to scan the area containing the QD cluster, and then held above the cluster for a certain distance<sup>29, 30</sup>. A fluorescence time trace is collected again, which shows the effects of the gold nanoparticle attached on the AFM probe on blinking of small QD clusters.

## 8.7 Temperature Dependence

The thermal effects on the photoluminescence properties of QDs were studied in single colloidal QDs<sup>31, 32</sup>, self-assembled QDs<sup>33, 34</sup> homogeneous solution phases<sup>35, 36</sup>, and colloidal QD solids and clusters<sup>37, 38</sup>. For single colloidal QDs, while the statistical studies of fluorescence blinking revealed a temperature-independent power law distribution of “on” and “off” times probability<sup>32</sup>, PL intensity decay showed temperature dependent characteristics<sup>31</sup>. At low temperature, the excited state population of the QDs would be mainly in the triplet state. The transition from this state to the ground state was spin-forbidden and characterized by a long decay time. For QD solids, ET via dipole-dipole interaction plays the main role. ET rate decreased at lower temperatures because of the weaker oscillator strengths of energy donor in homonuclear QD solids.<sup>37</sup> For small QD clusters, interdot excitons or carriers coupling dominate within the QD clusters. Lower temperature slow the carrier tunneling or transfer rate.<sup>33, 34</sup> Small CdSe-ZnS QD clusters can be treated as quantum systems of CdSe QDs electronic coupling to other CdSe QDs through thin ZnS barrier layers.

## References:

1. Ji XJ, Wang CS, Xu JM, Zheng JY, Gattas-Asfura KM, Leblanc RM: Surface chemistry studies of (CdSe)ZnS quantum dots at the air-water interface. *Langmuir* **2005**, 21:5377.
2. Kalyuzhny G, Murray RW: Ligand effects on optical properties of CdSe nanocrystals. *Journal of Physical Chemistry B* **2005**, 109:7012.
3. Aldana J, Wang YA, Peng XG: Photochemical instability of CdSe nanocrystals coated by hydrophilic thiols. *Journal of the American Chemical Society* **2001**, 123:8844.
4. Hohng S, Ha T: Near-complete suppression of quantum dot blinking in ambient conditions. *Journal of the American Chemical Society* **2004**, 126:1324.
5. Koole R, Liljeroth P, Donega CD, Vanmaekelbergh D, Meijerink A: Electronic coupling and exciton energy transfer in CdTe quantum-dot molecules. *Journal of the American Chemical Society* **2006**, 128:10436.
6. Talapin DV, Murray CB: PbSe nanocrystal solids for n- and p-channel thin film field-effect transistors. *Science* **2005**, 310:86.
7. Joseph M. Luther MCB, Qing Song, Matt Law, Randy J. Ellingson, and Arthur J. Nozik: Multiple Exciton Generation in Films of Electronically Coupled PbSe Quantum Dots. *Nano Letters* **2007**, 7:1779.
8. Talapin DV, Rogach AL, Kornowski A, Haase M, Weller H: Highly luminescent monodisperse CdSe and CdSe/ZnS nanocrystals synthesized in a hexadecylamine-trioctylphosphine oxide-trioctylphosphine mixture. *Nano Letters* **2001**, 1:207.
9. Heyes CD, Kobitski AY, Breus VV, Nienhaus GU: Effect of the shell on the blinking statistics of core-shell quantum dots: A single-particle fluorescence study. *Physical Review B* **2007**, 75:125431.
10. Battaglia D, Blackman B, Peng XG: Coupled and decoupled dual quantum systems in one semiconductor nanocrystal. *Journal of the American Chemical Society* **2005**, 127:10889.
11. Dias EA, Sewall SL, Kambhampati P: Light harvesting and carrier transport in core/barrier/shell semiconductor nanocrystals. *Journal of Physical Chemistry C* **2007**, 111:708.
12. Tang ZY, Ozturk B, Wang Y, Kotov NA: Simple preparation strategy and one-dimensional energy transfer in CdTe nanoparticle chains. *Journal of Physical Chemistry B* **2004**, 108:6927.
13. Fu AH, Gu WW, Boussert B, Koski K, Gerion D, Manna L, Le Gros M, Larabell CA, Alivisatos AP: Semiconductor quantum rods as single molecule fluorescent biological labels. *Nano Letters* **2007**, 7:179.
14. Muller J, Lupton JM, Rogach AL, Feldmann J, Talapin DV, Weller H: Monitoring surface charge migration in the spectral dynamics of single CdSe/CdS nanodot/nanorod heterostructures. *Physical Review B* **2005**, 72:205339.
15. Rothenberg E, Kazes M, Shaviv E, Banin U: Electric field induced switching of the fluorescence of single semiconductor quantum rods. *Nano Letters* **2005**, 5:1581.
16. Yong KT, Qian J, Roy I, Lee HH, Bergrey EJ, Trampusch KM, He SL, Swihart MT, Maitra A, Prasad PN: Quantum rod bioconjugates as targeted probes for

- confocal and two-photon fluorescence imaging of cancer cells. *Nano Letters* **2007**, 7:761.
17. Li LS, Hu JT, Yang WD, Alivisatos AP: Band gap variation of size- and shape-controlled colloidal CdSe quantum rods. *Nano Letters* **2001**, 1:349.
  18. Li LS, Walda J, Manna L, Alivisatos AP: Semiconductor nanorod liquid crystals. *Nano Letters* **2002**, 2:557.
  19. Peng XG, Manna L, Yang WD, Wickham J, Scher E, Kadavanich A, Alivisatos AP: Shape control of CdSe nanocrystals. *Nature* **2000**, 404:59.
  20. Huynh WU, Dittmer JJ, Alivisatos AP: Hybrid nanorod-polymer solar cells. *Science* **2002**, 295:2425.
  21. Wang S, Querner C, Emmons T, Drndic M, Crouch CH: Fluorescence blinking statistics from CdSe core and core/shell nanorods. *Journal of Physical Chemistry B* **2006**, 110:23221.
  22. Shimizu KT, Woo WK, Fisher BR, Eisler HJ, Bawendi MG: Surface-enhanced emission from single semiconductor nanocrystals. *Physical Review Letters* **2002**, 89:117401.
  23. Huang FM, Festy F, Richards D: Tip-enhanced fluorescence imaging of quantum dots. *Applied Physics Letters* **2005**, 87:183101.
  24. Komarala VK, Rakovich YP, Bradley AL, Byrne SJ, Gun'ko YK, Gaponik N, Eychmuller A: Off-resonance surface plasmon enhanced spontaneous emission from CdTe quantum dots. *Applied Physics Letters* **2006**, 89:253118.
  25. Kulakovich O, Strelak N, Yaroshevich A, Maskevich S, Gaponenko S, Nabiev I, Woggon U, Artemyev M: Enhanced luminescence of CdSe quantum dots on gold colloids. *Nano Letters* **2002**, 2:1449.
  26. Oh E, Hong MY, Lee D, Nam SH, Yoon HC, Kim HS: Inhibition assay of biomolecules based on fluorescence resonance energy transfer (FRET) between quantum dots and gold nanoparticles. *Journal of the American Chemical Society* **2005**, 127:3270.
  27. Yu M, Van Orden A: Enhanced fluorescence intermittency of CdSe-ZnS quantum-dot clusters. *Physical Review Letters* **2006**, 97:237402.
  28. Barsegova I, Lewis A, Khatchaturiants A, Manevitch A, Ignatov A, Axelrod N, Sukenik C: Controlled fabrication of silver or gold nanoparticle near-field optical atomic force probes: Enhancement of second-harmonic generation. *Applied Physics Letters* **2002**, 81:3461.
  29. Hecht B, Sick B, Wild UP, Deckert V, Zenobi R, Martin OJF, Pohl DW: Scanning near-field optical microscopy with aperture probes: Fundamentals and applications. *Journal of Chemical Physics* **2000**, 112:7761.
  30. Kramer A, Trabesinger W, Hecht B, Wild UP: Optical near-field enhancement at a metal tip probed by a single fluorophore. *Applied Physics Letters* **2002**, 80:1652.
  31. Labeau O, Tamarat P, Lounis B: Temperature dependence of the luminescence lifetime of single CdSe/ZnS quantum dots. *Physical Review Letters* **2003**, 90:257404.
  32. Shimizu KT, Neuhauser RG, Leatherdale CA, Empedocles SA, Woo WK, Bawendi MG: Blinking statistics in single semiconductor nanocrystal quantum dots. *Physical Review B* **2001**, 63:205316.

33. Jin H, Zhang LG, Zheng ZH, An LN, Lu YM, Zhang JY, Fan XW, Shen DZ: Temperature-dependent photoluminescence in coupling structures of CdSe quantum dots and a ZnCdSe quantum well. *Chinese Physics Letters* **2005**, 22:1518.
34. Zhang XB, Ryou JH, Dupuis RD, Walter G, Holonyak N: Temperature-dependent luminescence of InP quantum dots coupled with an InGaP quantum well and of InP quantum dots in a quantum well. *Applied Physics Letters* **2005**, 87:201110.
35. Wuister SF, Donega CDM, Meijerink A: Luminescence temperature anti-quenching of water-soluble CdTe quantum dots: Role of the solvent. *Journal of the American Chemical Society* **2004**, 126:10397.
36. Liu TC, Huang ZL, Wang HQ, Wang JH, Li XQ, Zhao YD, Luo QM: Temperature-dependent photoluminescence of water-soluble quantum dots for a bioprobe. *Analytica Chimica Acta* **2006**, 559:120.
37. Wuister SF, Koole R, Donega CD, Meijerink A: Temperature-dependent energy transfer in cadmium telluride quantum dot solids. *Journal of Physical Chemistry B* **2005**, 109:5504.
38. Biju V, Makita Y, Sonoda A, Yokoyama H, Baba Y, Ishikawa M: Temperature-sensitive photoluminescence of CdSe quantum dot clusters. *Journal of Physical Chemistry B* **2005**, 109:13899.

# Appendix

## Programming with MatLab

### 1 Probability Density Distribution of “on” and “off” Times from a Fluorescence Blinking Trajectory

**File name: weighted\_fitting\_slop\_PDFdata\_onofftime\_recordingdata.m**

```
%Modified since 12/02/05
%change of the probability density  $p(s-1)$  vs time  $y/(a+b/2)$ 
%weight  $y$  with  $(a+b)/2$ 
%Refer to Kuno's paper (J. Chem. Phys., 115, 1028) for details
```

```
%Open file
function photoncounting = single
fname='538_032206_1.asc';
fid=fopen(fname);
Gtemp=[];
```

```
%Skip the first 5 lines
for i=1:5
    str=fgetl(fid);
end
```

```
%Read the PCH data until a blank line is encountered
cmp=0;
while cmp ~=1
    str=fgetl(fid);
    cmp=strcmp(str,"");
    if str == -1
        cmp = 1;
    end
    if cmp ~=1
        Gtemp=[Gtemp;str2num(str)];
    end
end
a=size(Gtemp);
a=a(1);
```

```
%Make a matrix from the original data
K=[];
timebin=10;%in ms
for j=1:timebin:a*timebin;
    k=j;
```

```

    K=[K;k];
end
b=size(K);
b=b(1);
G=[K Gtemp];

%%%%%%%%%%%%Make on and off times matrixes by setting a threshold
j=1;
noff=0;
non=0;
ton=[];
toff=[];

thres=22; %%%%%%%%%Set threshold manually
% g=G(1:50,2);
while j<=a;

    while j<=a & G(j,2)<=thres;
        noff=noff+1;
        j=j+1;

    end

    if non~=0;
        ton=[ton;non];
        non=0;
    end

    while j<=a & G(j,2)>thres;
        non=non+1;
        j=j+1;

    end

    if noff~=0;
        toff=[toff;noff];
        noff=0;
    end

end
ton=ton;
toff=toff;

%%%%%%%%%%%%Make weighted on times histogram distribution (Kuno's paper)
xx=min(ton):1:max(ton);
[tn,x]=hist(ton,xx);
c=[tn;x];
d=size(c);
e=d(2);
xxx=[];
yyy=[];

```

```

p=1;
while p<=e;
    if c(1,p)~=0;
        xxx=[xxx,c(2,p)];
        yyy=[yyy,c(1,p)];
    end
    p=p+1;
end

c=[yyy;xxx];
f=size(c);
ff=f(2);
Q=[];
j=2;
while j<=ff-1;
    cc=c(1,j)*2/(c(2,j+1)-c(2,j-1));
    Q=[Q;cc];
    j=j+1;
end
q1=c(1,1);
Q=[q1;Q];
Q=Q;
x=size(xxx);
X=x(2);
XX=[];
for j=1:X-1;
    XX=[XX;xxx(1,j)];
end
XX=XX;
QX=[XX*0.01 Q/0.01]; %original on times distribution data
timeon=XX*0.01;
Pon=Q/0.01;
tn=log10(Q/0.01);
XX=log10(XX*0.01);
LLQX=[XX tn]; %log on times distribution data
LLtimeon=XX;
LLPon=tn;
on=[QX LLQX];
figure(1)
plot(XX,tn,'k.')

```

```

%%%%%%%%%%%%%Make weighted off times histogram distribution (Kuno's paper)
zz=min(toff):1:max(toff);
[tff,z]=hist(toff,zz);
cc=[tff;z];
dd=size(cc);
ee=dd(2);
zzz=[];
sss=[];
pp=1;
while pp<=ee;
    if cc(1,pp)~=0;
        zzz=[zzz,cc(2,pp)];
    end
    pp=pp+1;
end

```

```

        sss=[sss,cc(1,pp)];
    end
    pp=pp+1;
end

c=[sss;zzz];
f=size(c);
ff=f(2);
Q=[];
j=2;
while j<=ff-1;
    cc=c(1,j)*2/(c(2,j+1)-c(2,j-1));
    Q=[Q;cc];
    j=j+1;
end
q1=c(1,1);
Q=[q1;Q];
Q=Q;
z=size(zzz);
Z=z(2);
ZZ=[];
for j=1:Z-1;
    ZZ=[ZZ;zzz(1,j)];
end
ZZ=ZZ;
QZ=[ZZ*0.01 Q/0.01]; %original off times distribution data
timeoff=ZZ*0.01;
Poff=Q/0.01;
tff=log10(Q/0.01);
ZZ=log10(ZZ*0.01);
LLQZ=[ZZ tff]; %log off times distribution data
LLtimeoff=ZZ;
LLPoff=tff;
off=[QZ LLQZ];

figure(2)
plot(ZZ,tff,'k.')

```

%%%%%%%%%% Recording Data

```

[fname,pname] = uinputfile('* .txt','on&off_distribution_');
if fname~=0
    filename=strcat(pname,fname);
    fid=fopen(filename,'w');
    fprintf(fid,'%s %s\n',File name:',fname);
    fprintf(fid,'%s\n',On times');
    fprintf(fid,'%6.4f\n',timeon);
    fprintf(fid,'%s\n',On times distribution');
    fprintf(fid,'%6.4e\n',Pon);
    fprintf(fid,'%s\n',Off times');
    fprintf(fid,'%6.4f\n',timeoff);
    fprintf(fid,'%s\n',Off times distribution');
    fprintf(fid,'%6.4e\n',Poff);
    fprintf(fid,'%s\n',log On times');

```

```
fprintf(fid,'%6.4f\n',LLtimeon);
fprintf(fid,'%s\n','log On times distribution');
fprintf(fid,'%6.4f\n',LLPon);
fprintf(fid,'%s\n','log Off times');
fprintf(fid,'%6.4f\n',LLtimeoff);
fprintf(fid,'%s\n','log Off times distribution');
fprintf(fid,'%6.4f\n',LLPoff);

    sta=fclose(fid);
end
end
```

## 2 Threshold for Distinguishing “on” and “off” States

**File name: threshold.m**

```
%ref to Kuno's Paper
%Open file
function photoncounting = single
fname='538_032206_1.asc';
fid=fopen(fname);
Gtemp=[];

%skip the first 10 lines
for i=1:5
    str=fgetl(fid);
end

%read the PCH data until a blank line is encountered
cmp=0;
while cmp ~=1
    str=fgetl(fid);
    cmp=strcmp(str,"");
    if str == -1
        cmp = 1;
    end
    if cmp ~=1
        Gtemp=[Gtemp;str2num(str)];
    end
end
Gtemp=Gtemp;

%%%%%%%%%%%%%Get the matrix containing only off times
a=size(Gtemp);
a=a(1);
off=[];
i=1;
threshold=20; %input an initial counts according to the trace
while i<=a;
    if Gtemp(i,1)<=threshold;
        off=[off;Gtemp(i,1)];
    end
    i=i+1;
end
off=off;

%%%%%%%%%%%%%Calculate standard deviation s from the off time matrix
b=sum(off);
c=size(off);
d=c(1);
e=b/d;
s=std(off);

%%%%%%%%%%%%%Set the threshold with this equation
S=e+2.*s
```

### 3 Photon Counting Histogram for the Single Detector Setup

**File name: photon\_counting\_histogram.m**

```
%04/24/05
%photon counting histogram H(I),H(Ion), and H(Ioff)
%paul Barara's paper (conjugated polymer)

%open file
function photoncounting = single
fname='QDcluster_121305_1';
fid=fopen(fname);
Gtemp=[];

%skip the first 10 lines
for i=1:5
    str=fgetl(fid);
end

%%%%%%%%%%%%%%read the PCH data until a blank line is encountered
cmp=0;
while cmp ~=1
    str=fgetl(fid);
    cmp=strcmp(str,"");
    if str == -1
        cmp = 1;
    end
    if cmp ~=1
        Gtemp=[Gtemp;str2num(str)];
    end
end
coun=min(Gtemp):1:max(Gtemp);
[n,coun]=hist(Gtemp,coun);
figure(1);
plot(coun,n,'-k.');
```

```
%%%%%%%%%%%%%%
%recording photon-counting histogram data to transfer into igor file
[fname,pname] = uinputfile(*.txt,'PCH_data');
if fname~=0
    filename=strcat(pname,fname);
    fid=fopen(filename,'w');
    fprintf(fid,'%s %s\n','File name:',fname);
    fprintf(fid,'%s\n','counts ');
    fprintf(fid,'%6.4f\n',coun);
    fprintf(fid,'%s\n','PCH_');
    fprintf(fid,'%6.4f\n',n);
    sta=fclose(fid);
end
```

## 4 Photon Counting Histogram for the Two-detector Setup

**File name: PCH\_2blocks.m**

```
%for two-detector setup
%04/30/07
%photon counting histogram H(I),H(Ion), and H(Ioff)
%paul Barara's paper (conjugated polymer)

%open file
function photoncounting = single
fname='121707_1.asc';
fid=fopen(fname);
Gtemp=[];

%%%%%%%%%%%%%read the blinking data (block A and B) until a blank line is encountered

cmp=0;
while cmp ~=1
    str=fgetl(fid);
    cmp=strcmp(str,"");
    if str == -1
        cmp = 1;
    end
    if cmp ~=1
        Gtemp=[Gtemp;str2num(str)];
    end
end
Gtemp=Gtemp;
a=size(Gtemp);
a=a(1);

%%%%%%%%%%%%%split matrix GG into block A (white trace/transmitted)and block B (Yellow fluorescence
trace/reflected light)
GtempA=[];
GtempB=[];
i=1;
j=1;
aa=a/2;
while i<=a
    if i<=aa;
        GtempA=[GtempA;Gtemp(i)];
        i=i+1;
    end
    if i>aa
        GtempB=[GtempB;Gtemp(i)];
        i=i+1;
    end
end
end
GtempA=GtempA;
GtempB=GtempB;
```

```

%% photon counting histogram (PCH) of block A (white trace, red
curve)
counA=min(GtempA):1:max(GtempA);
[nA,counA]=hist(GtempA,counA);
figure(1);
plot(counA,nA,'-r. ');
hold on

```

```

%% photon counting histogram (PCH) of block B (yellow trace, yellow
curve)
counB=min(GtempB):1:max(GtempB);
[nB,counB]=hist(GtempB,counB);
plot(counB,nB,'-y. ');

```

```

%% recording photon-counting histogram data to transfer into igor file
[fname,pname] = uinputfile('* .txt','PCH_data');
if fname~=0
    filename=strcat(pname,fname);
    fid=fopen(filename,'w');
    fprintf(fid,'%s %s\n','File name:',fname);
    fprintf(fid,'%s\n','counts-A ');
    fprintf(fid,'%6.4f\n',counA);
    fprintf(fid,'%s\n','PCH-A');
    fprintf(fid,'%6.4f\n',nA);
    fprintf(fid,'%s\n','counts-B ');
    fprintf(fid,'%6.4f\n',counB);
    fprintf(fid,'%s\n','PCH-B');
    fprintf(fid,'%6.4f\n',nB);
    sta=fclose(fid);
end
return

```

## 5 Auto-correlation Function for the Single Detector Setup

**File name: ACF\_QD\_R.m**

```
%10/04/06
%Auto-correlation function of QDs
% $G(t)-1=(M-K)\text{sum}I(t)I(t+\tau)/\text{sum}I(t)\text{sum}I(t+\tau)$ 

%Open file
fname='538_033006_6.asc';
fid=fopen(fname);
Gtemp=[];

%skip the first 5 lines
for i=1:6;
    str=fgetl(fid);
end

%%%%%%%%%% read the PCH_blinking data until a blank
cmp=0;
while cmp ~=1
    str=fgetl(fid);
    cmp=strcmp(str,"");
    if str == -1
        cmp = 1;
    end
    if cmp ~=1
        Gtemp=[Gtemp;str2num(str)];
    end
end
a=size(Gtemp);
a=a(1);

%%%%%%%%%% make a two-column matrix from the above matrix
KK=[];
timebin=0.01;%in second
for j=0.01:timebin:a*timebin;
    k=j;
    KK=[KK;k];
end
b=size(KK);
b=b(1);
GG=[KK Gtemp];
```

```

%%%%calculate auto-correlation function
G=[];
M=a;
K=0;

while K<M;
    i=1;
    j=2;
    count1=0;
    count2=0;
    count3=0;
    for i=1:a-K;
        c1=GG(i,j)*GG(i+K,j);
        count1=count1+c1;
        c2=GG(i,j);
        count2=count2+c2;
        c3=GG(i+K,j);
        count3=count3+c3;
        i=i+1;
    end
    Gk=count1*(M-K)/(count2*count3);
    G=[G;Gk];
    K=K+1;
end
GK=[G KK];
% figure(1)
% plot(KK,G,'k.')
% figure(2)
% semilogx(KK,G,'k.')
% hold on
% figure(3)
% plot(KKK,G,'k.')
% hold on
% return

%%%%Get rid of the noisy tail
ACF
%cut x to (0.01-10), then get xy array.
%then export to Exel to fit
KKshort1=[];
for i=0.01:timebin:1000*timebin;
    k=i;
    KKshort1=[KKshort1;k];
    i=i+1;
end

Gshort1=[];
GC=[];
for i=1:1000;
    GC=G(i);
    Gshort1=[Gshort1;GC];
    i=i+1;
end

```

```

KKK1=log10(KKshort1);
KKK1=KKK1;
Gshort1=Gshort1;
Gshort1=Gshort1-1;
figure(3)
plot(KKK1,Gshort1,'k.')
hold on

```

```

%%%%%%%%%%%%%%%%%%%%%%%%%%%%%%%%%%%%%%%%%%%%%%%%%%%%%%%%
%recording 0.01-10s data to transfer into igor file
[fname,pname] = uinputfile(*.txt,'ACF_data');
if fname~=0
    filename=strcat(pname,fname);
    fid=fopen(filename,'w');
    fprintf(fid,'%s %s\n','File name:',fname);
    fprintf(fid,'%s\n','time ');
    fprintf(fid,'%6.4e\n',KKshort1);
    fprintf(fid,'%s\n','logtime ');
    fprintf(fid,'%6.4f\n',KKK1);
    fprintf(fid,'%s\n','ACF_');
    fprintf(fid,'%6.4f\n',Gshort1);
    sta=fclose(fid);
end

```

## 6 Auto-correlation Function for the Two-detector Setup

**File name: ACF\_QD\_R\_2blocks.m**

```
%02/13/07
%Auto-correlation functions of QDs from two detectors
%G(t)-1=(M-K)sumI(t)I(t+tau)/sumI(t)sumI(t+tau)

%%%%%%%%%Open file
fname='071207_2.asc';
fid=fopen(fname);
Gtemp=[];

%%%%%%%%% read the blinking data (block A and B) until a blank
cmp=0;
while cmp ~=1
    str=fgetl(fid);
    cmp=strcmp(str,"");
    if str == -1
        cmp = 1;
    end
    if cmp ~=1
        Gtemp=[Gtemp;str2num(str)];
    end
end
Gtemp=Gtemp;
a=size(Gtemp);
a=a(1);

KK=[];
timebin=0.01;%in second
for j=0.01:timebin:a/2*timebin;
    k=j;
    KK=[KK;k];
end
b=size(KK);
b=b(1);
% GG=[KK Gtemp];

%%%%%%%%%split matrix GG into block A (white trace/transmitted)and block B (Yellow fluorescence
trace/reflected light)
GtempA=[];
GtempB=[];
i=1;
j=1;
aa=a/2;
while i<=a
    if i<=aa;
        GtempA=[GtempA;Gtemp(i)];
        i=i+1;
    end
end
```

```

    if i>aa
        GtempB=[GtempB;Gtemp(i)];
        i=i+1;
    end
end
GtempA=GtempA;
GtempB=GtempB;
GGA=[KK GtempA];
GGB=[KK GtempB];

% %%%auto-correlation function of block A
G=[];
M=aa;
K=0;

while K<M;
    i=1;
    j=2;
    count1=0;
    count2=0;
    count3=0;
    for i=1:M-K;
        c1=GGA(i,j)*GGA(i+K,j);
        count1=count1+c1;
        c2=GGA(i,j);
        count2=count2+c2;
        c3=GGA(i+K,j);
        count3=count3+c3;
        i=i+1;
    end
    Gk=count1*(M-K)/(count2*count3);
    G=[G;Gk];
    K=K+1;
end
GK=[G KK];

% %%%auto-correlation function of block B
GB=[];
M=aa;
KB=0;

while KB<M;
    i=1;
    j=2;
    count1=0.000001;
    count2=0.000001;
    count3=0.000001;
    for i=1:M-KB;
        c1=GGB(i,j)*GGB(i+KB,j);
        count1=count1+c1;
        c2=GGB(i,j);
        count2=count2+c2;
        c3=GGB(i+KB,j);
        count3=count3+c3;
        i=i+1;
    end
end

```

```

end
GkB=count1*(M-KB)/(count2*count3);
GB=[GB;GkB];
KB=KB+1;
end
GKB=[GB KK];

% %%%%%%%%%%
%For fitting of ACF of QD clusters for block A.
%cut x to (0.01-10), then get xy array.
%then export to Exel to fit
KKshort1=[];
for i=0.01:timebin:1000*timebin;
    k=i;
    KKshort1=[KKshort1;k];
    i=i+1;
end

Gshort1=[];
GC=[];
for i=1:1000;
    GC=G(i);
    Gshort1=[Gshort1;GC];
    i=i+1;
end
KKK1=log10(KKshort1);
KKK1=KKK1;
Gshort1=Gshort1;
Gshort1=Gshort1-1;
figure(1)
plot(KKK1,Gshort1,'k.')
hold on

% %%%%%%%%%%
%For fitting of ACF of QD clusters for block B.
%cut x to (0.01-10), then get xy array.
%then export to Exel to fit
KKshort1B=[];
for i=0.01:timebin:1000*timebin;
    k=i;
    KKshort1B=[KKshort1B;k];
    i=i+1;
end

Gshort1B=[];
GCB=[];
for i=1:1000;
    GCB=GB(i);
    Gshort1B=[Gshort1B;GCB];
    i=i+1;
end
KKK1B=log10(KKshort1B);
KKK1B=KKK1B;
Gshort1B=Gshort1B;

```

```

Gshort1B=Gshort1B-1;
% figure(2)
plot(KKK1B,Gshort1B,'y.')

%%%%%%%%%%%%%%%%%%%%%%%%%%%%%%%%%%%%%%%%%%%%%%%%%%%%%%%%
%recording 0.01-10s data to transfer into igor file
[fname,pname] = uiputfile('*.txt','ACF_2blocks_data');
if fname~=0
    filename=strcat(pname,fname);
    fid=fopen(filename,'w');
    fprintf(fid,'%s %s\n','File name:',fname);
    % fprintf(fid,'%s\n','time-A');
    % fprintf(fid,'%6.4e\n',KKshort1);
    fprintf(fid,'%s\n','time-B');
    fprintf(fid,'%6.4e\n',KKshort1B);
    % fprintf(fid,'%s\n','logtime-A');
    % fprintf(fid,'%6.4f\n',KKK1);
    fprintf(fid,'%s\n','logtime-B');
    fprintf(fid,'%6.4f\n',KKK1B);
    % fprintf(fid,'%s\n','ACF-A');
    % fprintf(fid,'%6.4f\n',Gshort1);
    fprintf(fid,'%s\n','ACF-B');
    fprintf(fid,'%6.4f\n',Gshort1B);
    sta=fclose(fid);
end
return

```

## 7 Auto-correlation and Cross-correlation Functions for the Two-detector Setup

**File name: CCF\_QD\_R\_spectraldiffusion.m**

```
%04/08/07
%cross-correlation functions of QDs from two detectors
% $G(\tau)-1=(M-K)\sum I_i(t)I_j(t+\tau)/\sum I_i(t)\sum I_j(t+\tau)$ 
%For spectral diffusion, BW=0.1s

%%%%%%%%%Open file
fname='041507_4.asc';
fid=fopen(fname);
Gtemp=[];

%%%%%%%%%read block A (white fluorescence trace/transmitted light)
%%%%%%%%%skip the first 5 lines
% for i=1:9;
%   str=fgetl(fid);
% end

%%%%%%%%% read the PCH_blinking data (block A and B) until a blank
cmp=0;
while cmp ~=1
    str=fgetl(fid);
    cmp=strcmp(str,"");
    if str == -1
        cmp = 1;
    end
    if cmp ~=1
        Gtemp=[Gtemp;str2num(str)];
    end
end
Gtemp=Gtemp;
a=size(Gtemp);
a=a(1);

KK=[];
timebin=0.1;%in second
for j=0.1:timebin:a/2*timebin;
    k=j;
    KK=[KK;k];
end
b=size(KK);
b=b(1);
% GG=[KK Gtemp];

%%%%%%%%%split matrix GG into block A (white trace/transmitted)and block B (Yellow fluorescence
trace/reflected light)
GtempA=[];
```

```

GtempB=[];
i=1;
j=1;
aa=a/2;
while i<=a
    if i<=aa;
        GtempA=[GtempA;Gtemp(i)];
        i=i+1;
    end
    if i>aa
        GtempB=[GtempB;Gtemp(i)];
        i=i+1;
    end
end
GtempA=GtempA;
GtempB=GtempB;
GGA=[KK GtempA];
GGB=[KK GtempB];
test=[GtempA,GtempB];

```

%%%%%%%%%%auto-correlation function of block A

```

G=[];
M=aa;
K=0;

while K<M;
    i=1;
    j=2;
    count1=0;
    count2=0;
    count3=0;
    for i=1:M-K;
        c1=GGA(i,j)*GGA(i+K,j);
        count1=count1+c1;
        c2=GGA(i,j);
        count2=count2+c2;
        c3=GGA(i+K,j);
        count3=count3+c3;
        i=i+1;
    end
    Gk=count1*(M-K)/(count2*count3);
    G=[G;Gk];
    K=K+1;
end
GK=[G KK];

```

%%%%%%%%%%auto-correlation function of block B

```

GB=[];
M=aa;
KB=0;

```

```

while KB<M;
    i=1;
    j=2;
    count1=0;
    count2=0;
    count3=0;
    for i=1:M-KB;
        c1=GGB(i,j)*GGB(i+KB,j);
        count1=count1+c1;
        c2=GGB(i,j);
        count2=count2+c2;
        c3=GGB(i+KB,j);
        count3=count3+c3;
        i=i+1;
    end
    GkB=count1*(M-KB)/(count2*count3);
    GB=[GB;GkB];
    KB=KB+1;
end
GKB=[GB KK];

```

```

%%cross-correlation function from block A and block B
GCC=[];
M=aa;
KCC=0;

```

```

while KCC<M;
    i=1;
    j=2;
    count1=0;
    count2=0;
    count3=0;
    for i=1:M-KCC;
        c1=GGA(i,j)*GGB(i+KCC,j);
        count1=count1+c1;
        c2=GGA(i,j);
        count2=count2+c2;
        c3=GGB(i+KCC,j);
        count3=count3+c3;
        i=i+1;
    end
    GkC=count1*(M-KCC)/(count2*count3);
    GCC=[GCC;GkC];
    KCC=KCC+1;
end
GKC=[GCC KK];

```

```

% For fitting of ACF of QD clusters for block A.
%cut x to (0.1-100), then get xy array.
%then export to Exel to fit

```

```

KKshort1=[];
for i=0.1:timebin:1000*timebin;
    k=i;
    KKshort1=[KKshort1;k];
    i=i+1;
end

```

```

Gshort1=[];
GC=[];
for i=1:1000;
    GC=G(i);
    Gshort1=[Gshort1;GC];
    i=i+1;
end
KKK1=log10(KKshort1);
KKK1=KKK1;
Gshort1=Gshort1;
Gshort1=Gshort1-1;
figure(1)
plot(KKK1,Gshort1,'r.')
hold on

```

```

% %%%%%%%%%%
%For fitting of ACF of QD clusters for block B.
%cut x to (0.1-100), then get xy array.
%then export to Exel to fit
KKshort1B=[];
for i=0.1:timebin:1000*timebin;
    k=i;
    KKshort1B=[KKshort1B;k];
    i=i+1;
end

```

```

Gshort1B=[];
GCB=[];
for i=1:1000;
    GCB=GB(i);
    Gshort1B=[Gshort1B;GCB];
    i=i+1;
end
KKK1B=log10(KKshort1B);
KKK1B=KKK1B;
Gshort1B=Gshort1B;
Gshort1B=Gshort1B-1;
% figure(2)
plot(KKK1B,Gshort1B,'y.')
% hold on

```

```

% %%%%%%%%%%
%For fitting of CCF of QD clusters for block A and B.
%cut x to (0.1-100), then get xy array.
KKshort1C=[];
for i=0.1:timebin:1000*timebin;

```

```

k=i;
KKshort1C=[KKshort1C;k];
i=i+1;
end

Gshort1C=[];
GCCC=[];
for i=1:1000;
    GCCC=GCC(i);
    Gshort1C=[Gshort1C;GCCC];
    i=i+1;
end
KKK1C=log10(KKshort1C);
KKK1C=KKK1C;
Gshort1C=Gshort1C;
Gshort1C=Gshort1C-1;
% figure(3)
plot(KKK1C,Gshort1C,'k.')
hold on

```

```

%%%%%%%%%%%%%%%%%%%%%%%%%%%%%%%%%%%%%%%%%%%%%%%%%%%%%%%%%%
%recording 0.01-10s data to transfer into igor file
[fname,pname] = uinputfile(*.txt','CCF_SD_data');
if fname~=0
    filename=strcat(pname,fname);
    fid=fopen(filename,'w');
    fprintf(fid,'%s %s\n','File name:',fname);
    fprintf(fid,'%s\n','time-A ');
    fprintf(fid,'%6.4e\n',KKshort1);
    fprintf(fid,'%s\n','time-B ');
    fprintf(fid,'%6.4e\n',KKshort1B);
    fprintf(fid,'%s\n','time-Cr ');
    fprintf(fid,'%6.4e\n',KKshort1C);
    fprintf(fid,'%s\n','logtime-A ');
    fprintf(fid,'%6.4f\n',KKK1);
    fprintf(fid,'%s\n','logtime-B ');
    fprintf(fid,'%6.4f\n',KKK1B);
    fprintf(fid,'%s\n','logtime-Cr ');
    fprintf(fid,'%6.4f\n',KKK1C);
    fprintf(fid,'%s\n','ACF-A');
    fprintf(fid,'%6.4f\n',Gshort1);
    fprintf(fid,'%s\n','ACF-B');
    fprintf(fid,'%6.4f\n',Gshort1B);
    fprintf(fid,'%s\n','ACF-Cr');
    fprintf(fid,'%6.4f\n',Gshort1C);
    sta=fclose(fid);
end
return

```

## 8 Auto-correlation and Cross-correlation Functions for the Two-detector Setup

**File name: ACFCCF\_QD\_R\_2blocks.m**

```
%04/08/07
%auto- and cross-correlation functions of QDs from two detectors
%G(tau)-1=(M-K)sumIi(t)Ij(t+tau)/sumIi(t)sumIj(t+tau)

%%%%%%%%%Open file
fname='053107_12.asc';
fid=fopen(fname);
Gtemp=[];

%%%%%%%%%read block A (white fluorescence trace/transmitted light)
%%%%%%%%%skip the first 5 lines
% for i=1:5;
%   str=fgetl(fid);
% end

%%%%%%%%% read the blinking data (block A and B) until a blank
cmp=0;
while cmp ~=1
    str=fgetl(fid);
    cmp=strcmp(str,"");
    if str == -1
        cmp = 1;
    end
    if cmp ~=1
        Gtemp=[Gtemp;str2num(str)];
    end
end
Gtemp=Gtemp;
a=size(Gtemp);
a=a(1);

KK=[];
timebin=0.01;%in second
for j=0.01:timebin:a/2*timebin;
    k=j;
    KK=[KK;k];
end
b=size(KK);
b=b(1);
% GG=[KK Gtemp];

%%%%%%%%%split matrix GG into block A (white trace/transmitted)and block B (Yellow fluorescence
trace/reflected light)
GtempA=[];
GtempB=[];
i=1;
```

```

j=1;
aa=a/2;
while i<=a
    if i<=aa;
        GtempA=[GtempA;Gtemp(i)];
        i=i+1;
    end
    if i>aa
        GtempB=[GtempB;Gtemp(i)];
        i=i+1;
    end
end
GtempA=GtempA;
GtempB=GtempB;
GGA=[KK GtempA];
GGB=[KK GtempB];
test=[GtempA, GtempB];

```

```

%%%auto-correlation function of block A
G=[];
M=aa;
K=0;

```

```

while K<M;
    i=1;
    j=2;
    count1=0;
    count2=0;
    count3=0;
    for i=1:M-K;
        c1=GGA(i,j)*GGA(i+K,j);
        count1=count1+c1;
        c2=GGA(i,j);
        count2=count2+c2;
        c3=GGA(i+K,j);
        count3=count3+c3;
        i=i+1;
    end
    Gk=count1*(M-K)/(count2*count3);
    G=[G;Gk];
    K=K+1;
end
GK=[G KK];

```

```

%%%auto-correlation function of block B
GB=[];
M=aa;
KB=0;

```

```

while KB<M;
    i=1;
    j=2;
    count1=0;
    count2=0;
    count3=0;
    for i=1:M-KB;
        c1=GGB(i,j)*GGB(i+KB,j);
        count1=count1+c1;
        c2=GGB(i,j);
        count2=count2+c2;
        c3=GGB(i+KB,j);
        count3=count3+c3;
        i=i+1;
    end
    GkB=count1*(M-KB)/(count2*count3);
    GB=[GB;GkB];
    KB=KB+1;
end
GKB=[GB KK];

```

```

%%%%%%%%%%cross-correlation function from block A and block B
GCC=[];
M=aa;
KCC=0;

```

```

while KCC<M;
    i=1;
    j=2;
    count1=0;
    count2=0;
    count3=0;
    for i=1:M-KCC;
        c1=GGA(i,j)*GGB(i+KCC,j);
        count1=count1+c1;
        c2=GGA(i,j);
        count2=count2+c2;
        c3=GGB(i+KCC,j);
        count3=count3+c3;
        i=i+1;
    end
    GkC=count1*(M-KCC)/(count2*count3);
    GCC=[GCC;GkC];
    KCC=KCC+1;
end
GKC=[GCC KK];

```

```

%%%%%%%%%%Whole functions
% KKK1=log10(KK);
% KKK1=KKK1;
% GCC=GCC-1;
% GB=GB-1;

```



```

    Gshort1B=[Gshort1B;GCB];
    i=i+1;
end
KKK1B=log10(KKshort1B);
KKK1B=KKK1B;
Gshort1B=Gshort1B;
Gshort1B=Gshort1B-1;
% figure(2)
plot(KKK1B,Gshort1B,'y.')
% hold on

```

```

% %%%%%%%%%%
%For double exponential fitting of CCF of QD clusters for block A and B.
%cut x to (0.01-10), then get xy array.
KKshort1C=[];
for i=0.01:timebin:1000*timebin;
    k=i;
    KKshort1C=[KKshort1C;k];
    i=i+1;
end

```

```

Gshort1C=[];
GCCC=[];
for i=1:1000;
    GCCC=GCC(i);
    Gshort1C=[Gshort1C;GCCC];
    i=i+1;
end
KKK1C=log10(KKshort1C);
KKK1C=KKK1C;
Gshort1C=Gshort1C;
Gshort1C=Gshort1C-1;
% figure(3)
plot(KKK1C,Gshort1C,'k.')
hold on

```

```

% %%%%%%%%%%
% KKC=log10(KK);
% GC=GC-1;
% % figure(2)
% plot(KKC,GC,'k.')
% % hold on

```

```

% %%%%%%%%%%
%recording 0.01-10s data to transfer into igor file
[fname,pname] = uiputfile('*.txt','ACF_CCF_data');
if fname~=0
    filename=strcat(pname,fname);

```

```

fid=fopen(filename,'w');
fprintf(fid,'%s %s\n', 'File name:',fname);
fprintf(fid,'%s\n', 'time-A ');
fprintf(fid,'%6.4e\n',KKshort1);
fprintf(fid,'%s\n', 'time-B ');
fprintf(fid,'%6.4e\n',KKshort1B);
fprintf(fid,'%s\n', 'time-Cr ');
fprintf(fid,'%6.4e\n',KKshort1C);
fprintf(fid,'%s\n', 'logtime-A ');
fprintf(fid,'%6.4f\n',KKK1);
fprintf(fid,'%s\n', 'logtime-B ');
fprintf(fid,'%6.4f\n',KKK1B);
fprintf(fid,'%s\n', 'logtime-Cr ');
fprintf(fid,'%6.4f\n',KKK1C);
fprintf(fid,'%s\n', 'ACF-A');
fprintf(fid,'%6.4f\n',Gshort1);
fprintf(fid,'%s\n', 'ACF-B');
fprintf(fid,'%6.4f\n',Gshort1B);
fprintf(fid,'%s\n', 'ACF-Cr');
fprintf(fid,'%6.4f\n',Gshort1C);
sta=fclose(fid);
end
return

```